

## **UC Irvine**

### **UC Irvine Electronic Theses and Dissertations**

#### **Title**

Interactions between PFAS and Microplastics in Wastewater Systems

#### **Permalink**

<https://escholarship.org/uc/item/7zz7b373>

#### **Author**

Salawu, Omobayo Adio

#### **Publication Date**

2023

Peer reviewed|Thesis/dissertation

UNIVERSITY OF CALIFORNIA,  
IRVINE

Interactions between PFAS and Microplastics in Wastewater Systems

DISSERTATION

submitted in partial satisfaction of the requirements.  
for the degree of

DOCTOR OF PHILOSOPHY

in Civil and Environmental Engineering

by

Omobayo Adio Salawu

Dissertation Committee:  
Assistant Professor Adeyemi Adeleye, Chair  
Associate Professor Russell Detwiler  
Professor Sunny Jiang

2023



## **DEDICATION**

To

my mum, who first taught me how to write and whose spirit lives on through me.

# TABLE OF CONTENTS

TABLE OF CONTENTS .....	iii
LIST OF FIGURES .....	v
LIST OF TABLES .....	vi
ACKNOWLEDGEMENTS .....	vii
VITA .....	viii
ABSTRACT OF THE DISSERTATION .....	xv
Chapter 1 Introduction .....	1
1.1 Background .....	1
1.2 Fate of microplastics and PFAS in wastewater .....	4
1.3 Hypothesis and Objectives .....	8
Chapter 2 Literature Review .....	10
2.1 Interaction between PFAS and suspended solids .....	10
2.2 Interaction between PFAS and microplastics .....	11
2.3 Microplastics aging .....	16
2.3.1 Physical aging .....	16
2.3.2 Chemical aging .....	18
2.4 Effect of aging on adsorption of contaminants onto microplastics .....	20
Chapter 3 Residential contributions to occurrence and concentrations of PFAS in Raw wastewater .....	23
3.1 Introduction .....	23
3.2 Materials and Methods .....	25
3.2.1 Description of study area .....	25
3.2.2 Sample collection .....	26
3.2.3 Physical and chemical properties measurement .....	26
3.2.4 PFAS extraction and instrumental analysis .....	27
3.2.5 Quality assurance/Quality .....	28
3.3 Results and Discussions .....	29
3.3.1 Physical and chemical properties of wastewater .....	29
3.3.2 PFAS occurrence and concentration in municipal raw wastewater .....	29
3.3.3 Correlations of PFAS with heavy metals .....	33
3.4 Conclusions and Limitations .....	35
Chapter 4 Adsorption of PFAS onto secondary microplastics: A mechanistic study .....	37
4.1 Introduction .....	37
4.2 Materials and Methods .....	40

4.2.1 Production of secondary MPs from PET bottles.....	40
4.2.2 Characterization of secondary PET MPs .....	41
4.2.3 PFAS adsorption studies .....	42
4.2.4 Statistical analyses .....	44
4.3 Results and Discussions .....	45
4.3.1 Characterization of secondary PET MPs .....	45
4.3.2 Kinetics of PFAS adsorption onto secondary PET MPs.....	47
4.3.3 Effect of water chemistry on adsorption of PFAS onto secondary PET MPs.....	52
4.3.3.1 Role of pH.....	52
4.3.3.2 Role of ionic strength.....	54
4.3.3.3 Role of NOM .....	57
4.3.3.4 Role of temperature.....	58
4.3.4 Mechanism of adsorption.....	59
4.3.5 Conclusions and Limitations.....	63
Chapter 5 Adsorption of PFAS onto aged secondary microplastics .....	65
5.1 Introduction.....	65
5.2 Materials and Methods.....	67
5.2.1 Production of secondary MPs from PET bottles.....	67
5.2.2 Aging of secondary PET MPs by Na <sub>2</sub> S treatment and loading with natural organic matter .....	68
5.2.3 Characterization of PET MPs .....	68
5.2.4 PFAS adsorption studies .....	69
5.3 Results and Discussions .....	70
5.3.1 Characterization of secondary PET MPs .....	70
5.3.2 Effect of aging on adsorption of PFAS in deionized water .....	74
5.3.2.1 Na <sub>2</sub> S treatment .....	74
5.3.2.2 Loading with NOM.....	77
5.3.3 Effect of aging on adsorption of PFAS in synthetic wastewater .....	79
5.3.3.1 Na <sub>2</sub> S treatment .....	79
5.3.3.2 Loading with NOM.....	81
5.3.4 Conclusion, environmental implications, and limitations.....	83
Chapter 6 Summary .....	85
Chapter 7 Future perspectives.....	89
References.....	90
Appendix.....	104

## LIST OF FIGURES

Figure 1.1 Summary of the scope of this dissertation.....	6
Figure 2.1 Abundance of different polymers in WWTP analyzed by collecting data from 10 articles that reported microplastics in WWTP.....	15
Figure 3.1 Available studies on occurrence and fate of PFAS in a sewershed target areas around the treatment plant.....	25
Figure 3.2(a) Detection frequency of PFAS in raw wastewater (b) Box plot showing the distribution of PFAS concentrations. The vertical lines drawn above and below the boxes (whiskers) show variability outside the upper and lower quartiles. The mean values are shown as open markers (o) while the outliers are shown as full markers (•). The median values are shown by a horizontal line across the boxes. ....	31
Figure 3.3 Total PFAS concentration in (a) Tap (b) wastewater samples .....	33
Figure 3.4 Correlations between PFAS and heavy metals in raw wastewater.....	35
Figure 4.1(a) surface morphology of commercial PET MPs (b) particle size distribution of commercial PET microplastics. (c) adsorption kinetics rate constant and (b) capacity of commercial PET MPs for PFAS in single-analyte systems. Initial concentration = 200 µg/L for each PFAS; MPs dose = 2 g/L; pH = 7; shaker speed = 150 rpm. ....	39
Figure 4.2 (a) The appearance (b) particle size distribution (c) SEM micrograph of secondary PET MPs used in this study. (d) A comparison of the FTIR spectra of the secondary PET MPs and the parent PET water bottle.....	46
Figure 4.3 (a) adsorption kinetics rate constant and (b) capacity of secondary PET MPs for PFAS in single-analyte systems; (c) adsorption kinetics rate constant and (d) capacity of secondary PET MPs for PFAS in mixed-PFAS systems; Initial concentration = 200 µg/L for each PFAS ; MPs dose = 2 g/L; pH = 7; shaker speed = 150 rpm.....	50
Figure 4.4 Effect of pH on (a) the adsorption capacity and (b) ζ potential of PET MPs; ionic strength on (c) the adsorption capacity and (d) ζ potential of PET MPs; humic acid concentration on (e) the adsorption capacity and (f) ζ potential of PET MPs; temperature on (g) the adsorption capacity of PET MPs. Gibb’s free energy (ΔG) of adsorption at 25°C is shown in (h). Initial PFAS concentration = 200 µg/L; MPs dose = 2 g/L; shaker speed = 150 rpm. ....	56
Figure 4.5 (a) FTIR spectra the secondary PET MPs before and after PFAS adsorption. PCA score plot of transformed FTIR spectra of PET before and after adsorption of (b) PFBA, (c) PFOA, (d) PFBS, (e) PFOS, and (f) GenX. The ellipses in the PCA score plots represent the 95% confidence range: n = 5.....	60
Figure 4.6 HOMO-LUMO diagrams of (a) PFBA, (b) PFOA, (c) PFBS, and (d) PFOS.....	61
Figure 5.1 Particle size distribution of (a) pristine (b) Na <sub>2</sub> S treated (c) NOM loaded MPs (d) mean surface roughness as obtained from AFM analysis. (e) FTIR spectra of pristine and aged MPs (f) PCA analysis showing the difference in the FTIR spectra of pristine and aged MPs. XPS survey spectra of (g) pristine (h) Na <sub>2</sub> S treated (i) NOM loaded MPs.....	74

## LIST OF TABLES

Table 2-1. Studies on the adsorption of PFAS to suspended particles in aquatic environment. ..	10
Table 2-2: Densities of microplastics detected in WWTP* .....	15
Table 4-1. Physicochemical properties of studied PFAS.....	44



## ACKNOWLEDGEMENTS

I extend my heartfelt gratitude to the Almighty Allah, for guiding me on this journey. I am profoundly indebted to my supervisor, Professor Adeyemi S. Adeleye, for his unwavering support and guidance throughout my PhD studies. I also wish to express my sincere appreciation to my thesis committee members: Professor Russell Detwiler and Professor Sunny Jiang for their encouragement, invaluable comments, and support.

I am also thankful to the past and present members of the Department of Civil and Environmental Engineering and the Environmental Chemistry and Technology Lab at University of California, Irvine for their constant assistance, which enriched my studies. I deeply appreciate the words of encouragement and support from Professor Diego Rosso, Professor Christopher Olivares, Dr. Sergio Carnalla, Dr. Jenny Zenobio, Ziwei Han, Naomi Senehi, Sarah Kadiri, Hyungwoo and the help from all the mentees that have worked me throughout my study. I am immensely grateful to Dr. Felix Grun, Dr. Abduljamiu Amao, and Dr. Xiaofeng Liu for their support. To my friends who made UC Irvine a home, your support has been invaluable. Thank you, Keiland, Marina, Mohannad, Gaëlle, Pedro, Mukesh. In the words of Gandalf, "All we have to decide is what to do with the time that is given to us." Your guidance has helped me make the most of my time in pursuit of knowledge. I extend my gratitude to Water UCI and Brown and Caldwell for their generous research support, facilitated through the UCI Water-Energy Nexus Center.

My family has been a steadfast pillar of support throughout my PhD journey. I cannot thank my brother, Omotayo Salawu, enough for his love, understanding, support, and sacrifices. My sons, Hamdan and Zaydan, gave me the reasons to see this through and I am also deeply indebted to my sister, Medinat Salawu, for always offering encouragement when I needed it most. I am immensely grateful for the prayers and blessings constantly received from my father. Thank you, sir.

To my biggest supporter, my late mother, Jummai Salawu: This success would not have been possible without your dreams. Rest in peace, Momma.

## VITA

### **EDUCATION**

- PhD, Civil and Environmental Engineering 2019 - 2023  
The Henry Samueli School of Engineering  
University of California, Irvine, USA
- Master of Science, Environmental Science 2013 - 2016  
College of Petroleum and Geosciences  
King Fahd University of Petroleum and Minerals (KFUPM), Saudi Arabia
- B. Eng., Agricultural and Environmental Resources Engineering 2005 - 2011  
Faculty of Engineering  
University of Maiduguri, Nigeria

### **RESEARCH INTEREST**

- Fate and transport of emerging contaminants including per- and polyfluorinated alkyl substances (PFAS) and microplastics in the environment.
- Application of membrane technology and nanotechnology in water treatment.
- Advanced oxidation and adsorption of water contaminants.

### **RESEARCH EXPERIENCE**

**Graduate Research Assistant** 2019 - Present  
Civil and Environmental Engineering  
University of California, Irvine

- Investigated the use of porous carbon adsorbent synthesized from shrimp waste for adsorption of ciprofloxacin and per- and polyfluoroalkyl substances (PFAS) from water.
- Carried out research on the synthesis and use of manganese oxide nanoparticles for remediation of PFAS.
- Studied the mechanism of interaction between secondary microplastics and PFAS in aqueous media.
- Researched the occurrence and concentration of PFAS in raw wastewater from a sewer shed
- Investigated the interaction between PFAS and biofilm.
- Extracted PFAS from aqueous samples using EPA 1633 method.
- Researched the environmental effects of quantum dots.
- Mentored undergraduate and master's students.

**Lecturer** 2017 - 2019  
Department of Chemistry  
King Fahd University of Petroleum and Minerals

- Lectured freshmen in basic laboratory chemistry and mentored students in undergraduate research.

- Researched novel bio-based products and their application in Food-Energy-Water Nexus

**Research Intern**

2016 - 2017

Dr. Basheer Research Group, Department of Chemistry  
King Fahd University of Petroleum and Minerals

- Researched synthesis and application of functionalized activated carbon in water treatment.
- Studied calcium carbonate scale formation on membrane.

**Research Assistant**

2014 - 2016

Center for Environment and Water  
King Fahd University of Petroleum and Minerals

- Reviewed articles on clean development mechanisms, solar energy in Saudi Arabia.
- Collected data and wrote reports on urban heat island and alternative renewable energy in Saudi Arabia.

**Graduate Research Assistant**

2013 - 2016

Earth Sciences  
King Fahd University of Petroleum and Minerals

- Studied adsorption of heavy metals from crude oil using activated carbon.
- Researched synthesis of nanocomposites of nanoparticles and electrospun polyacrylonitrile for the remediation of mercury.
- Investigated the synthesis of silver and iron nanoparticles for the removal of heavy metals from water.

**TEACHING EXPERIENCE**

Teaching Assistant – University of California, Irvine  
Course: Environmental challenges  
Course level: Undergraduate

Fall 2022

- Duties – Held discussion sessions on different environmental challenges.
- Taught a lecture “Fate of PFAS in raw wastewater”.

Teaching Assistant – University of California, Irvine  
Course: Environmental challenges  
Course level: Undergraduate

Fall 2021

- Duties – Held discussion sessions on different environmental challenges.
- Taught a lecture “Introduction to PFAS”.

Teaching Assistant – University of California, Irvine  
Course: Introduction to environmental chemistry  
Course level: Undergraduate

Winter 2020

- Duties – Assisted student during the course, prepared reagents, and chemicals for the laboratory part of the course and taught the laboratory class.

Invited Lecturer – University of California, Irvine  
Course: Environmental chemistry  
Course level: Graduate

Spring 2020

- Duties: Gave two lectures on “Basics of Adsorption”

Graduate Assistant – Kaduna Polytechnic, Nigeria  
 Department of Agricultural and Bioenvironmental Engineering  
 Kaduna Polytechnic, Nigeria

2011 – 2012

- Duties: Lectured undergrads in strength of materials and fluid mechanics. Also, co-supervised two diploma final year projects.

### **PEER-REVIEWED PUBLICATIONS**

1. Han, Z., Oyeyemi, B. F., Zenobio, J. E., **Salawu, O. A.**, & Adeleye, A. S. (2023). Perfluorooctanoic acid dominates the molecular-level effects of a mixture of equal masses of perfluorooctanoic acid and perfluorooctane sulfonic acid in earthworm. *Journal of Hazardous Materials*, 457, 131718.
2. Zenobio, J. E., **Salawu, O. A.**, Han, Z., & Adeleye, A. S. (2022). Adsorption of per-and polyfluoroalkyl substances (PFAS) to containers. *Journal of Hazardous Materials Advances*, 100130.
3. **Salawu, O. A.**, Ziwei Han, and Adeyemi S. Adeleye. "Shrimp Waste-derived Porous Carbon Adsorbent: Performance, Mechanism, and Application of Machine Learning." *Journal of Hazardous Materials* (2022): 129266.
4. Adeleye, A. S., Xue, J., Zhao, Y., Taylor, A. A., Zenobio, J. E., Sun, Y., Ziwei, H., **Salawu, O.A.**, & Zhu, Y. (2022). Abundance, fate, and effects of pharmaceuticals and personal care products in aquatic environments. *Journal of Hazardous Materials*, 424, 127284.
5. Giroux, M. S., Zahra, Z., **Salawu, O. A.**, Burgess, R. M., Ho, K. T., & Adeleye, A. S. (2022). Assessing the environmental effects related to quantum dot structure, function, synthesis, and exposure. *Environmental Science: Nano*.
6. Han, Z., **Salawu, O. A.**, Zenobio, J. E., Zhao, Y., & Adeleye, A. S. (2021). Emerging investigator series: immobilization of arsenic in soil by nanoscale zerovalent iron: role of sulfidation and application of machine learning. *Environmental Science: Nano*, 8(3), 619-633.
7. Ganiyu, S. A., Ajumobi, O., Tanimu, A., Abdulazeez, I., **Salawu. O.A.**, Muhammad, Q., & Alhooshani, K. (2021). Mechanistic insights into the ultra-deep desulfurization of liquid fuel on date-seed derived hierarchical porous carbon. *Surfaces and Interfaces*, 26, 101413.
8. Shaikh, A. R., Chawla, M., Hassan, A. A., Abdulazeez, I., **Salawu, O. A.**, Siddiqui, M. N., ... & Cavallo, L. (2021). Adsorption of industrial dyes on functionalized and

nonfunctionalized asphaltene: A combined molecular dynamics and quantum mechanics' study. *Journal of Molecular Liquids*, 337, 116433.

9. Hassan, A. A., Abdulazeez, I., **Salawu, O. A.**, & Al-Betar, A. R. (2020). Electrochemical deposition and characterization of polyaniline-grafted graphene oxide on a glassy carbon electrode. *SN Applied Sciences*, 2(7), 1-8.
10. **Salawu, O. A.**, Ganiyu, S. A., Usman, M., Abdulazeez, I., & Alhooshani, K. (2019). Facile and efficient nitrogen modified porous carbon derived from sugarcane bagasse for CO<sub>2</sub> capture: Experimental and DFT investigation of nitrogen atoms on carbon frameworks. *Chemical Engineering Journal*, 122964.
11. Saleh, T. A., **Salawu, O.A.**, Parthasarathy, P., & Danmaliki, G. I. (2020). Scientific insights into modified and non-modified biomaterials for sorption of heavy metals from water. In *Waste Management: Concepts, Methodologies, Tools, and Applications* (pp. 807-827). IGI Global.
12. **Salawu, O. A.**, Basheer C., Mohammed Omar H., Bassam Tawabini, Siddiqui Nahid (2018). Comparative evaluation of biosynthesized nanoscale zero valent iron and iron Oxide nanoparticles in mercury adsorption. *Journal of Environmental Engineering*
13. **Salawu, O. A.**, Mohammad Asif, Abdul-Rashid I. Mohammed, Nadeem Baig, Abdurrahman A. Al-Arfaj, Tawfik A. Saleh (2018). Poly (amidoxime) modified magnetic activated carbon for chromium and thallium adsorption: Statistical analysis and regeneration. *Process Safety and Environmental Protection*.
14. **Salawu, O.A.**, Rana, A., Chanabsha, B., BoAli, A. A. K., Essa, M., & Alsaadi, A. (2019). Silver nanoparticle-loaded activated carbon as an adsorbent for the removal of mercury from Arabian gas-condensate. *Arabian Journal for Science and Engineering*, 44(7), 6285-6293.
15. Saleh, T. A., **Salawu, O. A.**, Asif, M., & Dafalla, H. (2018). Statistical analysis of phenols adsorption on diethylenetriamine-modified activated carbon. *Journal of Cleaner Production*, 182, 960-968.
16. Sajid, M., Nazal, M. K., & **Salawu, O. A.** (2018). Applications of Nanomaterials in Miniaturized Extraction Techniques. In *Nanomaterials in Chromatography* (pp. 157-200).
17. **Salawu, O. A.**, Omar, M. H., Asif, M., & Saleh, T. A. (2017). Arsenic and Selenium removal from water using Biosynthesized Nanoscale zero-valent iron: A factorial design analysis. *Process Safety and Environmental Protection*.

18. Alsharaa, A., Basheer, C., **Salawu, O. A.**, Alhooshani, K., & Lee, H. K. (2016). Removal of haloethers, trihalomethanes and haloketones from water using *Moringa oleifera* seeds. *International Journal of Environmental Science and Technology*, 13(11), 2609-2618.
19. **Salawu, O. A.**, Basheer, C., Zafarullah, K., Alsharaa, A., & Siddiqui, Z. (2016). Biogenic synthesis of silver nanoparticles; study of the effect of physicochemical parameters and application as nanosensor in the colorimetric detection of Hg<sup>2+</sup> in water. *International Journal of Environmental Analytical Chemistry*, 96(8), 776-788.

## **PATENT**

1. Chanbasha Chanbasha B., **Salawu O. A.** Method for detecting Hg (II) in an aqueous solution. Docket Number: 453661US8 (Patent Submission).

## **CONFERENCES**

- August 2023: ACS Fall conference, San Francisco  
Paper presented: Influence of water chemistry and microplastics ageing on the adsorption of per- and polyfluoroalkyl substances to secondary microplastics.
- June 2022: AEESP Conference, St. Louis  
Paper presented: Roles of compounds and water chemistries in the adsorption of per- and polyfluoroalkyl substances to microplastics.
- March 2022: ACS Spring conference, San Diego  
Paper presented: Interactions between secondary microplastics and per- and polyfluoroalkyl substances.
- August 2021: ACS Fall conference, Atlanta  
Paper presented: Experimental and DFT studies of the adsorptive properties of porous carbon derived from shrimp shell.
- March 2020: PANNANO conference, Brazil  
Papers presented:  
Synthesis of manganese-iron oxide nanoparticle embedded on nitrogen-modified porous carbon (MnFe<sub>2</sub>O<sub>4</sub>@N-C) for selective adsorption of perfluorooctanesulfonate (PFOS) and its precursor from water.  
Biosynthesized silver nanoparticles and electrospun silver-nanoparticle-polyacrylonitrile nanohybrid for mercury (II) adsorption at low concentration.
- November 2015: NanoSpain 201 Conference, Spain  
Paper Presented: Biosynthesis of Silver Nanoparticles and Its application in the Removal of Mercury (II) from water.
- February 2015: Water Arabia 2015 Conference and Exhibition, Al-Khobar Saudi Arabia

Paper Presented: Removal of Dichloromethane from Groundwater Samples using Photodegradation.

- October 2014: 3rd International Laboratory Technology Conference & Exhibition, Bahrain  
Paper Presented: Removal of mercury from Water samples using biosynthesized silver nanoparticle membrane filter.
- November 2012: 15th National Engineering Conference, Kaduna Nigeria  
Paper Presented: Nuclear Technology: Possible Solution to Nigeria's Agricultural Challenges.

### **FELLOWSHIPS AND AWARDS**

- |  |      |
|--|------|
| • AEESP Research and Education Conference Travel grant               | 2022 |
| • Marquette University Water Quality Center Scholarship              | 2022 |
| • AGS Travel Grant   | 2021 |
| • Marquette University Water Quality Center Scholarship              | 2021 |
| • Henry Samueli Endowed Fellowship                                   | 2021 |
| • Ministry of Higher Education Scholarship, Kingdom of Saudi Arabia. | 2013 |
| • Bode Amao Foundation Scholarship, Nigeria                          | 2010 |

### **RESEARCH AND ANALYTICAL SKILLS**

- Instruments used: Mercury Analyzer, UV-Spectrophotometer, Ion Chromatography, Rigaku Miniflex-XRD, Liquid Chromatography tandem Mass Spectroscopy (LC/MS).
- Operating system: Windows and Linux.
- Graphic and Data Analysis tools: AutoCad, Originlab, Sigmaplot, Minitab, Chemometrics.

### **TECHNICAL TRAINING/SEMINARS**

- Emerging Contaminants in Water and Wastewater. Organized virtually by Marquette University, October 25, 2022.
- Emerging Contaminants in Water and Wastewater. Organized virtually by Marquette University, October 26, 2021.
- PFAS: Advanced Discussion of Data Defensibility and DOD QSM, Part 4. Organized by Eurofins Environment Testing America. Presented by Taryn McKnight & David Kaminski, October 19, 2021.
- PFAS Sample Collection, State of the Science, Part 2. Organized by Eurofins Environment Testing America. Presented by Taryn McKnight & David Kaminski, September 21, 2021.

### **TEACHING AND MENTORING EXPERIENCE**

Student Mentoring – University of California, Irvine

- Masters' student: Junya Zheng, Sarah Kadiri.
- Undergraduates: Lauren Nicole Obrien, Natasha Thandi, Luz Alexandra Valle, Hugo Yao, Zachary Wharton.

Student Mentoring – King Fahd University of Petroleum and Minerals

- Masters' students: Mustapha Umar, Mohammed Altahir.

### **REVIEWING DUTIES**

- Journal of Nanoparticle Research. ISSN: 1388-0764
- Journal of Environmental Engineering. ASCE ISSN: 0733-9372
- Journal of Cleaner Production. ISSN: 0959-6526

### **PROFESSIONAL AFFILIATIONS**

- Student Member: American Chemical Society.
- Student Member: American Society of Civil Engineers.
- Student Member: Association of Environmental Engineering and Science Professors.



# ABSTRACT OF THE DISSERTATION

Interactions between PFAS and Microplastics in Wastewater Systems

by

Omobayo Adio Salawu

Doctor of Philosophy in Civil and Environmental Engineering

University of California, Irvine, 2023

Professor Adeyemi S. Adeleye, Chair

Microplastics interact with per- and polyfluoroalkyl substances (PFAS), potentially acting as vectors for these contaminants. However, little is known about how residential sources, physicochemical properties, and water chemistry influence these interactions and the subsequent fate of microplastics and PFAS. Elucidating the role of residential PFAS inputs, sorption mechanisms, and microplastics aging is critical to understand microplastic-mediated PFAS proliferation. This work aimed to address these knowledge gaps by investigating PFAS in wastewater sources, sorption to microplastics, and effect of aging (sodium sulfide treatment and natural organic matter loading) on adsorption of PFAS onto microplastics. Raw wastewater sampling at three sites revealed complex PFAS profiles, with 9 compounds detected - 5 carboxylates, 2 sulfonates, and 2 precursors. Long-chain PFAS including perfluorododecanoic acid and perfluoropentanesulfonic acid dominated, contrasting with the lower levels of legacy PFAS like PFOS. Fluorotelomer precursors, especially 6:2 FTS, were frequently detected and abundant. PFAS showed distinct variation from heavy metals, although PFOA uniquely correlated with iron. Controlled experiments found PFAS rapidly sorb to microplastics within hours, following thermodynamically favorable and spontaneous partitioning. Perfluoroalkyl sulfonic

acids preferentially adsorbed over carboxylates, attributed to hydrophobicity. Water chemistry parameters like pH, salinity, and natural organic matter impacted sorption. Na<sub>2</sub>S treatment enhanced adsorption capacity by 28-95%, while NOM loading increased it by 16-42%, highlighting the impact of aging on PFAS uptake. This work advances understanding of residential PFAS inputs, microplastic interactions, and effects of MPs aging and aqueous matrices on PFAS adsorption. The results can inform source control and treatment strategies targeting these ubiquitous contaminants.

# Chapter 1 Introduction

## 1.1 Background

Plastic debris and per- and polyfluoroalkyl substances (PFAS) are contaminants of emerging concern that share similar transport routes and fates in the environment. Plastics are a diverse array of polymeric materials mainly derived from petrochemical sources. Plastics' versatile properties and low cost enabled their widespread incorporation into products and processes (Frias & Nash, 2019; Jessieleena et al., 2023). Plastics are widely produced and used in different sectors, including packaging, electronics, construction, health, agriculture, transportation, and the production of household products (Er et al., 2023; Flury et al., 2021; Shah & Wu, 2020). It is estimated that approximately 7 billion metric tons of plastic waste have been generated globally, with a mere 9% undergoing recycling while a substantial 79% enters landfills, wastewater, or the natural environment (Geyer et al., 2017b; Z. Liu et al., 2021). In addition, plastics production is expected to double by 2040 from a current estimate of about 390 million metric tons annually (McGuinty & Walker, 2023). The ubiquitous use, improper disposal, limited recycling, and persistence of plastics make them abundant in the environment (Er et al., 2023; Wong et al., 2020).

In wastewater streams, plastic debris act as sinks and vectors of contaminants during transport (Windsor et al., 2019). Plastics' surface area and hydrophobic nature also influence their interaction with contaminants (Vivekanand et al., 2021). For instance, the fragmentation of plastics increases their surface area for adsorption of different contaminants. These fragments vary in size,

from macroplastics (larger than 25 mm) to nanoplastics (1–100 nm), with microplastics (0.1 µm–5 mm) being particularly relevant. Microplastics are particularly relevant in the context of adsorption of contaminants because they are small enough to be ingested by a wide range of organisms, including plankton, fish, and birds (Khan et al., 2022; Thompson et al., 2009). This can lead to bioaccumulation of contaminants in the food chain, with potential impacts on human health and ecosystem functioning. In addition, fragmentation of plastics increases their surface area for adsorption of different contaminants, with microplastics being particularly relevant due to their small size and abundance in the environment. Microplastics (MPs) can be 'secondary,' resulting from fragmentation, or 'primary,' engineered for various uses. The ecological risks of microplastics are due to their physical characteristics, chemical composition, and ability to accumulate and transport co-contaminants like per- and polyfluoroalkyl substances (PFAS).

Per- and polyfluoroalkyl substances (PFAS) constitute a class of fluorinated compounds that have been in production since the 1940s and find extensive use in both industrial and domestic processes (Cousins et al., 2019; Gagliano et al., 2020; Noyma et al., 2016). PFAS molecules consist of hydrophobic carbon backbones, either fully or partially enveloped by fluorine atoms, and hydrophilic heads containing carboxylic, sulfonate, or other functional groups (Cui et al., 2020). The pronounced electronegativity of fluorine results in a strong bond between the central carbon and their linked fluorine atoms in PFAS molecules. Due to these strong C-F bonds, PFAS molecules are thermally and chemically stable (Rahman et al., 2014). Given this stability, PFAS have garnered interest for use in industrial processes and a wide array of commercial and consumer

products, such as nonstick cookware, adhesives, coatings, and aqueous firefighting foams (Glüge et al., 2020; Schaidler et al., 2017). PFAS are also integral components of aqueous firefighting foams (AFFF), extensively employed in firefighting at military bases and airports (Wang et al., 2017). The hydrophobic and oleophobic properties of PFAS further render them effective as surfactants, surface coating agents, and personal care products (Glüge et al., 2020; Knepper & Lange, 2011). However, these very attributes that make PFAS so versatile also contribute to their resistance to environmental removal, complicating efforts to address their presence (Bentel et al., 2019).

PFAS are bio-accumulative, ubiquitous, and easy to transport in aquatic environments (Bamai et al., 2020; Dixit et al., 2019; Suja et al., 2009). Some PFAS are toxic to human health and have been linked to harmful health effects such as liver and kidney damage, reproductive defects, immune system dysfunction, and hormone disruption (Backe et al., 2013; Campo et al., 2014). Recent epidemiological investigations have also revealed that human exposure to PFAS is linked with increased risk of cholesterol, testicular and prostate cancer, thyroid disease, and pregnancy-induced hypertension (Agency for Toxic & Disease, 2018; Benbrahim-Tallaa et al., 2014; Tarapore & Ouyang, 2021). Unfortunately, the U.S. Centers for Disease Control and Prevention (CDC) has reported PFAS compounds in the blood of up to 98% of all Americans (Calafat et al., 2007; Lewis et al., 2015; Sunderland et al., 2019). The growing understanding, potential effects, and wide distribution of many legacy PFAS have resulted in increased regulatory attention to the concentrations of PFAS in the environment.

## 1.2 Fate of microplastics and PFAS in wastewater

The fate of MPs and PFAS within WWTPs depends on complex interactions with other components in wastewater. Microplastics exhibit particle-like behavior, accumulating in sewage sludge (up to 37.7 – 286.5 microplastics/gram of sludge) through aggregation (Borthakur et al., 2022; Harley-Nyang et al., 2022). However, MPs also permeate through treatment processes and are discharged within the effluent (Talvitie et al., 2017). In contrast, the surface activity of PFAS results in preferential partitioning to the aqueous phase, especially in PFAS with short chain length (less than 5 carbon atoms). While sorption of some PFAS to sewage sludge occurs, higher proportions (up to 60 %) end up in treated effluent (Tavasoli et al., 2021). Thus, MPs and PFAS display differential fate within WWTP processes based on their distinct properties.

The release of incompletely removed MPs and PFAS from WWTPs causes their ubiquitous detection in surface waters worldwide (Podder et al., 2021; Sun et al., 2019). Discharge contributes to accumulation in sediments and biota near outfalls (Jaubet et al., 2021; McCormick et al., 2016). Land application of sewage sludge as biosolids also risks spreading MPs and PFAS contamination (Gianico et al., 2021; Pozzebon & Seifert, 2023). However, interactions between MPs and PFAS within wastewater may alter their partitioning and fate. Recent studies indicate MPs could act as carriers facilitating PFAS transfer to solids (Parashar et al., 2023; Scott et al., 2021). Factors influencing PFAS-microplastics interaction require further investigation both at mechanistic level and under realistic conditions.

While pristine microplastics exhibit some affinity for PFAS, the microplastics entering wastewater treatment plants are typically aged particles with modified surface properties. Aging processes during sewer transport such as exposure to sulfur rich environment, oxidation, and natural organic matter fouling alter the surface chemistry of microplastics, changing their hydrophobicity, charge, and aggregation tendencies (Bhagat et al., 2022). Aged microplastics with increased surface roughness and polarity have shown enhanced adsorption of some PFAS like PFOS compared to pristine plastics. However, aging mechanisms that reduce hydrophobicity could decrease PFAS binding affinity. Furthermore, coating of microplastics by organic matter or biofilms may inhibit PFAS adsorption by blocking reactive sites. Elucidating the complex effects of realistic wastewater aging on microplastic-PFAS interactions is crucial for understanding their co-fate. Research on binding kinetics, surface characterization, and separation behavior with aged microplastics can provide insights into how aging transformations impact PFAS partitioning and facilitate risk assessment of microplastic-mediated PFAS transport in wastewater systems.

This dissertation (summarized in Figure 1.1) seeks to investigate the role of interactions between microplastics and PFAS on the fate of both contaminants in wastewater. Chapter two provides a literature review and research gaps identified within the scope of this work. In Chapter three, I quantified household contributions to PFAS loads in WWTP influent to establish domestic activities as a major ongoing source. This is also to establish the fact that even if industrial PFAS uses are phased out, residential inputs will persist and so will the interaction between MPs and PFAS. Chapter four is a mechanistic study of the adsorption of PFAS onto pristine secondary MPs. This work investigates the role of physicochemical properties of PFAS and MPs, and aqueous

chemistry on the interactions between PFAS and secondary MPs. Chapter five builds on the findings of chapter four and aims to explore the influence of MPs ageing in wastewater on the adsorption of PFAS. I hypothesize that aging processes such as loading MPs with natural organic matter and sodium sulfide ( $\text{Na}_2\text{S}$ ) treatment may enhance MPs vector potential for PFAS by increasing their surface area and altering surface chemistry. I also hypothesize that altering surface chemistry and area will increase adsorption of PFAS. Elucidating mechanisms governing MPs - PFAS binding across these scenarios will provide insights into their co-fate in wastewater. Outcomes can inform management strategies to control MPs and PFAS releases into the environment.

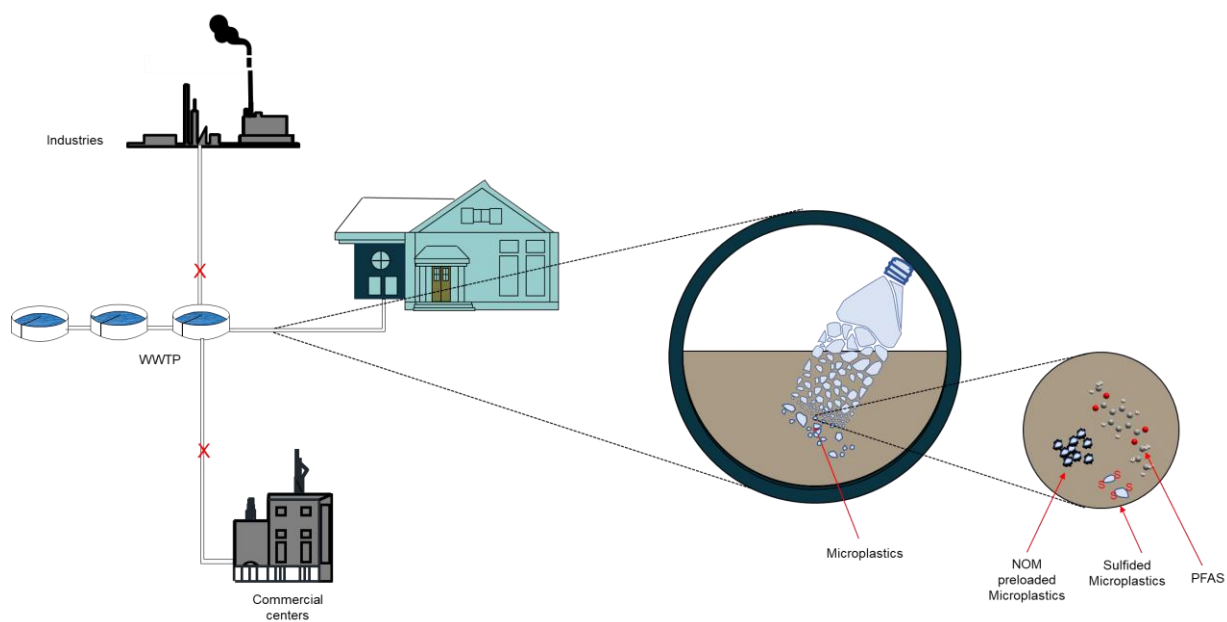


Figure 1.1 Summary of the scope of this dissertation



The findings from this dissertation will significantly advance our fundamental understanding of the interactions between microplastics (MPs) and per- and polyfluoroalkyl substances (PFAS) that affect their fate and transport in wastewater systems. By thoroughly characterizing the contribution of residential sources to PFAS loads in wastewater and elucidating the sorptive properties of both pristine and aged microplastics for PFAS, we can better predict the co-partitioning of MPs and PFAS through wastewater treatment plants (WWTPs). The results will directly aid in developing novel treatment methods that target microplastics as vectors in order to mitigate PFAS discharges into the environment. This research tackles crucial knowledge gaps at the intersection of these two ubiquitous and concerning pollutants within the context of wastewater systems and environmental plastic pollution. The outcomes will enable science-based solutions for controlling releases of both MPs and PFAS.

Specifically, this work investigates interactions between microplastics and PFAS and the effect of these interactions on the fate of MPs and PFAS during wastewater conveyance and treatment. Quantifying household PFAS contributions establishes that domestic activities will be an ongoing source to WWTPs even if industrial uses are phased out, necessitating control of MPs-PFAS interactions. Elucidating adsorption mechanisms of PFAS onto pristine and aged MPs reveals how plastic properties and aqueous chemistry impact binding. Providing better understanding of these mechanisms provides invaluable insights into MP-PFAS co-fate and behavior in wastewaters. The knowledge gained can directly inform management strategies to minimize MP vectoring and

enable removal of PFAS prior to environmental release. Overall, this timely research makes important advances in understanding two critical water pollutants.

### 1.3 Hypothesis and Objectives

The overarching hypothesis of this work is that per- and polyfluoroalkyl substances (PFAS) originating from residential sources interact with polyethylene terephthalate (PET) microplastics present in wastewater systems, resulting in sorption that is governed by microplastics properties, solution chemistry, and sewer transformations.

The key elements covered in this hypothesis are:

1. Identifying residential sources as contributors of PFAS to wastewater.
2. Stating that PFAS interacts with and adsorbs onto PET microplastics in wastewater.
3. Suggesting that the interaction process is mechanistic in nature.
4. Highlighting that aqueous chemistry parameters influence the sorption.
5. Implying that microplastics aging in sewers is an important factor.

This provides a broad hypothesis that residential PFAS inputs interact with microplastics through an intricate, chemistry-dependent process influenced by sewer conditions. Testing this hypothesis through the outlined objectives can provide fundamental insights into PFAS sources, fate, and microplastic interactions in wastewater systems.

- a. To highlight residential sources as contributors of PFAS in raw wastewater
- b. To develop a mechanistic understanding of the interaction between secondary polyethylene terephthalate (PET) MPs and PFAS
- c. To investigate the influence of aqueous chemistry on the interaction process

- d. To investigate the influence of aging and aquatic matrix in the adsorption of PFAS

## Chapter 2 Literature Review

### 2.1 Interaction between PFAS and suspended solids

Result of extensive literature search shows that adsorption of PFAS on such as activated carbon (Gagliano et al., 2020; Hansen et al., 2010; Park et al., 2020), polymeric materials (Lu et al., 2020; Senevirathna et al., 2010) and other engineered materials (Du et al., 2014; Xu et al., 2015; Zhang et al., 2019) have been well researched for the purpose of remediation. Studies also exist on the adsorption of PFAS to suspended particles in the environment. Adsorption on suspended solid surfaces play a huge role in the fate and transport of PFAS in aquatic environment (Alves et al., 2020). Table 1 shows some studies on the adsorption of PFAS to suspended solids. Most of the studies are focused on the adsorption of PFAS on mineral surfaces. Very few studies have investigated the adsorption of PFAS to microplastics and these studies are reviewed in section 2.2.1.

Table 2-1. Studies on the adsorption of PFAS to suspended particles in aquatic environment.

<b>PFAS compounds</b>	<b>Particulates</b>	<b>Study details</b>	<b>Reference</b>
PFOA, PFHpA, PFOS, PFNA, PFDA, PFUnDA	Kaolinite	Mechanistic study	(Xiao et al., 2011)
PFOS, PFOA	Boehmite	Mechanistic study	(Shih & Wang, 2013; Wang & Shih, 2011)

PFOS	Kaolinite and montmorillonite	Mechanistic study	(Zhang et al., 2014)
PFOS, PFHxS, PFOA, PFHXA	montmorillonite, kaolinite, and hematite	Mechanistic study	(Zhao et al., 2014)
PFOS and PFOA	Alumina	Mechanistic study	(Hellsing et al., 2016; Wang & Shih, 2011)
PFOS	Sand, clay, and iron oxide surfaces	Mechanistic study	(Johnson et al., 2007)

## 2.2 Interaction between PFAS and microplastics

Few studies have investigated the interaction between PFAS and microplastics. The few studies available are focused on the interaction between microplastics and PFAS in natural environments (Llorca et al., 2018; Scott et al., 2021). Only one study was found that performed a complete investigation of the adsorption mechanism of PFAS on microplastics. Wang et al., (F. Wang et al., 2015) investigated adsorption mechanism of PFOS and FOSA under batch conditions. Microplastics sizes, PFAS functional group, and organic matter content are the factors that influence adsorption of PFAS in natural environment (Atugoda et al., 2021). Microplastics sizes

influence the uptake rate and adsorption capacity of PFAS in natural waters with smaller particle sizes showing faster adsorption of PFAS compared to larger ones (Llorca et al., 2018; Scott et al., 2021). Presence of organic material from the environment also resulted in higher adsorption capacity of microplastics for PFAS (Scott et al., 2021). The increase in organic adsorption of PFAS at higher organic matter concentration may be due to co-adsorption and increase in surface active sites available for the adsorption of PFAS by heterogeneous surface complexation (Ateia et al., 2020; Gagliano et al., 2020; Joo et al., 2021a; Scott et al., 2021). Although, research that has reported influence of organic matter on the adsorption of PFAS was done outside controlled environment and using incubated microplastics which may introduce higher probability for error. As such, the role of organic matter on the adsorption capacities of microplastics is an area that required further research (Amaral-Zettler et al., 2020), and this study intend to fill this research gap.

In controlled environmental conditions, achieved by batch adsorption experiments, adsorption of PFAS to microplastics (Polyethylene (PE), polystyrene (PS), and polyvinyl chloride (PVC)) is linear and sorption mechanism is due to hydrophobic and electrostatic interaction (Gagliano et al., 2020; F. Wang et al., 2015). An increase in ionic strength also results in higher adsorption of PFOS but no effect on the adsorption of perfluorooctanesulfonamide (FOSA), a PFAS precursor. The difference in effect observed in both PFAS was attributed to difference in adsorption mechanism. Adsorption of PFOS to the microplastics investigated was partly due to electrostatic and hydrophobic interactions while the adsorption of FOSA was governed by hydrophobic interaction only. However, under natural environmental conditions, adsorption mechanism of PFAS on

microplastics were due to hydrophobic interactions especially in long-chain PFAS and electrostatic interactions. Salting out effect were predominant in seawater especially in the adsorption of long chain PFAS due to an increase in hydrophobicity (Llorca et al., 2018; Lohmann, 2012; Sacks & Lohmann, 2011). It is important to note that electrostatic interactions are influenced by solution pH which can change the surface charge of the microplastics. Thus, the effect of solution pH and ionic strength are also important to investigate adsorption mechanism.

Notably, the only study on the adsorption of PFAS to microplastics under batch conditions was carried out using primary microplastics (F. Wang et al., 2015). Ateia et al., (Ateia et al., 2020) used secondary microplastics in the adsorption of PFAS and other personal care products, although the study was limited to adsorption kinetic study which doesn't give a detail understanding of the adsorption mechanism. Study of adsorption mechanism using secondary microplastics is necessitated by the fact that these microplastics are often made up of other constituents such as plasticizers, pigments, fillers, and other additives that may influence the adsorption of contaminants. Primary microplastics also often come in defined and uniform shapes and sizes which makes it difficult to understand the effect of irregular shapes and size distribution on the adsorption of contaminants. Difference in adsorption of contaminants including PFAS has been observed using primary and secondary microplastics (Ateia et al., 2020; Müller et al., 2018; Zhang et al., 2018). One of the novelties of this work is to produce secondary microplastics to study the adsorption mechanism of PFAS. To the best of our knowledge and within our literature search, this is yet to be studied.

The scope of this work will be limited to adsorption of PFOS, PFOA, PFBS, PFBA and GenX on polyethylene terephthalate (PET) and high-density polyethylene (HDPE). PET microplastics have been selected based on the result of data gathered from the literature. Data was collected from ten (10) articles that reported microplastics in wastewater treatment plants and the three most abundant microplastics reported in each of these papers were collected. The frequency of each polymer was calculated, and the result (Figure 2.1.1 1) shows that polyethylene (PE, high and low density), PET and PP are the most frequently detected microplastics in WWTP. In addition, the density of the microplastics was also considered (Table 2). PET is considered a high-density plastic (Li et al., 2018) and this property has been suggested as one of the reasons why it is abundant in sludge. Polypropylene was overlooked despite more frequency of detection in WWTP because of its low density (0.83 – 0.92, Table 2). Microplastics of sizes within 50 – 250  $\mu\text{m}$  will be used in this study. As shown in Table S2, plastics within this size range are reported in wastewater treatment plants.



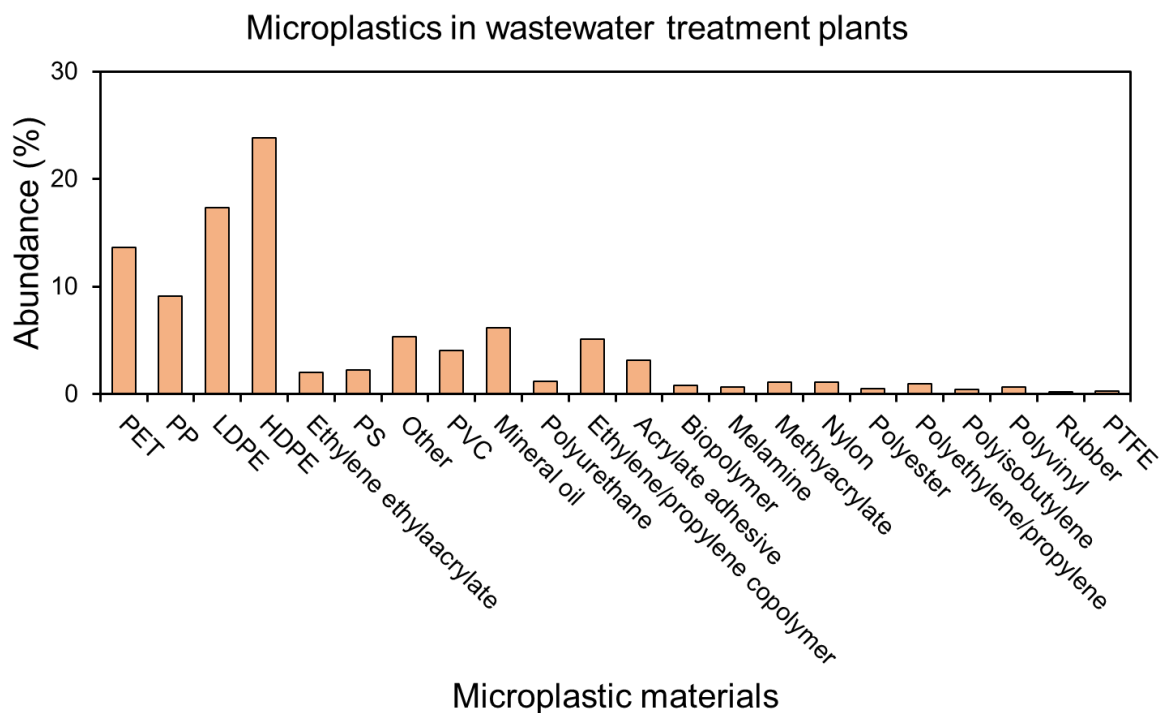


Figure 2.1 Abundance of different polymers in WWTP analyzed by collecting data from 10 articles that reported microplastics in WWTP.

Table 2-2: Densities of microplastics detected in WWTP\*

Polymer	Abbreviation	Density g/cm <sup>3</sup>
Acrylic	–	1.09–1.20
Alkyd	–	1.24–2.01
Polyethylene terephthalate	PET	0.96–1.45
Polyamide (nylon)	PA	1.02–1.16
Polyaryl ether	PAE	1.14
Polyester	PES/PEST	1.24–2.3
Polyethylene	PE	0.89–0.98
Polypropylene	PP	0.83–0.92
Polystyrene	PS	1.04–1.1
Polyurethane	PU/PUR	1.2
Polyvinyl fluoride	PVF	1.7
Polyvinyl acetate	PVAC	1.19
Polyvinyl chloride	PVC	1.16–1.58
Polytetrafluoroethylene	PTFE	2.1–2.3
Styrene acrylonitrile	SAN	1.08

Ethylene vinyl acetate	EVA	0.92–0.95
Polyvinyl alcohol	PVAL	1.19–1.31
Acrylonitrile butadiene styrene	ABS	1.04–1.06
Poly lactide	PLA	1.21–1.43
polycarbonate	PC	1.2–1.22
Poly(oxymethylene)	POM	1.41
Polysulfone	PSU	1.24
Silicone	–	1.1–1.2

\*(Sun et al., 2019)

## 2.3 Microplastics aging

In aquatic environments, MPs often undergo different physical, chemical, and biological processes that lead to their degradation, and alteration over time (Dey et al., 2022; Wu et al., 2022a). These aging processes result in changes to surface, textural, and chemical properties of MPs which can have significant implications for their environmental persistence, interactions with pollutants, and potential impacts on aquatic organisms (Zha et al., 2022). Below, the common MPs aging mechanisms are classified into physical, and chemical processes based on the factors that drive the changes in the MPs.

### 2.3.1 Physical aging

MPs age because of their interactions with suspended particles (sediment, pebbles) or exposure to environmental stressors such as waves, tides, and temperature fluctuations during transport (Luo et al., 2022; Rangel-Buitrago et al., 2023). Mechanical forces, including wave action and abrasion, can fragment MPs, eroding their surfaces through friction with sediment and other particles (Andrady & Koongolla, 2022; Rangel-Buitrago et al., 2023). This turbulence and abrasion

repeatedly roughen the surfaces, causing pits and cracks (Kokalj et al., 2019) that render the particles more susceptible to fragmentation and could enhance sorption capabilities.

Wave turbulence, through incremental abrasion, progressively breaks plastic particles into smaller fragments, increasing their surface area (Born et al., 2023; Weinstein et al., 2016). Additionally, photodegradation weakens polymer bonds (Ding et al., 2022; Zhang et al., 2021b) until shear forces or microorganisms ultimately break the pieces apart (Luo et al., 2022). These physical aging processes modify MPs characteristics, including size distribution, shape, density, and surface roughness (X. Liu, Q. Deng, Y. Zheng, D. Wang, & B.-J. Ni, 2022; Rummel et al., 2017). Over time, abrasion and fragmentation produce smaller, more irregularly shaped, or angular MPs. Density of the MPs may also increase due to coating or biofouling (Halsband, 2021; S. Liu et al., 2022). Alterations in size, shape, and density have notable effects on microplastic transport and settling (Ding et al., 2021; Waldschläger & Schüttrumpf, 2019).

Mechanical and hydrodynamic forces, driving abrasion, cracking, and fragmentation, significantly contribute to the physical aging of microplastics (Kumar et al., 2021; Mattsson et al., 2021). These processes modify particle size distribution, shape, density, and surface roughness over time (Luo et al., 2023). While chemical aging has been more widely studied, integrating physical aging mechanisms into fate models can improve predictions of microplastic transport and accumulation. Physical aging alters microplastic properties, which can affect their interactions with contaminants and organisms as well as their environmental fate. Despite advances, more research on physical aging is still needed, as it both increases microplastic numbers through breakdown and reduces

their size. Overall, physical aging transforms microplastic characteristics in ways that likely influence their behavior and impacts in aquatic systems.

### 2.3.2 Chemical aging

MPs undergo various chemical aging processes that alter their composition and properties over time. Major chemical aging mechanisms include photodegradation, thermal oxidation, ozone oxidation, and hydroxyl radical degradation. Although exposure to UV light is often classified as a chemical aging process, degradation caused by UV irradiation can trigger chemical reactions in the polymer materials that make up the MPs. For instance, broken polymer chain in MPs under UV exposure may undergo chemical reactions with other compounds present in the environment, leading to chemical changes and degradation of MPs.

Exposure to ultraviolet (UV) radiation from sunlight is a predominant aging process for MPs (P. Liu et al., 2022). The potential for photodegradation varies among different types of MPs, primarily because of their polymeric structure and distinct capacity to absorb ultraviolet (UV) light and generate free radicals (P. Liu et al., 2022; Song et al., 2017). MPs with phenyl rings in their polymeric structure are more susceptible to photodegradation due to easy excitation by UV radiation (Gewert et al., 2015). UV radiation also induces scission of polymer chains through both direct photolysis reactions and radical-mediated pathways (Chen et al., 2019; Zhang et al., 2021a). Chain scission progressively reduces the molecular weight of the plastic polymer (Shi et al., 2021; Zhang et al., 2021a). Photodegradation makes microplastics more brittle and prone to fracturing under mechanical forces or turbulence (Priya et al., 2022). Studies have shown enhanced

photodegradation of microplastics under environmentally relevant conditions (Ouyang et al., 2022; Sait et al., 2021; C. Wang et al., 2020).

An unexplored pathway that could substantially contribute to the aging of MPs is reactions induced by sulfides (Zhao et al., 2021). Sulfidation of MPs is relevant in anoxic zones within aquatic environments and engineered systems like wastewater treatment plants (Duan et al., 2023; Wei et al., 2020). In wastewater systems, sulfidation of MPs is more likely to occur during their transport through sewer lines and wastewater treatment plants (WWTPs). Sulfide, even at environmentally relevant concentrations (e.g., tens of micromolar), can initiate the alteration of MPs by radical oxidation and sulfide addition leading to physical damage, as well as surface oxidation and sulfidation of the MPs (Duan et al., 2023). Sulfidation introduces hydrophilic, polar functional groups that change surface charge, and functional groups. Sulfides undergoes spontaneous reactions with dissolved organic matter, often through nucleophilic substitution and/or addition mechanisms. To date, the impact of sulfide on the transformation processes of MPs remain uncertain (Zhao et al., 2021). Some studies have examined sulfidation of microplastics. Zhao et al. (2021) showed that sulfide treatment resulted in physical and chemical changes on the surface of thermoplastic polyurethane, polystyrene, polyethylene terephthalate and polyethylene.

These chemical reactions increase microplastic surface area due to cracks and pits formed during oxidation (Guo and Wang, 2019). Overall, photodegradation, sulfidation, and loading with NOM affects the physical and chemical properties of MPs over time. Elucidating chemical aging mechanisms and kinetics is crucial for modeling microplastic fate across environments (Song et

al., 2019). Chemical aging processes fundamentally change microplastic properties and behavior and must be considered when assessing their interaction with co-contaminants and overall environmental impacts.

Loading microplastics with natural organic matter (NOM) is an important aging process in aquatic environments. NOM readily sorbs to microplastic surfaces, creating an organic coating that alters surface properties and behavior (Shams et al., 2021). This fouling process transforms pristine plastic particles into more aged forms. NOM is ubiquitous in natural and wastewaters, containing a complex mixture of hydrophobic and hydrophilic organic molecules from sources like decomposing plant matter (Liang et al., 2023). NOM loading changes microplastic surface charge, energy, and hydrophobicity (Ali et al., 2022; Chen et al., 2018).

#### 2.4 Effect of aging on adsorption of contaminants onto microplastics

The adsorption of organic contaminants to microplastics is affected by various aging processes that alter the physicochemical surface properties of the plastic particles over time. Aging mechanisms can either enhance or inhibit contaminant adsorption, depending on the specific changes induced. Several studies have shown increased adsorption of heavy metals (Q. Fu et al., 2021; Lang et al., 2020; Mao et al., 2020) and pharmaceuticals (Fan et al., 2021; Liu et al., 2020; Wang et al., 2022) to aged microplastics compared to pristine particles. Duan et al. (2023) compared the effect of sulfide and UV- induced aging of three MPs materials (polypropylene, polystyrene, and polyethylene terephthalate) on adsorption of pyrene and ciprofloxacin and showed that adsorption of the model contaminant is enhanced due to sulfidation. However, aging

processes such as UV irradiation of MPs have little or no effect on the adsorption tendencies for organic contaminants like polycyclic aromatic hydrocarbons (PAHs) (Ding et al., 2020a; Li et al., 2020). Aging processes that enhance oxygen-containing surface functional groups on the aged microplastics can reduce the accessibility of sorption sites for hydrophobic contaminants such as PAH. For instance, Hüffer et al. (2018a) observed that the sorption coefficients of organic compounds by UV-aged polystyrene microplastics were lower than for pristine particles because aging led to significant surface oxidation and the formation of oxygen-containing surface groups on the microplastics. These groups form hydrogen bonds with surrounding water molecules, making it less favorable for sorption to occur. Similar explanations were provided by Luo et al. (2023) and (Wang et al., 2022).

Thermal oxidation and photodegradation increase surface polarity, roughness, and porosity, which improves adsorption through hydrophobic effects and enlarged surface area (Wang et al., 2019). Natural organic matter (NOM) fouling also enhances adsorption by providing additional sorption sites on the NOM coating (Wang et al., 2016).

Few studies have investigated the effect of aging on adsorption of PFAS to MPs. (Ateia et al., 2020) showed that loading MPs with NOM can enhance the adsorption of PFAS to microplastics, but the effect may depend on the specific type of PFAS. This result is consistent with that reported by Scott et al. (2021) that showed that adsorption of PFAS was higher on field-incubated MPs compared to pristine MPs. To the best of our knowledge, these are the only available studies on

the effect of aging on adsorption of PFAS and as such, more studies are needed to understand the role of different aging processes on the interaction between PFAS and MPs. The complex effects of aging on microplastic-contaminant interactions demonstrate the need to consider realistic aging processes in a study aimed at investigating the interactions between PFAS and MPs. Advanced characterization of aged particle surface morphology and chemistry will provide better insights into adsorption mechanisms. Further studies should investigate a wider range of contaminants and plastic types. Overall, elucidating the relationships between microplastic aging and contaminant adsorption is critical for assessing their combined environmental transport and impacts.



## Chapter 3 Residential contributions to occurrence and concentrations of PFAS in Raw wastewater

### 3.1 Introduction

The extensive production and use of per- and polyfluoroalkyl substances (PFAS) in industrial and consumer applications has led to their widespread presence across environmental matrices, raising concerns related to their persistence and potential for adverse effects (Glüge et al., 2020; Lenka et al., 2022). PFAS compounds are widely used in industrial activities such as metal plating, packaging, textile production, and corrosion prevention, fluoropolymer, and plastics manufacturing (Ankley et al., 2021; Guelfo et al., 2021). Consumer products such as nonstick cookware, adhesives, household appliances also contain PFAS (Dery et al., 2019; Gaines, 2023). The number of PFAS compounds on the commercial market increased from 950 compounds in 2007 to over 4,700 by 2018 (OECD, 2018; Olsson, 2014). In addition to concerns on the persistence and effect of PFAS, the widespread use of PFAS increases their potential release into the environment, ultimately finding their way into water systems (Meegoda et al., 2020; Podder et al., 2021). PFAS are recalcitrant through conventional water treatment processes and are released into wastewater effluents (Timothy L Coggan et al., 2019; Tavasoli et al., 2021). Investigating the occurrence and concentration of PFAS in raw wastewater gives better understanding of the dynamics of contamination, potential implications for downstream water treatment processes and the types of PFAS that may interact or be found in biosolids.

Wastewater treatment plants (WWTPs) have been identified as a pathway facilitating PFAS release into the environment through effluent discharges and biosolids reuse (Becker et al., 2008; Timothy L. Coggan et al., 2019). PFAS compounds have been detected in biosolids and influent/effluent streams of WWTPs worldwide, with some research reporting higher effluent concentrations compared to influents due to biotransformation of precursors (Lenka et al., 2022). As such, determining the occurrence and concentration of PFAS in raw wastewater is important for source identification, regulatory compliance, understanding contaminant fate, and guiding research and policy initiatives. Also, wastewater may serve as a key indicator of PFAS contamination within communities. Elucidating PFAS levels and forms in raw wastewater provides insight into contributions from different sources within communities.

Establishing domestic contributions to PFAS loads in WWTP influents is crucial for understanding the role of everyday residential activities in PFAS discharges to sewers. (Bilela et al., 2023; Nguyen et al., 2022). Raw wastewater, collected from manholes that predominantly receive wastewater from residential areas, also provides beneficial information on the types of PFAS contributed by residential sources. To the best of our knowledge, this is the first research that investigates the occurrence and concentration of PFAS in a location at proximity to domestic sources with the aim of establishing domestic contributions of PFAS to WWTP. Most works (Figure 3.1) on spatial and temporal variation of PFAS in wastewater are focused on areas around the influent and effluents of treatment plants, which gives extra significance to this study. This knowledge would demonstrate that even if industrial inputs are reduced, ongoing household releases will sustain PFAS presence. This knowledge will also demonstrate that interactions of

PFAS with suspended solids such as microplastics from consumer product debris will continue regardless of industrial phase-outs.

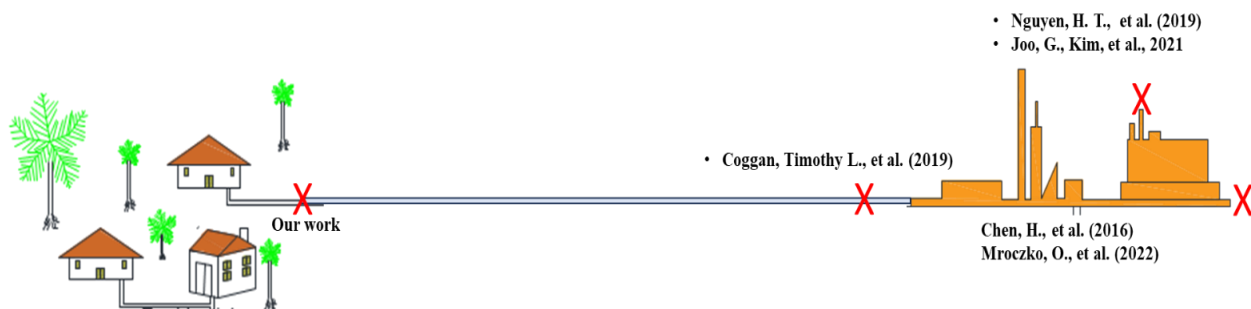


Figure 3.1 Available studies on occurrence and fate of PFAS in a sewershed target areas around the treatment plant.

## 3.2 Materials and Methods

### 3.2.1 Description of study area

Wastewater samples were collected from three different sewers (through a manholes) located in three different cities but in the same county. The locations of the manholes are classified as residential according to information from the respective cities. The exact locations of the sewers are not revealed in this document. The sites will be identified as Site A, B, and C for the purpose of this work. Site A is 8.2 miles from Site B and 10.1 miles from Site C, while Site B is 4 miles from Site C. The manholes in Site A, B, and C are 11.10, 11.58', and 7.12' deep, respectively. The manhole in Site A connects to an area with a domestic population of about 2,256 people, while the manhole in Site B connects to an area with a domestic population of about 2,300. The manhole in

Site C connects an area with an estimated population of 2,436 people. This information was collected from documents provided by the public municipalities.

### 3.2.2 Sample collection

Prior to each sample collection, all sampling materials were decontaminated by rinsing or wiping with LC-MS grade water, LC-MS grade methanol, and PFAS free water, in that order. Composite raw wastewater samples were collected daily from each manhole for 7 days, consecutively. The autosamplers were programmed to collect 66 grab samples of 150 mL each in 24 hours. The autosamplers were programmed to have higher sample collections during peak periods and lower sample collection at off – peak periods. The expected total sample volume at the end of 24 h was 9.24 L. Hach autosamplers (AS950, Loveland, CO) equipped with a 10 L low density polyethylene (LDPE) carboy and silicone tubing (Hach #4600, Loveland, CO) were used to collect samples daily. The autosamplers were also packed with ice to ensure the sample temperature was maintained at  $\leq 6^{\circ}\text{C}$  during sampling. The carboys were not reused to avoid carryover contamination. After sample collection, the autosamplers were opened and the carboy gently inverted 10 times to homogenize the samples collected and subsequently transferred into 500 mL high density polyethylene (HDPE) containers. The samples were stored at  $< - 20^{\circ}\text{C}$  until sample extraction.

### 3.2.3 Physical and chemical properties measurement

Physical and chemical properties of the collected wastewater were analyzed after sampling. Initial temperature immediately after recovering the autosampler from the manholes was taken using a

temperature gun (Lasergrip 774, Etekcity, China). Subsequently, pH and conductivity of the samples were measured immediately after sample collection using pH/conductivity meter (YSI – Pro 1030, Yellow Springs, OH).

For chemical oxygen demand (COD) analysis, the wastewater samples were mixed by shaking the sample tubes vigorously. Next, 2 mL aliquots of each sample were transferred into Hach COD test tubes, and the caps were closed. The test tubes were then inverted upside down approximately 20 times to mix the wastewater samples with the reagent in the Hach COD test tubes. The test tubes were placed in the COD digester (DRB 200, Loveland, CO) and heated at 150°C for 2 hours. After cooling down, the test tubes were inverted upside down approximately 20 times while holding the caps to mix the solution. The COD value was then read using a colorimeter (Hach DR 900, Loveland, CO). Total ammonia nitrogen (TAN) analysis was done by shaking each sample tube vigorously. Then, 0.1 mL aliquots of each sample were transferred into a Hach TAN test tube. The Ammonia Salicylate Reagent was added to each test tube, and the caps were closed. Each test tube was inverted upside down approximately 20 times to dissolve the reagent particles. The test tubes were then left for 20 minutes to let the reactions occur, after which the ammonia concentration in the samples was determined using a colorimeter (Hach DR 900, Loveland, CO).

### 3.2.4 PFAS extraction and instrumental analysis

The extraction and analysis of PFAS was done according to the EPA 1633 method. EPA Method 1633 is an analytical method for quantitative determination of 40 target per- and polyfluoroalkyl substances (Table S1) in environmental matrices. The method concentrates the samples by solid

phase extraction (SPE) coupled with liquid chromatography and tandem mass spectrometry (LC/MS/MS). Briefly, vacuum manifold was set up with SPE cartridges (Waters Oasis WAX 150 mg) and a reservoir for each cartridge. Cartridges were preconditioned with 15 mL of 1 % methanolic ammonium hydroxide followed by 5 mL of 0.3 M formic acid. The sample was spiked with isotopically labeled standards (Wellington, Ontario, Canada) and mixed by swirling the sample container. Subsequently, the liquid level in the 500 mL HDPE container was marked, followed by gently inverting the samples 4 times, before pouring each sample into the reservoir. The samples were allowed to pass through the cartridge at 5 mL/min. The empty HDPE containers were allowed to dry while the reservoirs were rinsed with 5 mL reagent water twice followed by 5 mL of 1:1 M formic acid/methanol. Subsequently, the cartridges were allowed to dry for 15 s after which the rinse solution was discarded. Elution of the cartridge was done into a clean 15 mL polypropylene centrifuge tubes using 5 mL of 1% methanolic ammonium hydroxide. Twenty-five microliter concentrated acetic acid was added to each sample and filtered with through 25-mm, 0.2- $\mu$ m syringe filter. Finally, Non-Extracted Internal Standard (NIS) was added to the samples before analysis in an Agilent 6470 LC/TQ (Santa Clara, CA) LC-MS/MS.

### 3.2.5 Quality assurance/Quality

Samples collected for quality assurance and quality control (QA/QC) are Instrument blanks, field blanks, and sample duplicates. QA/QC samples were collected for each sample location. Storage and treatment of QA/QC was done in the same manner as all wastewater samples. Instrument blanks were collected by passing PFAS free water through the autosampler after installation of the tubing while field blanks were collected by transferring 500 mL of PFAS free water into a HDPE

container. The field blank container was left open while samples were transferred from the carboy into sample collection containers.

Calibration curves were prepared in accordance with the guidelines provided in EPA 1633 draft method. A seven-point calibration standard containing target analytes, EIS, and NIS compounds at concentrations described in the EPA 1633 draft method was prepared. The calibration standards were only accepted when  $r^2$  was  $> 0.99$ . Calibration verification and analysis of ongoing precision and recovery (OPR) were done, and recovery of target analyte were within 70 – 130 % (Figure A1), which is acceptable according to the EPA 1633 guidelines.

### 3.3 Results and Discussions

#### 3.3.1 Physical and chemical properties of wastewater

The results of the physicochemical analysis of the collected wastewater samples are presented in Table S2. The pH of the samples ranged from 7.63 to 8.57. The organic matter content, expressed as chemical oxygen demand (COD), was between 173 – 680 mg/L. The total ammonia nitrogen concentrations spanned 48.9 – 54.6 mg/L. Overall, the measured pH, COD, and ammonia nitrogen levels were within typical ranges reported for raw wastewater in previous studies.

#### 3.3.2 PFAS occurrence and concentration in municipal raw wastewater

Nine different PFAS compounds were detected across all collected raw wastewater samples from the three sites. Of the 9 PFAS identified, 5 were carboxylates, 2 were sulfonates, and 2 were PFAS precursors. Figure 3.2a illustrates the frequency of detection (DF) for each PFAS.

Perfluorododecanoic acid (PFDOA) displayed the highest frequency, being present in all samples (DF = 100%). Perfluoropentanesulfonic acid (PFPeS) had the second highest detection frequency at 91%. In contrast, the legacy PFAS compounds perfluorooctanoic acid (PFOA) and perfluorooctanesulfonic acid (PFOS) exhibited lower occurrence, with DFs of 14.3% and 0% respectively. Two PFAS precursors were also found - 1H,1H,2H,2H-perfluorooctane sulfonate (6:2 FTS) (DF 52%) and perfluoro-1-octanesulfonamide (PFOSA) (DF 19%). Overall, the detection frequency trend was: PFDOA > PFPeS > PFPeA > 6:2 FTS > PFHxA = PFOSA > PFOA = PFTTrDA > PFNS.

The concentrations of each PFAS presented in a box plot (Figure 3.3b, Table S3) provide valuable insights into their distribution in the raw wastewater samples collected. The concentration of 6:2 FTS (mean = 59.84 ng/L, median = 44.06 ng/L) was the highest of all the PFAS detected. The carboxylates, PFOA (mean = 4.08 ng/L, median = 2.92 ng/L) and PFHxA (mean = 4.67 ng/L, median = 4.48 ng/L) had similar mean concentrations and were the lowest. The concentration range for PFHxA, PFOA, PFTTrDA, PFNS, and PFOSA were narrower than the rest of the PFAS detected, signifying more consistent concentrations within these compounds. In contrast, PFDoA, PFPeA, PFPeS, and 6:2 FTS exhibited a wider concentration range, suggesting a broader range of concentrations. The variation in the concentration ranges observed implies that while the first group of PFAS (PFHxA, PFOA, PFTTrDA, PFNS, and PFOSA) tend to exhibit more consistent concentration levels the subsequent group (PFDoA, PFPeA, PFPeS, and 6:2 FTS) displayed greater variability, potentially indicating variations in its sources or behavior within the sampled environment. Despite having similar, PFPeA (mean = 27.83 ng/L, median = 26.11 ng/L) had



relatively higher concentration than PFPeS (mean = 19.22 ng/L, median = 28.62 ng/L). The mean concentrations were lower than those reported in raw wastewater collected closer to the influents of the wastewater treatment plant. The difference in concentration observed in this study compared to the those taken closer to WWTP might indicate differences in spatial or temporal patterns.

While the exact causes of the observed trends are currently uncertain, usage patterns of PFAS-containing consumer products likely contribute. Further studies on major residential PFAS sources are needed to elucidate their distinct characteristics and distribution behaviors. These results provide initial insights into the occurrence of these emerging PFAS in municipal wastewater.

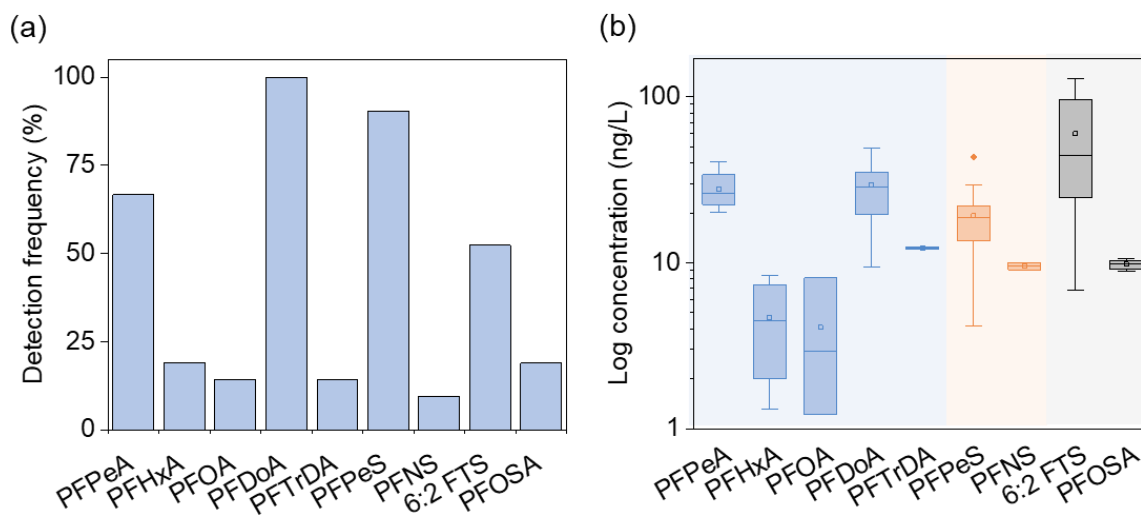


Figure 3.2(a) Detection frequency of PFAS in raw wastewater (b) Box plot showing the distribution of PFAS concentrations. The vertical lines drawn above and below the boxes (whiskers) show variability outside the upper and lower quartiles. The mean values are shown as

open markers (o) while the outliers are shown as full markers (•). The median values are shown by a horizontal line across the boxes.

Four PFAS were detected in tap water collected from the sampling locations (Figure 3.5a) out of which 2 are PFAS precursors. 6:2 FTS had the highest total concentration (38.60 ng/L) of the PFAS detected with a DF of 66.6% followed by PFOSA with a total concentration of 19.23 ng/L and the same DF (66.6 %) as 6:2 FTS. The other two PFAS detected are long chain carboxylates PFTTrDA (Total concentration = 13.29 ng/L, DF = 33.3 %) and long chain sulfonates, PFNS (Total concentration = 13.29 ng/L, DF = 33.3 %). The total PFAS concentration in the tap water samples is 80.53 ng/L. These PFAS are not among the most detected PFAS in drinking water. According to a study that assessed tap water from 716 locations across the United States, PFBS (16%), PFHxS (15%), and PFOA (14%) are the most frequently detected PFAS in tap water samples with cumulative PFAS concentration of 346 ng/L (Smalling et al., 2023). In a similar study, total PFAS concentration in tap water range from 4.59 – 365.04 ng/L. However, none of the PFAS detected in our study was reported.

Unsurprisingly, all 4 PFAS measured in tap water were also detected in the raw wastewater samples (Figure 3.6b). 6:2 FTS has the highest total concentration (658.25 ng/L) in the wastewater samples collected followed by PFDoA (618.44 ng/L). In deviation to what has been reported in some literature, PFOA (12.23 ng/L) had the lowest total concentrations of the 9 PFAS detected. Sulfonates with similar carbon chain length PFPeS and PFPeA had similar total concentrations,

365.22 and 389.64 respectively. Total concentrations of carboxylates (1075.79 ng/L) measured was almost thrice that of sulfonates (384.07 ng/L) and higher than the total concentrations of the precursors (697.37 ng/L). The fluorotelomer 6:2 FTS has been reported at similar concentrations and DF frequency. Nguyen et al. (2019) detected 6:2 FTS in 100 % samples collected at the influent of WWTP with average concentrations that range from 2.5 – 76 ng/L. Similarly Schultz et al. (2006) reported between 4.9 – 13 ng/L.

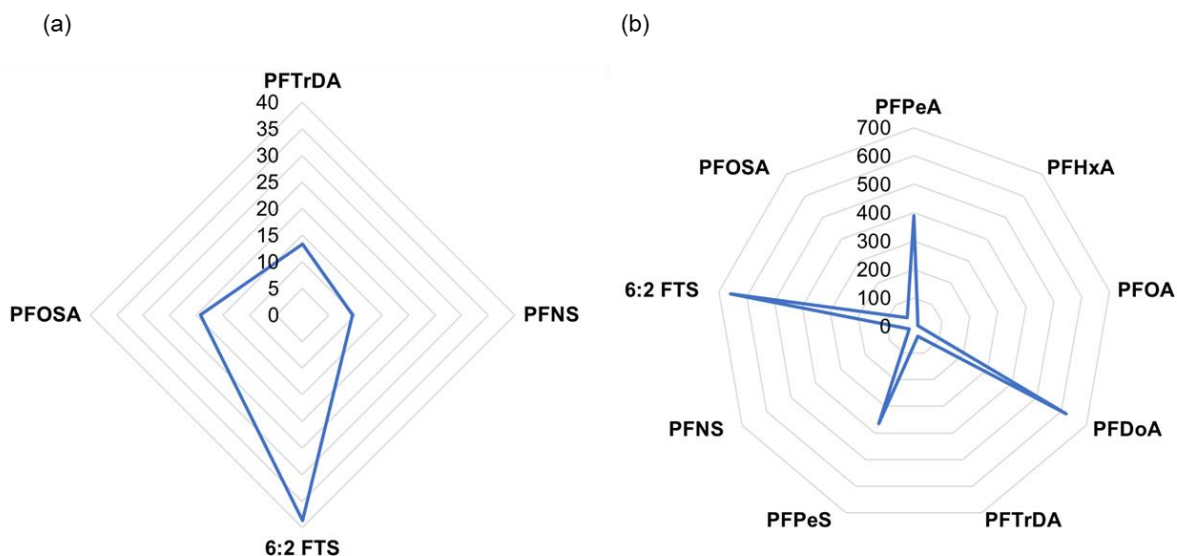


Figure 3.3 Total PFAS concentration in (a) Tap (b) wastewater samples

### 3.3.3 Correlations of PFAS with heavy metals

The heat map analysis of PFAS and heavy metal concentrations in raw wastewater samples reveals distinctive patterns (Figure 3.4). The data clustered into two main groups, segregating heavy

metals and PFAS compounds. Within the heavy metals group, including elements like cobalt, zinc, calcium, manganese, and chromium, a coherent clustering highlights their shared variability across the samples. While the absence of industrial contributions to the raw wastewater might have removed certain external influences, their common presence could arise from sources like household cleaning agents (Aonghusa & Gray, 2002). In contrast, the PFAS compounds - encompassing PFOA, PFOS, PFNA, and PFHpA - create an independent cluster. This isolation concurs with existing literature, underscoring how domestic inputs, including consumer disposals and food packaging, significantly shape the prevalence of PFAS compounds in municipal wastewater. Noteworthy is the cross-cluster correlation between PFOA and iron. This correlation prompts further inquiry into localized mechanisms that might associate the two even in the absence of industrial contributions.

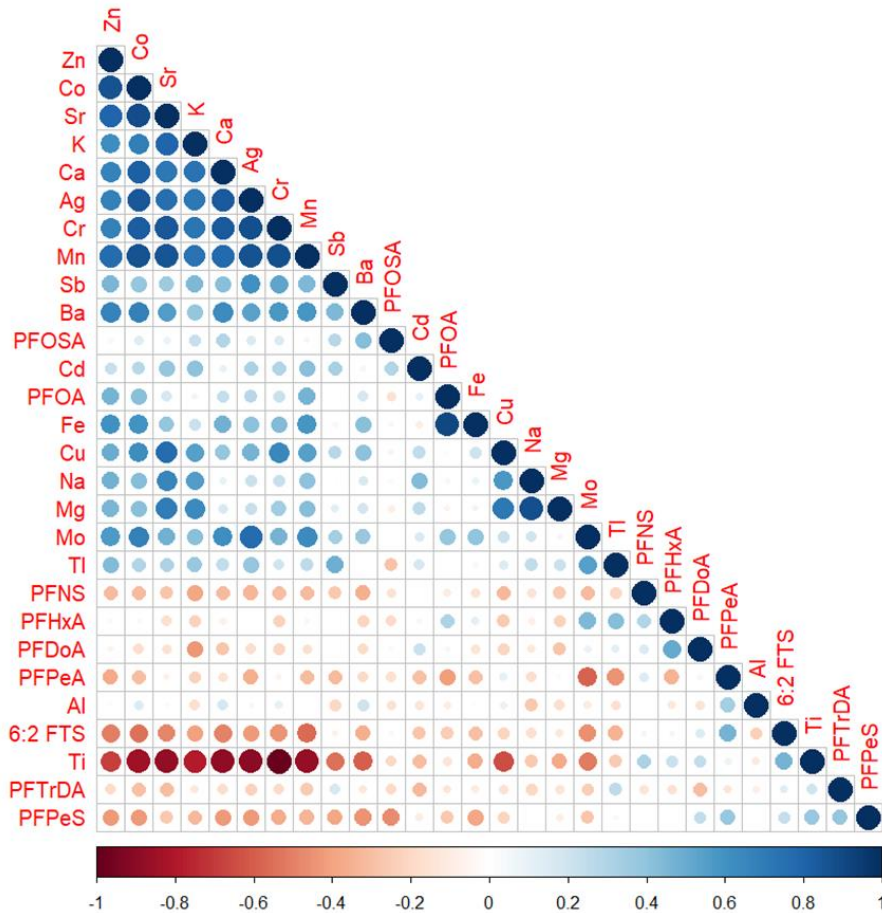


Figure 3.4 Correlations between PFAS and heavy metals in raw wastewater

### 3.4 Conclusions and Limitations

This study provides valuable insights into the occurrence and concentration of per- and polyfluoroalkyl substances (PFAS) in raw wastewater from residential areas. Nine PFAS compounds were detected, with perfluorododecanoic acid (PFDoA) and perfluoropentanesulfonic acid (PFPeS) exhibiting the highest frequencies. The fluorotelomer precursor 6:2 FTS occurred at the highest concentrations, contrasting with the lower levels of legacy PFAS like PFOA. PFAS profiles clustered distinctly from heavy metals, however PFOA was uniquely correlated with iron.

Overall, the results reveal the complexity of PFAS inputs even in predominantly residential wastewater. Long-chain PFAS are still regularly occurring, likely from ongoing releases from consumer goods, while shorter short-chain replacements are being detected. The study provides an initial exploration of PFAS near domestic sources, complementing research at wastewater treatment plant influents. These findings can inform source control and treatment strategies by elucidating residential PFAS uses, forms, behaviors, and concentrations. Additional work should aim to trace detected PFAS to specific household sources. Overall, this study significantly enhances understanding of these ubiquitous contaminants in municipal wastewaters. The outcomes can support efforts to control PFAS releases into sewers and reduce environmental discharges.

# Chapter 4 Adsorption of PFAS onto secondary microplastics: A mechanistic study

## 4.1 Introduction

Due to their lightweight, durability, and cost-effectiveness, plastics are widely used in a variety of domestic and industrial applications, which has led to skyrocketing production.(Geyer et al., 2017a; F. Wang et al., 2020) About 391 million tons of plastics was produced in 2021, and production is estimated to double in the upcoming 20 years.(Elias, 2018; Europe, 2022; Geyer et al., 2017a) High global plastic production and use have led to increasing amount of plastic waste in the environment,(Cheng et al., 2021; da Costa et al., 2016; Elhacham et al., 2020; Jambeck et al., 2015) with about 80% of the plastic waste generated accumulating in landfills or in natural waters.(Barnes et al., 2009; Geyer et al., 2017a; Shim et al., 2018) Plastics (and/or their debris) may occur as macroplastics (size > 25 mm), mesoplastics (5–25 mm), microplastics (0.1  $\mu\text{m}$ –5 mm), and nanoplastics (1–100 nm).(Alimi et al., 2018; da Costa et al., 2016; Ter Halle et al., 2017) Microplastics (MPs) have been identified as a major, global challenge in aquatic and terrestrial environments.(Barnes et al., 2009; Shim et al., 2018) MPs can be intentionally engineered to have small size (primary MPs) or may form from the fragmentation of larger plastics (secondary MPs).(Allouzi et al., 2021; Ateia et al., 2020; Cole et al., 2011; Song et al., 2017) The ecological risks of MPs may arise from their physical properties (e.g., sharp edges), chemical properties (e.g., leaching of additives),(da Costa et al., 2016; Petroody et al., 2020; Rochman et al., 2015; Ziajahromi et al., 2017) and/or their ability to concentrate and transport other contaminants.(Koelmans et al., 2016; F. Wang et al., 2020).

MPs have a tendency to adsorb a wide variety of legacy and emerging contaminants, including per- and polyfluoroalkyl substances (PFAS). (F. Wang et al., 2020; Yu et al., 2019) PFAS are currently one of the most important emerging contaminants due to their ubiquity, persistence, toxicity, and bioaccumulation in organisms. (Brusseau et al., 2020; Buck et al., 2011; Han et al., 2023) Both PFAS and MPs were recently detected in the guts of organisms in the Mississippi coast, (Navarathna et al., 2023) which suggests that MPs may transport PFAS into organisms. Cheng and coworkers detected up to 9  $\mu\text{g/g}$  total PFAS on MPs isolated from an urban river. (Cheng et al., 2021) The authors reported that perfluorooctane sulfonic acid (PFOS) and perfluorooctanoic acid (PFOA) were the most abundant PFAS adsorbed to the MPs. (Cheng et al., 2021) Although secondary MPs are more abundant in aquatic systems than primary MPs, (Shim et al., 2018) most existing studies of partitioning of PFAS onto MPs were performed using primary MPs. The physicochemical properties of secondary MPs, such as their shape, surface roughness, composition and functionality, and affinity, may differ from those of primary MPs. (Ateia et al., 2020; Bhagat et al., 2022; da Costa et al., 2016; Waldman & Rillig, 2020; Yu et al., 2019) The physical properties (shape and size distribution) of primary MPs is shown in Figure 4.1.1 (a) and (b) and we hypothesize that this properties will influence the rate constant (Figure 4.1.2c) and adsorption capacities (Figure 4.1.3d) of commercial MPs.



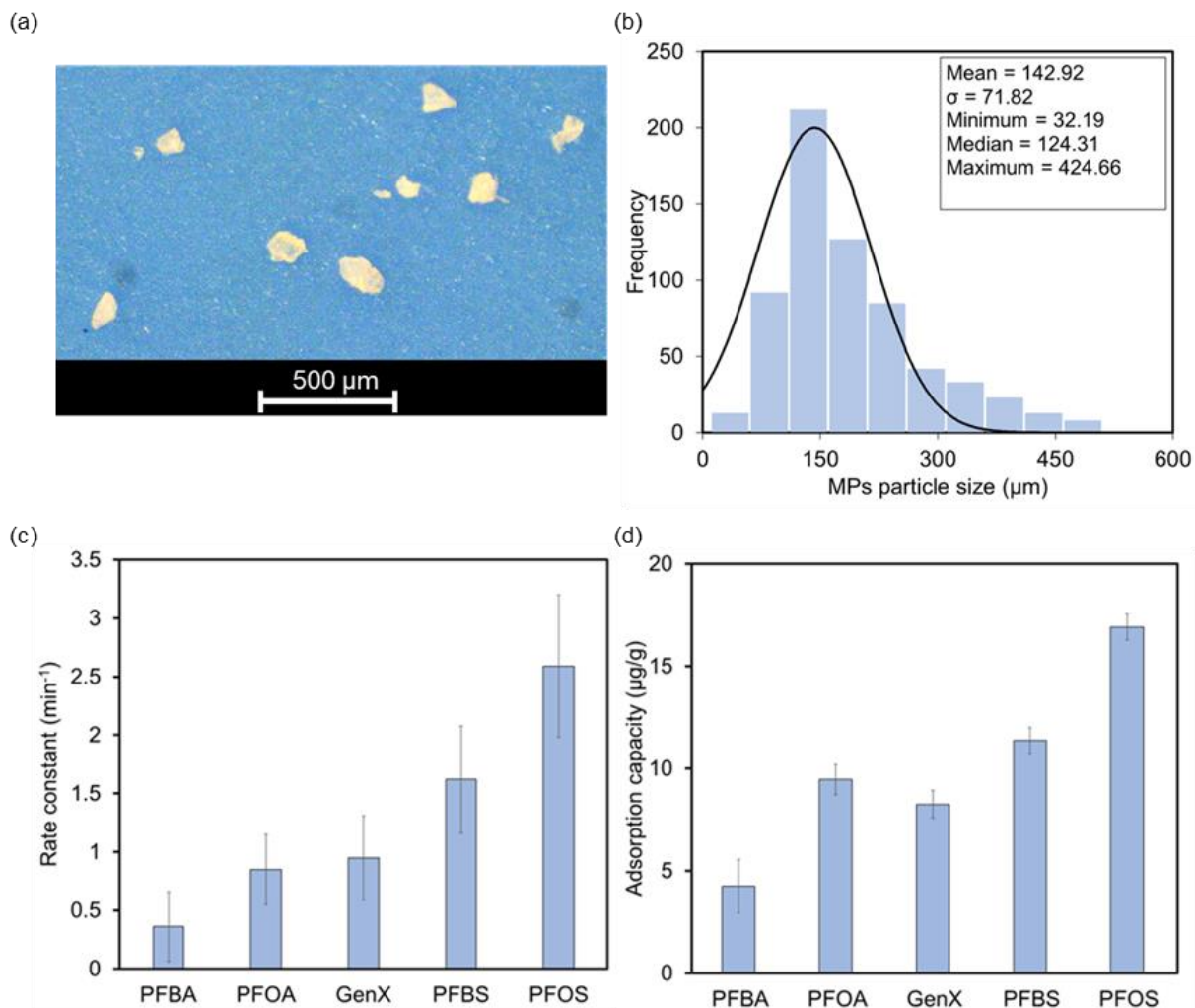


Figure 4.1(a) surface morphology of commercial PET MPs (b) particle size distribution of commercial PET microplastics. (c) adsorption kinetics rate constant and (b) capacity of commercial PET MPs for PFAS in single-analyte systems. Initial concentration = 200 μg/L for each PFAS; MPs dose = 2 g/L; pH = 7; shaker speed = 150 rpm.

Ateia et al. found that more PFAS (per unit surface area) partitioned to the surface of secondary MPs (which were prepared via mechanical milling of commercial and recycled plastics) than their

primary counterparts.(Ateia et al., 2020) The higher PFAS uptake by the secondary MPs was attributed to surface roughness and/or the presence of additives in the commercial parent plastics.(Ateia et al., 2020) Till date, there is no mechanistic investigation of the effect of PFAS chemistry and water chemistry on how they partition onto secondary MPs. While hydrophobic interaction is important in the partitioning of PFAS onto surfaces,(Ateia et al., 2020; F. Wang et al., 2015; Zenobio et al., 2022a) other interaction forces that may be sensitive to aqueous chemistry, such as electrostatic interactions (due to their head groups), may play important roles in PFAS partitioning onto MPs.(Llorca et al., 2018; F. Wang et al., 2015).

The main objectives of this study were to investigate the role of water chemistry (pH, ionic strength, natural organic matter [NOM], and temperature) and PFAS chemistry (chain length and functionality) on PFAS partitioning from water to the surface of secondary MPs. Polyethylene terephthalate (PET) was selected for this study because it is the second most produced thermoplastic, with a market of 53 million tonnes in 2010.(Kershaw, 2016) The most produced thermoplastic, polyethylene (market was 73 million tonnes in 2010), has been more widely studied compared to PET. This study is based on a central hypothesis that the extent to which water chemistry influences PFAS partitioning is a function of PFAS chain length.

## 4.2 Materials and Methods

### 4.2.1 Production of secondary MPs from PET bottles

We produced the secondary PET MPs used in this study by modifying a method described by Ji and co-workers.(Ji et al., 2020) Briefly, we rinsed PET water bottles with deionized (DI) water

(18.2 M $\Omega$  cm, Milli-Q Ultrapure Water Systems), dried and cut to card size using a pair of scissors. We then shredded the card-sized plastics to 0.5  $\times$  4.0 cm with a paper shredder. Finally, we further cut the plastics to smaller pieces ( $\sim$  0.5  $\times$  1.0 cm), and mechanically degraded them with a hand blender (Yissvic LB2108, Ningbo, China) for a total blending time of 240 min in a glass beaker that contains water with 0.05 % Bovine Serum Albumin (BSA,  $\geq$ 99.0%, Fisher BioReagents, Fair Lawn, NJ). We used the BSA to prevent MPs agglomerations during blending,(Guo et al., 2022; Ji et al., 2020) and blenders were used for 30 s at a time and allowed to cool down for 5 min thereafter. After blending, we sieved the MPs suspensions with stacked sieves (Hogentogler, Gerwig Lane, DC) to isolate MPs within 53 – 250  $\mu$ m, which falls within the range reported in different aquatic media.(Kameda et al., 2021; Uurasjärvi et al., 2020; Xu et al., 2019) To remove BSA from the surface of the MPs, we dialyzed the sieved MPs against DI water for 5 d using Spectra/Por 3 RC dialysis membrane (3,500 Da). Following dialysis, we dried the MPs in an oven at 50°C for 12 h and stored them until use.

#### 4.2.2 Characterization of secondary PET MPs

We determined the morphology of the secondary MPs using a FEI Magellan 400 scanning electron microscope (SEM; FEI, USA). Their size distribution was obtained using light microscopy coupled with ImageJ analysis. We characterized the functional groups on the surface of the MPs (and compared with that of the original PET bottle) via Fourier transformed infrared spectroscopy (FTIR) using a Jasco FT/IR-4700 spectrometer (Japan). Following established methods, (Adeleye et al., 2019; Salawu et al., 2022)we determined the surface charge of the MPs by measuring their zeta ( $\zeta$ ) potential using a NanoBrook 90Plus (Brookhaven Instruments, Holtsville, NY). We also characterized the Brunauer-Emmett-Teller (BET) surface area of the MPs through nitrogen

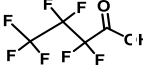

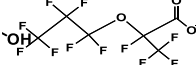


sorption using a Micromeritics 3Flex Surface Characterization Analyzer (Norcross, GA).

### 4.2.3 PFAS adsorption studies

We studied the adsorption of PFAS onto the secondary PET MPs by batch experiments. We considered five PFAS for this study, including perfluorobutanoic acid (PFBA), hexafluoropropylene oxide dimer acid (GenX), perfluorobutane sulfonic acid (PFBS), perfluorooctanoic acid (PFOA), and perfluorooctane sulfonic acid (PFOS). More details of the PFAS and their physicochemical properties are provided in Table 1 and Section S1. For the batch studies, we added 20 mg of PET MPs to 10 mL of each aqueous PFAS solution (200  $\mu\text{g/L}$ ) in 15 mL polystyrene tubes. We selected polystyrene tubes based on our previous study that shows low adsorption of the selected PFAS to the container.(Zenobio et al., 2022a) We performed all the experiments in triplicates with triplicate controls (that is, no MPs, to quantify partitioning to the container). We quantified the equilibrium PFAS concentrations via liquid chromatography with tandem mass spectrometry (LC-MS/MS) using an Agilent 6470 LC/TQ (Santa Clara, CA). We provided detailed information on equilibrium PFAS concentration determination and LC-MS/MS analysis in Section S2. We performed adsorption kinetics studies to determine the equilibrium adsorption time and maximum adsorption capacity of the MPs for (1) each PFAS (200  $\mu\text{g/L}$ ) and a mixture of the five PFAS (each PFAS in the mixture = 200  $\mu\text{g/L}$ ). To understand the effect of water chemistry on the adsorption of PFAS to the MPs, we varied pH (3 – 11), ionic strength (0 – 100 mM), and NOM concentration (0 – 100 mg/L). We also conducted adsorption studies at different temperatures (25-50°C) to obtain adsorption thermodynamics parameters. See the details of these studies in Sections S3-S5 and Table S1. We determined MPs adsorption capacity ( $q_e$ ) for each PFAS, and fit classical models to the kinetics and isotherm data, as detailed in Sections S4

and S5.

Table 4-1. Physicochemical properties of studied PFAS

	PFBA	PFOA	GenX	PFBS	PFOS
Molecular structure					
Molecular formula	C <sub>4</sub> HF <sub>7</sub> O <sub>2</sub>	C <sub>8</sub> HF <sub>15</sub> O <sub>2</sub>	C <sub>6</sub> H <sub>4</sub> F <sub>11</sub> NO <sub>3</sub>	C <sub>4</sub> HF <sub>9</sub> O <sub>3</sub> S	C <sub>8</sub> HF <sub>17</sub> O <sub>3</sub> S
CAS No.	375-22-4	335-67-1	13252-13-6	375-73-5	1763-23-1
Molecular weight (g/mol)	214.0	414.1	330.1	300.1	500.1
Boiling point (°C)	121	189-192	108	447	Nd
Melting point (°C)	-17.5	45-50	-21.0	188	>400
Log S <sub>w</sub> (mol/L)	0.42	-2.73	4.00	-1.00	-3.92
Log K <sub>oc</sub> (mL/g)	1.88	1.89-3.50	1.92	1.22-1.79	2.6-3.80
Log K <sub>ow</sub>	2.82- 2.91	5.30-6.26	4.0	3.90	4.67-7.66
pK <sub>a</sub>	0.05	-0.21	-0.77, 3.82	0.14	-3.27-0.14
Log D (pH 7)	-1.22	1.58	0.47	0.25	3.05
Log P <sub>L</sub> (Pa, 25 °C)	3.59	1.73	2.59	2.88	0.83
H (Pa·m <sup>3</sup> /mol, 20°C)	1.24	0.362	(2.05-7.47 × 10 <sup>-4</sup> )	nd	(4.34 × 10 <sup>-7</sup> )
CMC (mol/L)	0.8	0.01	0.175	0.00137	0.0002
Polarizability (Å <sup>3</sup> )	9.05	16.72	13.71	13.29	20.94
Molar refractivity (cm <sup>3</sup> /mol)	22.99	41.66	35.14	32.31	50.98
Hydrogen bond acceptor count	2	2	3	3	3
Hydrogen bond donor count	1	1	1	1	1

#### 4.2.4 Statistical analyses

We performed statistical analysis using RStudio (RStudio 2022.07.1+544). We checked the dataset for normality using the Shapiro-Wilk test and homogeneity of variance using Levene's test. We accepted data when normality and homogeneity of variance when  $p > 0.05$ . We evaluated statistical significance for normally distributed data using two-way analysis of variance (ANOVA) and post-

hoc Tukey's HSD test. Datasets that did not satisfy homoscedasticity were analyzed using Kruskal-Wallis non-parametric statistical analysis.

## 4.3 Results and Discussions

### 4.3.1 Characterization of secondary PET MPs

Unlike the PET bottles that are transparent, the produced PET MPs were pale white in color (Figure 4.2a). The overall particle size distribution was 39 – 493  $\mu\text{m}$ , with about 63% within 50 – 190  $\mu\text{m}$  (Figure 4.3b). The size distribution is close to what we intended to produce (53 – 250  $\mu\text{m}$ ), which suggests that the method we adopted can be used to produce secondary PET MPs of desired sizes. We also observed that the MPs had irregular shapes, sizes, and surface roughness (Figure 4.4c), similar to secondary MPs isolated in the natural environment (Malygina et al., 2021). The BET surface area of the MPs was  $3.82 \text{ m}^2/\text{g} \pm 0.05 \text{ m}^2/\text{g}$ . The BET surface area obtained was larger than the surface area reported for secondary PET MPs ( $1.42 \text{ m}^2/\text{g} \pm 0.03 \text{ m}^2/\text{g}$ ) with size range within 180 – 220  $\mu\text{m}$ , produced using a crusher (Duan et al., 2023), primary PET MPs (Zhao et al., 2021) (surface area =  $0.88 \pm 0.03 \text{ m}^2/\text{g}$ , size range = 11 – 28  $\mu\text{m}$ ), and aged PET MPs (Hanun et al., 2023) ( $1.22 - 1.56 \text{ m}^2/\text{g}$ , size = 125  $\mu\text{m}$ ). The difference in surface area may be due to the method of production, size, and shape of the MPs produced.

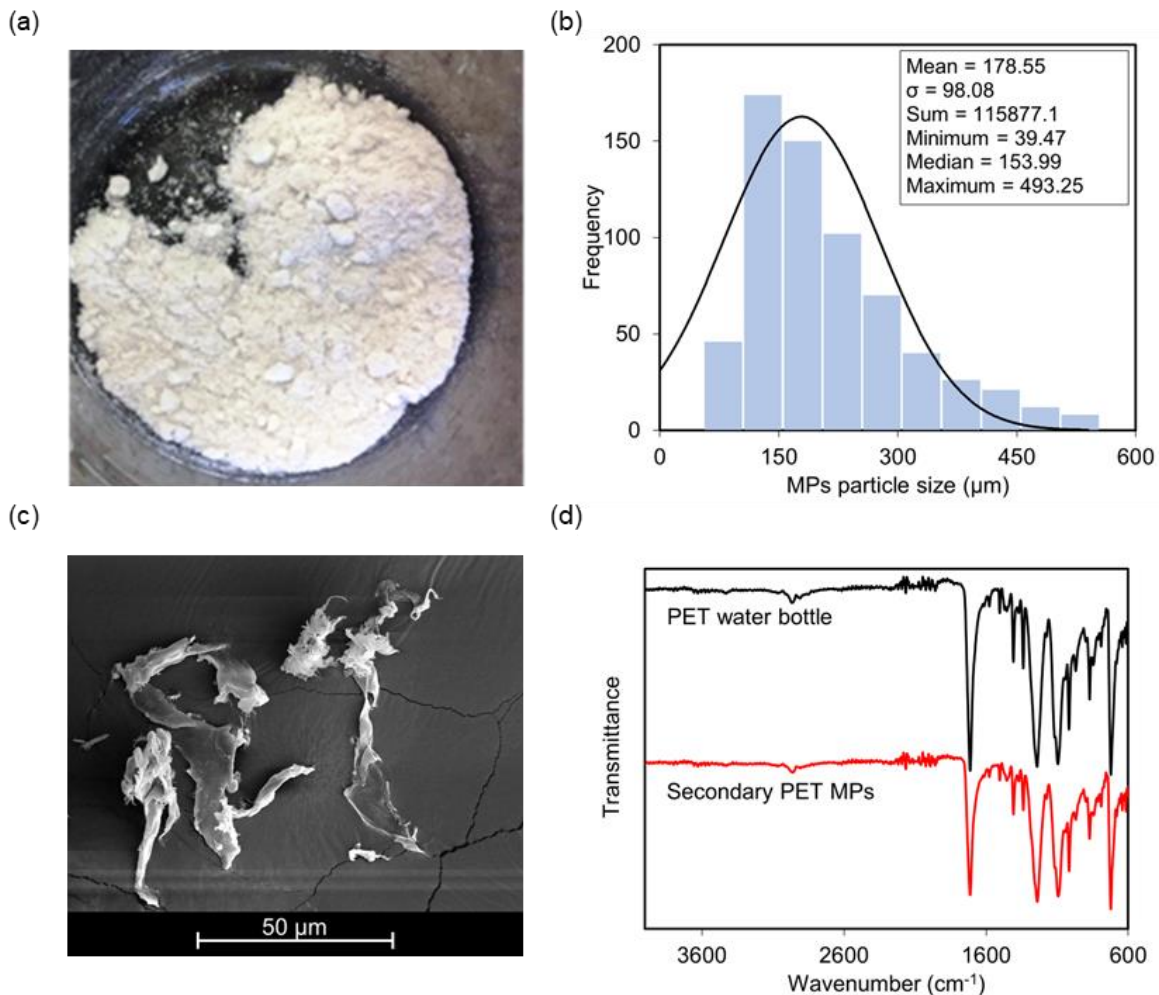


Figure 4.2 (a) The appearance (b) particle size distribution (c) SEM micrograph of secondary PET MPs used in this study. (d) A comparison of the FTIR spectra of the secondary PET MPs and the parent PET water bottle.

The FTIR spectra of the secondary MPs and that of the PET water bottle were similar (Figure 4.2d), which shows that the mechanical degradation approach used in this study did not alter the surface chemistry of the polymer. Both spectra match that of standard PET (Jiang et al., 2019). The ester group (-COO-), formed from the condensation of terephthalic acid and ethylene glycol, is the



main functional group present in PET. The peaks at 1089 and 1712  $\text{cm}^{-1}$  were assigned to stretching vibration of C-O and -C=O bond, respectively, in the -COO- group. We assigned the peak at 1021  $\text{cm}^{-1}$  to the stretching vibrations of the ester (-C-O-C-) group. We also observed symmetry C-H bending of aromatic rings at 2971  $\text{cm}^{-1}$ . Although PET may contain some residual hydroxyl (OH) group from ethylene glycol, most often, the OH group is converted to -COO- group. Therefore, it is not surprising that OH functional group was not observed in the spectrum obtained.

#### 4.3.2 Kinetics of PFAS adsorption onto secondary PET MPs

In single-analyte solutions, the five PFAS adsorbed rapidly within the first 30 min and reached equilibrium after 420 min (Figure B1), which implies that the partitioning of PFAS to the surface of PET MPs in waters likely occurs within hours or a few days. The kinetics of PFAS adsorption to the PET MPs was best described by the pseudo first order (PFO) model, although the pseudo second order (PSO) model was very suitable too (Table S2). The only exception we observed was for GenX, for which the intraparticle diffusion (IPD) and PSO models had the best correlation coefficients (both  $R^2 > 0.83$ ). It is somewhat surprising that the IPD model better describes the adsorption of GenX given that its large molecular size might limit its diffusion. Moreover, PET MPs are not very porous (Pore volume = 0.000947  $\text{cm}^3/\text{g}$ ). The good fit of the PFO and PSO models for describing the adsorption kinetics of the PFAS is not surprising, given their hydrophobic backbone (and hence, tendencies for physical interactions) and functional head groups (and hence, possibility of participating in chemical interactions such as hydrogen bonding).

Based on the PFO adsorption rate constant ( $k_1$ ) we obtained (Figure 4a, Table S2) perfluoroalkyl carboxylic acids (PFCAs) adsorbed faster to the secondary PET MPs ( $k_1 = 0.052 \pm 0.027$  /min for

PFOA and  $0.038 \pm 0.022$  /min for PFBA) compared to perfluoroalkyl sulfonic acids (PFSAs) with similar chain lengths ( $k_f = 0.036 \pm 0.016$  /min for PFOS and  $0.022 \pm 0.005$  /min for PFBS). The overall trend of  $k_f$  was PFOA > PFBA > PFOS > GenX > PFBS. Although more studies are needed to determine the exact reason for the faster adsorption of the PFCAs, we hypothesize that it may have to do with their lower molecular weight (compared to the corresponding PFCAs), which allows for faster diffusion from the bulk to the surface of the MPs.

According to the findings of Deng et al.,(Deng et al., 2012) when aminated rice husk was utilized for the removal of various PFAS, it was observed that PFOA and PFBA had a faster adsorption rate compared to PFOS, while more PFOS was adsorbed at equilibrium.(Deng et al., 2012) The authors attributed the slow adsorption of PFOS to its higher hydrophobicity and the formation of micelles and hemi-micelles on the surface of the adsorbent due to its lower critical micelle concentration.(Deng et al., 2012) Similarly, in 2015, Dong et al.(Dong et al., 2021) reported a comparable trend, where PFOA had a faster adsorption rate compared to PFOS when ionic liquid-modified natural clay was used as an adsorbent.(Dong et al., 2021) The authors attributed this observation to the relatively smaller size of PFOA, which resulted in less steric hindrance during the adsorption process compared to PFOS.(Dong et al., 2021)

Contrary to the trend in  $k_f$ , we observed that the adsorption capacity of the PET MPs ( $q_e$ ) was greater for PFSAs ( $q_e = 36.71$   $\mu\text{g/g}$  for PFOS and  $35.46$   $\mu\text{g/g}$  for PFBS) compared to their corresponding PFCAs ( $q_e = 18.98$   $\mu\text{g/g}$  for PFOA and  $5.17$   $\mu\text{g/g}$  for PFBA) (XXb). We hypothesize that the higher affinity of the sulfonates may be due to their higher hydrophobicity (see LogD

values in Table 1) and possession of a higher number of electronegative oxygen atoms compared to their corresponding carboxylates. This hypothesis of higher electronegativity was tested using density-functional theory (DFT) analysis (which will be discussed later). The possession of a higher number of electronegative oxygen atoms on sulfonates compared to carboxylates can create a stronger electrostatic interaction between the sulfonate functional group and the surface of the PET MPs. The higher hydrophobicity of the PFASs compared to their same chain-length PFCA counterparts likely arises from the extra  $\text{CF}_2$  group in the sulfonic acid.(Siriwardena et al., 2019) The overall trend of  $q_e$  was  $\text{PFOS} > \text{PFBS} > \text{GenX} > \text{PFOA} > \text{PFBA}$ , which is similar to our recent observation of PFAS partitioning to plastic containers.(Zenobio et al., 2022a)

Within the same functional group, the  $q_e$  of the secondary PET MPs for long-chain PFAS (PFOS and PFOA) was higher than that of their short-chain homologues (PFBS and PFBA). We attributed this to the stronger hydrophobic interactions between the MPs and long-chain PFAS due to their possession of higher numbers of hydrophobic  $\text{CF}_2$  moiety. Also, long chains allow PFAS to adsorb while experiencing much less electrostatic repulsion between the negatively charged MP and their anionic headgroups compared to short chains. Although micelle formation can enhance partitioning of PFAS from water to solid surfaces, and long-chain PFAS have lower critical micelle concentrations (CMCs),(Du et al., 2014; Yu et al., 2009) we do not believe that hemi-micelles and micelles formation played an important role in this study because the tested concentration (200  $\mu\text{g/L}$ ) is 4-5 orders of magnitude below PFAS CMC values.(Johnson et al., 2007; Yu et al., 2009)

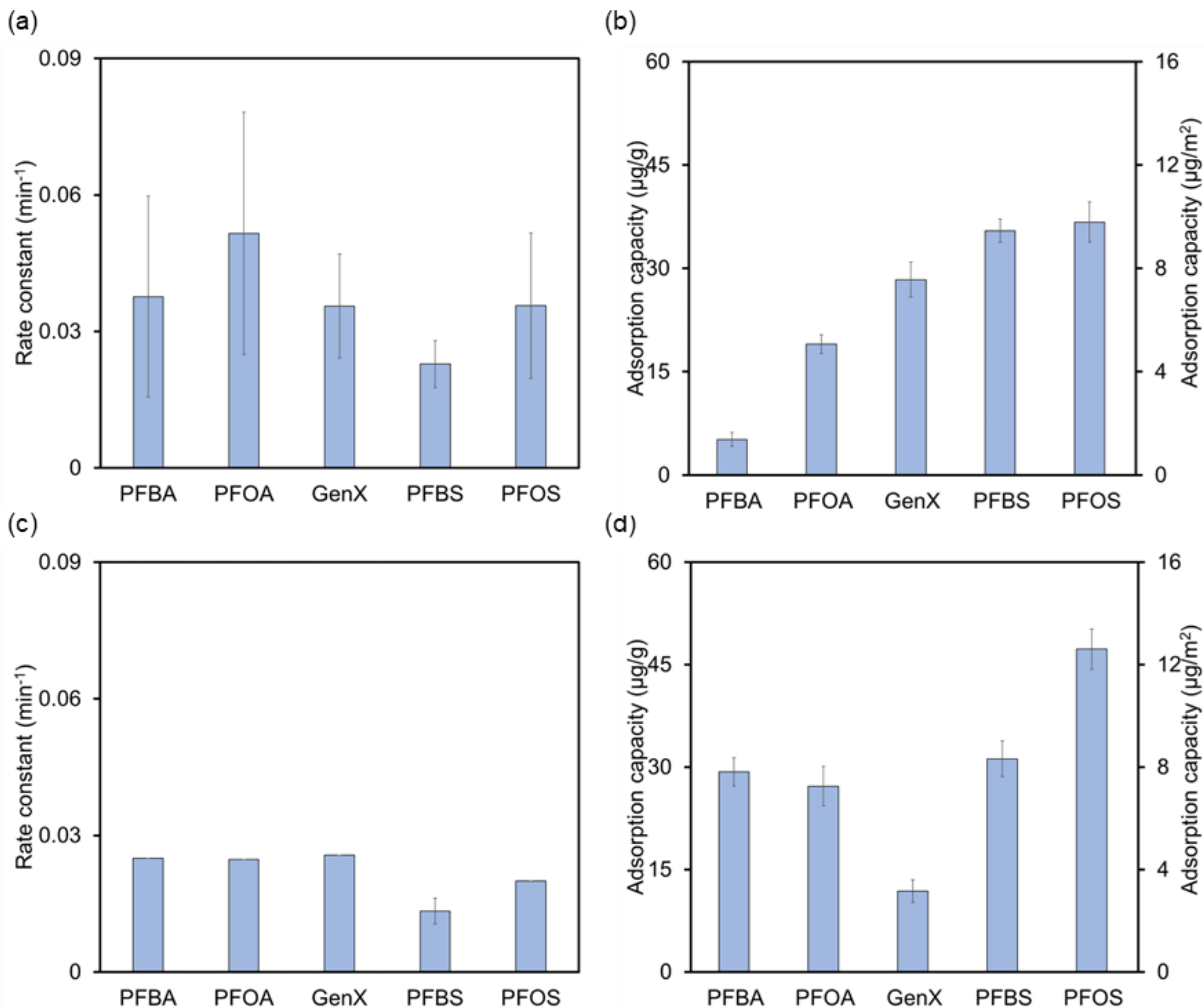


Figure 4.3 (a) adsorption kinetics rate constant and (b) capacity of secondary PET MPs for PFAS in single-analyte systems; (c) adsorption kinetics rate constant and (d) capacity of secondary PET MPs for PFAS in mixed-PFAS systems; Initial concentration = 200  $\mu\text{g/L}$  for each PFAS ; MPs dose = 2 g/L; pH = 7; shaker speed = 150 rpm.

When adsorption kinetics was studied using a mixture of the five PFAS (at 200  $\mu\text{g/L}$  each), equilibrium was reached after 540 min (Figure B2), which is longer than in the single-PFAS systems. Similar to the result we obtained in the single-analyte kinetic experiments, PFO and PSO

models adequately described the adsorption kinetics of most of the PFAS to the secondary PET MPs. However, both the  $q_e$  and  $k_1$  change for most PFAS compared to the single-analyte system (Figures 4b). This suggests that competition occurred among the PFAS, which needs to be thoroughly investigated in future studies.

We further compared the adsorption of PFAS to secondary MPs to that of commercial MPs with size range  $< 300 \mu\text{m}$  in single-analyte solutions. Similar to the adsorption of PFAS to the secondary MPs, the five PFAS adsorbed rapidly within the first 30 min. However, equilibrium was reached faster (after 300 mins) using commercial PET MPs (Figure B3) than secondary PET MPs in the adsorption of the respective PFAS. We observed good fits of the PFO and PSO models for describing the adsorption kinetics. Similar to adsorption of GenX on secondary PET MPs, adsorption of GenX was best described by the IPD. All the other PFAS were described suitably described by the PFO and PSO kinetics model. A comparison of the adsorption rate constant based on the PFO shows that all the PFAS adsorb faster to the commercial PET MPs compared to the secondary PET MPs (Figure 4c, Table S2). The trend was PFOS  $>$  PFBS  $>$  GenX  $>$  PFOA  $>$  PFBA. At equilibrium, we observed greater adsorption capacities of the secondary PET MPs (Figure 2b) for all the PFAS compared to the commercial PET MPs (Figure 4d). Although, while sulfonates adsorb more than carboxylates (as observed in the adsorption on secondary PET MPs), the overall trend was PFOS  $>$  PFBS  $>$  PFOA  $>$  GenX  $>$  PFBA as compared to PFOS  $>$  PFBS  $>$  GenX  $>$  PFOA  $>$  PFBA in secondary PET MPs. We attributed the difference in the adsorption rates to difference in particle size distribution. Commercial PET MPs are typically produced to a specific size range and may have less variation in the size distribution. We compared the size distribution

of both MPs (Figure 4b for secondary PET MPs and Figure B4a for commercial PET MPs) and observed less size variation in commercial PET MPs (32 – 424  $\mu\text{m}$ ) than secondary PET MPs (39 – 494  $\mu\text{m}$ ). The surface morphology of the MPs also differs (Figure B4a and b). The particles of commercial PET MPs are more regular compared to those of the secondary PET MPs which shows the presence of flakes and hence more irregular. The sharp edges in the secondary PET MPs may also be potential active sites for the adsorption of PFAS.

#### 4.3.3 Effect of water chemistry on adsorption of PFAS onto secondary PET MPs

We initially performed adsorption isotherm experiments in DI water using the equilibrium time determined for each PFAS in the adsorption kinetics study (Figure B5). Overall, the Freundlich model fits better to our experimental data ( $R^2 = 0.87\text{-}0.98$ ), except for GenX, which was better described by the Langmuir isotherm. The better fit of the Freundlich isotherm was expected based on the heterogeneity of the secondary MPs surface (Figure 4c). The maximum adsorption capacities of the secondary PET MPs for the PFAS ( $q_{\text{max}}$ ) that we determined from the isotherm studies (Table S3) agreed with the  $q_e$  values that we independently obtained in the kinetics study (Table S2), which reflects the occupation of the entire surface of the MPs by PFAS. To understand how important environmental factors would affect the adsorption of PFAS to secondary MPs in aquatic systems, we performed additional studies, considering the roles of pH, ionic strength, NOM, and temperature.

##### 4.3.3.1 Role of pH

Like other particles suspended in water, pH may influence the surface charge of MPs, (H. Wang et al., 2015) which may impact their adsorption of dissolved contaminants. We observed that the  $q_e$

of the secondary PET MPs for the five PFAS decreased significantly ( $p < 0.05$ ) as pH increased from 3 to 11 (Figure 4a, Table S4). Linear regression analyses revealed a statistically significant ( $p < 0.05$ ) inverse correlation between pH and the  $q_e$  of the PET MPs for the five PFAS ( $-0.57 \geq \text{slope} \geq -1.18$ ;  $R^2 > 0.87$ ), as shown in Figure B6. We hypothesized that the strong trend between pH and  $q_e$  was likely due to the impact of pH on the surface charge of the PET MPs, and thus, electrostatic interactions with the PFAS.

To test this hypothesis, we estimated the surface charge of the MPs by measuring their  $\zeta$  potential at pH 3 – 11. As expected, the surface negativity of the MPs increased as pH increased, with  $\zeta$  potential decreasing in magnitude from -12.2 mV at pH 3 to -22.8 mV at pH 11 (Figure 4b). The change in  $\zeta$  potential is primarily due to the deprotonation of PET MP's functional groups, such as carboxylic acids, and esters (Figure 4d), as pH increased. The PFAS considered in this study have  $pK_a < 1$  (Table 1), therefore are anionic at pH 3 – 11. Thus, the magnitude of electrostatic repulsion between the PET MPs and the anionic PFAS increases as water pH increases, limiting the partitioning of PFAS to the surface of the MPs.

Our observation agrees with the trend that has been reported for the adsorption of PFAS to solids such as MPs (Meng et al., 2023; F. Wang et al., 2015), soil/sediment,(Nguyen et al., 2020; You et al., 2010) carbon nanotubes,(Deng et al., 2012) etc. at different pH values by other researchers. In most studies, the trends were attributed to changes on the surface of the adsorbents brought about by pH change and not changes in the charges of PFAS since the  $pK_a$  values of common PFAS are below what is typically studied. In addition, hydrogen bonding have been reported to contribute to

the adsorption of PFAS to different adsorbents, including microplastics.(Enyoh et al., 2022; Gagliano et al., 2020; Joo et al., 2021b) The PET MPs we used in this study possess oxygen-rich functional groups, such as carbonyl and ester, that can form hydrogen bonds with PFAS.

#### 4.3.3.2 Role of ionic strength

Overall, we observed (1) that the  $q_e$  of the secondary PET MPs for the five PFAS increased as the ionic strength of the matrix increased; and (2) the increase in  $q_e$  as ionic strength increased from 0 to 100 mM was statistically significant ( $p < 0.05$ ) for only the short-chain PFAS (Figure 4c, Table S5). For instance, the  $q_e$  for PFBA increased significantly ( $p = 0.01$ ) from  $7.6 \pm 0.9 \mu\text{g/g}$  to  $23.7 \pm 7.6 \mu\text{g/g}$  as ionic strength increased from 0 to 100 mM, while the  $q_e$  for PFOS also increased from  $38.6 \pm 4.8 \mu\text{g/g}$  to  $58.2 \pm 8.9 \mu\text{g/g}$  across the same ionic strength range but not significantly ( $p = 0.11$ ). Overall,  $q_e$  is not significantly linearly correlated to ionic strength (Figure B7). Increased adsorption of PFAS to the secondary PET MPs as ionic strength increases may arise from impact of the ions on the surface charge of the adsorbents, and on the solubility of the adsorbates.



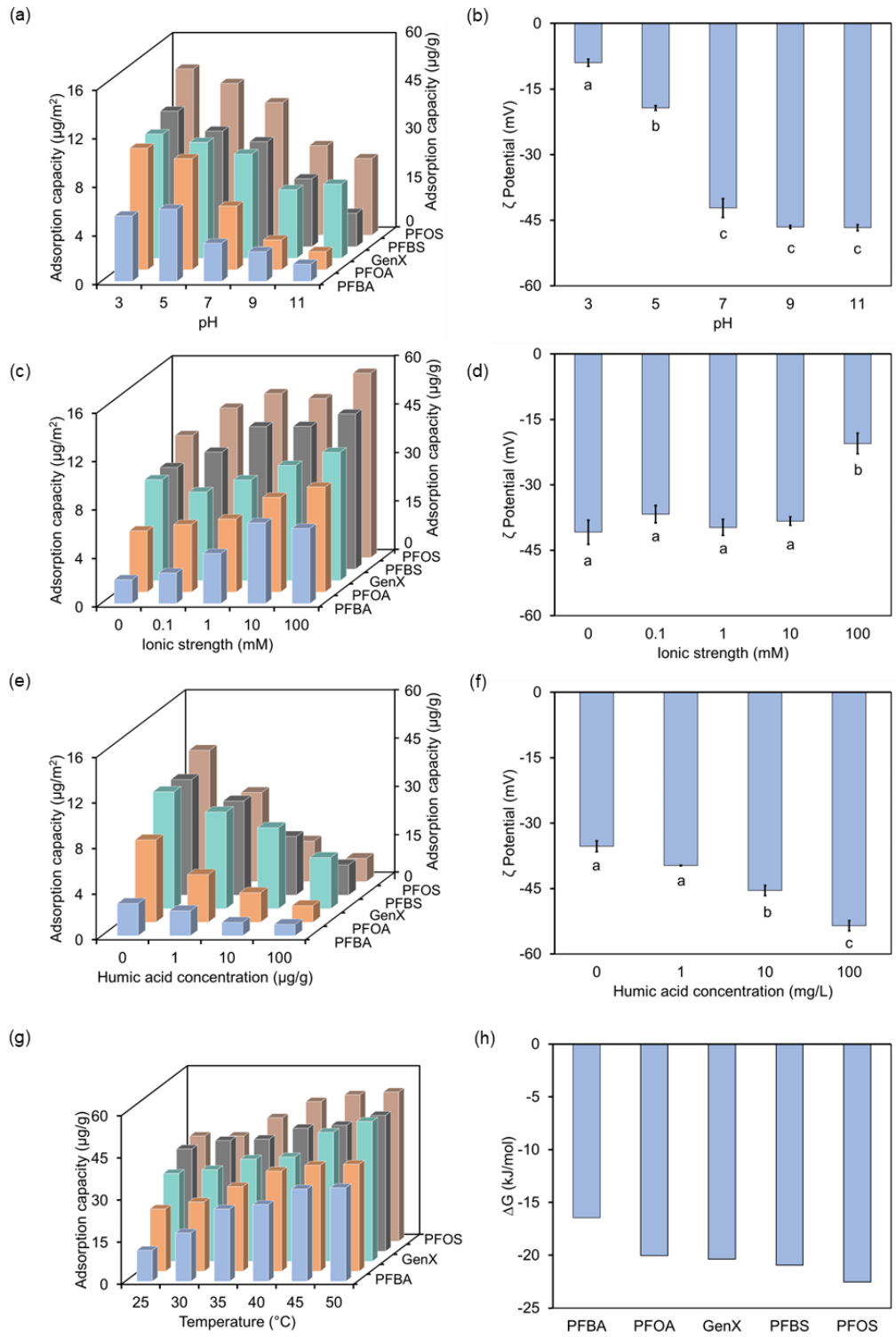


Figure 4.4 Effect of pH on (a) the adsorption capacity and (b)  $\zeta$  potential of PET MPs; ionic strength on (c) the adsorption capacity and (d)  $\zeta$  potential of PET MPs; humic acid concentration on (e) the adsorption capacity and (f)  $\zeta$  potential of PET MPs; temperature on (g) the adsorption capacity of PET MPs. Gibb's free energy ( $\Delta G$ ) of adsorption at 25°C is shown in (h). Initial PFAS concentration = 200  $\mu\text{g/L}$ ; MPs dose = 2 g/L; shaker speed = 150 rpm.

We observed increased positivity of the surface charge of the secondary PET MPs with increase in ionic strength as indicated by  $\zeta$  potential. The  $\zeta$  potential of the secondary MPs became less negative (increased from  $-36.7 \pm 1.97$  mV at 0.1 mM to  $-20.5 \pm 2.38$  mV) as ionic strength increased from 1 to 100 mM NaCl (Figure 4d). The charge screening that we observed with increased ionic strength is due to electrical double layer (EDL) compression by sodium ions, as predicted by the classical colloidal theory.(Elimelech et al., 1998; H. Wang et al., 2015) The increased positivity of the MPs' surface likely decreased the electrostatic repulsion between MPs and the anionic headgroups of the PFAS, therefore allowing for more adsorption. Increased ionic strength likely favored more adsorption of the short chain PFAS than the long chain PFAS because the short chain PFAS experience electrostatic repulsion much more than their long chain homologs due to the shorter distance between their hydrophobic tails and anionic headgroups.

Although increased ionic strength could enhance the adsorption of PFAS (especially the long chain homologs which are more hydrophobic) through salting-out effect (decreased solubility) and micelle/hemi-micelle formation,(L. Fu et al., 2021; Llorca et al., 2018) the concentrations of PFAS used in this study is several orders of magnitude below their solubility and CMC in water (Table

1). Our finding of increased adsorption of PFAS to PET MPs is in agreement with the observation of increased adsorption of PFOS to polyethylene, polystyrene, and polyvinyl chloride, reported by Wang and coworkers.(F. Wang et al., 2015) Based on our results, we expect weak adsorption of short chain PFAS (compared to their long chain homologs) to PET MPs in freshwaters, which typically have low salinity. Meanwhile, adsorption of short chain PFAS will be enhanced in estuaries and marine systems, which have much higher salt content that can compress the surface charge of MPs.

#### 4.3.3.3 Role of NOM

Using humic acid (0 – 100 mg/L) as a surrogate for NOM, which is abundant in aquatic environments,(Adeleye et al., 2019; Keller et al., 2010) we found that the adsorption of all five PFAS decreased significantly ( $p < 0.05$ ) as humic acid concentration increased (Figure 4e, Table S6), although there was no statistically significant linear correlation between  $q_e$  and humic acid concentration (Figure B8). Within the same functional groups, humic acid had a higher impact on the long chain PFAS compared to the short chain homologs. For instance, while the  $q_e$  for PFBA and PFBS decreased by 64.9% and 73.8%, respectively, when humic acid increased from 0 to 100 mg/L, the decrease in  $q_e$  MPs for PFOA and PFOS was 79.9% and 82.3%, respectively. The results suggest that humic acid competes with PFAS for adsorption on the surface of the MPs, which typically decreases  $q_e$ . Although the humic acid used here is orders of magnitude higher in concentration than the PFAS, it represents what is expected in natural and engineered aquatic systems.(Keller et al., 2010)

Humic acid can also change the surface properties of colloids; (H. Wang et al., 2015) hence, we

measured the  $\zeta$  potential of MPs in the presence of humic acid. Humic acid increased the negativity of the surface charge of PET MPs, decreasing  $\zeta$  potential from -35.3 mV to -53.5 mV as its concentration increased from 0 to 100 mg/L (Figure 4f). Therefore, in addition to steric exclusion of PFAS from the surface of the surface of the MPs, humic acid increased the electrostatic repulsion between the PET MPs and PFAS. While Mejías *et al.* similarly found a negative effect of NOM on the adsorption of PFAS to polyamide MPs,(Mejías *et al.*, 2023) Ateia and coworkers generally found that NOM promoted the adsorption of long chain PFAS onto MPs and had no negative effect on GenX.(Ateia *et al.*, 2020) The major difference between our experimental setup and that of Ateia *et al.* is that they mixed their MPs in NOM-containing water for 14 d (which loads the NOM on the MPs) before studying adsorption of PFAS. Thus, it is likely that the interactions among MPs, NOM, and PFAS changes over time, with competition (between NOM and PFAS) being the dominant process when MPs initially enters a water body, while cosorption become more dominant over time as NOM on the surface of MPs reaches equilibrium.

#### 4.3.3.4 Role of temperature

As we increased the temperature of the reactor from 25 to 50°C, the  $q_e$  of the MPs for the PFAS increased significantly ( $p > 0.05$ ), except for PFOS for which the increase was not statistically significant ( $p > 0.05$ ) (Figure 4g; Table S7). Linear regression analyses revealed a statistically significant ( $p < 0.05$ ) direct correlation between temperature and the  $q_e$  of the PET MPs for the five PFAS ( $0.91 \geq \text{slope} \geq 0.45$ ;  $R^2 > 0.92$ ), as shown in Figure B9. Increased  $q_e$  at elevated temperatures suggests a more favorable interaction between PFAS and the secondary PET MPs. This may have originated from increased collision between the adsorbate and adsorbent due to elevated kinetics energy as temperature increased, more collision occurring in the right orientation

in space due to increased PFAS mobility and increase in the fraction of collisions with enough energy for adsorption. Although we are unable to verify it in this work, Khumalo et al. hypothesized that plastic pore-filling could be an important mechanism of PFAS partitioning, especially at high temperatures due to polymer (pore) expansion.(Khumalo et al., 2022)

Based on the Gibb's free energy ( $\Delta G$ ) we obtained (Figure 4h), which ranged from -16.4 kJ/mol (for PFBA) to -22.5 kJ/mol (for PFOS), we concluded that the adsorption of the five PFAS to the secondary PET MPs is thermodynamically spontaneous at 25°C and would occur in surface waters. The  $\Delta G$  of the adsorption of PFAS to the secondary PET MPs became more negative as temperature increased (Table S8), which is reasonable given that it is an endothermic process ( $\Delta H = 14.0$  to  $41.0$  kJ/mol). Given the increase in adsorption spontaneity at higher temperatures, and the relatively low enthalpy values, we also concluded that the adsorption of the PFAS to the MPs is mainly via physical interactions.(Salawu et al., 2022) The spontaneity of PFAS adsorption to the MPs was mainly caused by increased randomness as indicated by positive entropy ( $\Delta S$ ). (T. Wang et al., 2020) Other researchers also reported spontaneous adsorption of PFOS to humic acid,(Jia et al., 2010) polyaniline nanotubes,(Xu et al., 2015) and carbon nitrides, (Yan et al., 2014) but this study is the first work to determine the spontaneity of PFAS adsorption to MPs.

#### 4.3.4 Mechanism of adsorption

To gain a better understanding of the mechanism of interactions between the secondary PET MPs and PFAS, we collected the FTIR spectra of the MPs before and after PFAS adsorption to assess any functional group changes after adsorption. The obtained spectra (Figure 4a) were transformed (second-derivative) and compared using principal component analysis (PCA), to separate

overlapping bands and magnify any minor spectral variations. (Zenobio et al., 2022a) PCA revealed clear separations between the spectra collected before and after PFAS adsorption except for PFBA. The separations we observed after PFAS adsorption indicates changes in infrared spectra of the MPs after adsorption, and it is reasonable that the changes in the MPs spectrum after PFBA adsorption was not substantial given that the  $q_e$  for PFBA ( $5.17 \pm 0.99 \mu\text{g/g}$ ) is a factor 4 (or more) lower than the other PFAS ( $18.98 \pm 1.37 - 36.71 \pm 2.94 \mu\text{g/g}$ ).

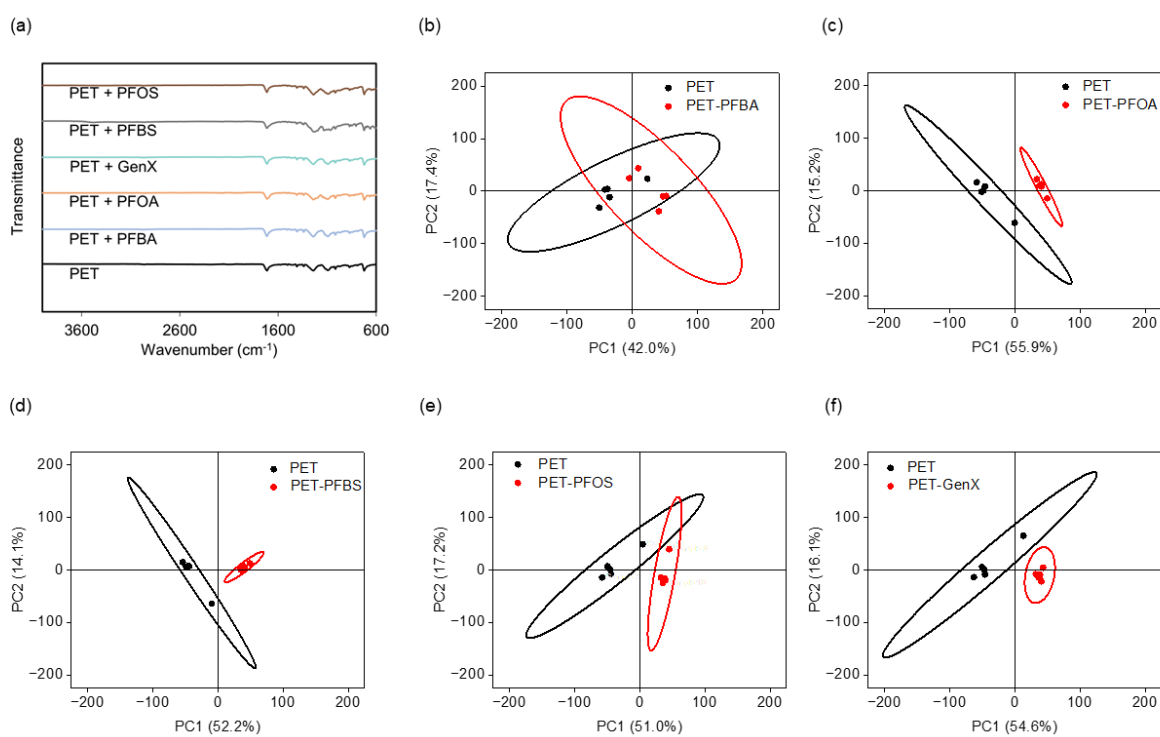


Figure 4.5 (a) FTIR spectra the secondary PET MPs before and after PFAS adsorption. PCA score plot of transformed FTIR spectra of PET before and after adsorption of (b) PFBA, (c) PFOA, (d) PFBS, (e) PFOS, and (f) GenX. The ellipses in the PCA score plots represent the 95% confidence range:  $n = 5$ .

We determined the bands (wavenumbers) with the highest square loadings, which represent the features that are altered and mainly responsible for the observed separations along the PCs. (Abdi & Williams, 2010) This check reveals a consistent decrease in the intensity of peaks assigned to the stretching vibration of C-O (at  $1089\text{ cm}^{-1}$ ) and -C=O (at  $1712\text{ cm}^{-1}$ ) bond in the ester group (-COO-) of the PET MPs after PFAS adsorption. We attributed the decrease in the intensities of these peaks to hydrophobic interactions between the MPs and PFAS, in which PFAS displaced the water molecules adsorbed to the surface of the PET MPs. The displacement of adsorbed water and thus, breaking of some hydrogen bonds water molecules formed with PET's -COO- group changed the chemical environment around these groups and decreased their intensity after PFAS adsorption. We calculated the change in the intensity of PET's -COO- group after the adsorption of each PFAS (Table S9) and found a strong correlation ( $R^2 = 0.96$ ;  $p = 0.003$ ) between it and  $\Delta S$  (Figure B10). This suggests that the increase in randomness after adsorption may be due to displacement of water by the PFAS.

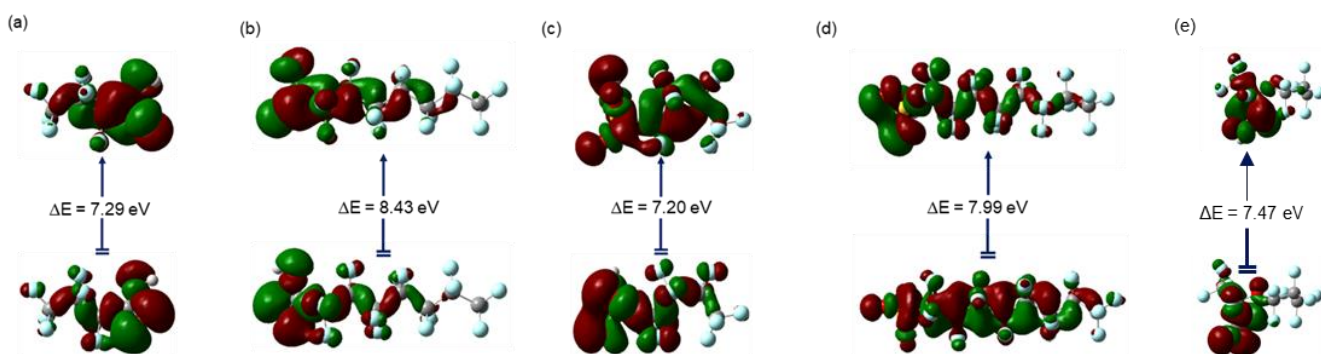


Figure 4.6 HOMO-LUMO diagrams of (a) PFBA, (b) PFOA, (c) PFBS, and (d) PFOS

We further investigated the adsorption mechanism of PFAS to the secondary PET MPs using DFT.

Molecular descriptors obtained from DFT improve understanding of the nature of chemical reactions at molecular levels. Details of the computational method adopted is provided in Section S6. Frontier orbital analysis of the optimized PET and PFAS structures shows interaction sites where the highest occupied molecular orbitals (HOMO) and lowest unoccupied molecular orbitals (LUMO) are localized on each molecule (Figure 4.6). According to frontier molecular orbital theory, the effectiveness of the interaction between two reacting molecules is linked to their frontier orbital distributions and the energy gaps maintained within. The HOMO-LUMO orbitals of the PFASs are spread out from the sulfonic head to the C-F tail while that of the PFCAs are localized on the carboxylic head and nearby fluorine atoms.

Considering the spread in the HOMO-LUMO of any molecule influences its dipole moment, and hence, likely interactions with solid surface, we explored the role of PFAS polarity on their adsorption to the secondary PET MPs. The solid water partitioning coefficients ( $K_d$ ) of the PET MPs that we obtained for the PFAS in our experiments has a strong correlation ( $R^2 = 0.89$ ;  $p = 0.015$ ) with the theoretical dipole moment obtained from DFT calculations (Table B10; Figure B11). This further confirms that electrostatic interactions are very important in the adsorption of PFAS to the PET MPs. The active sites of the PFCAs, that is PFBA and PFOA, are centered on the oxygen atoms located on the carboxylic head, with both oxygen atoms having the highest  $f_k^+$  and  $f_k^-$  values (Tables S11-12). Similarly, the three oxygen atoms double-bonded to the central sulfur atom in the sulfonic head group of the PFASs have the highest  $f_k^+$  and  $f_k^-$  values. These centers represent sites that are most prone to nucleophilic and electrophilic interactions, and likely interacted with PET. Based on the higher number of oxygen atoms in the sulfonic head of the



PFASs, we believe they have a higher tendency for electrostatic interaction with the PET MPs than their PFCA homologs.

#### 4.3.5 Conclusions and Limitations

The thermodynamics studies we performed in this study revealed that the adsorption of PFAS to secondary PET MPs (that we produced from PET water bottle) is spontaneous at 25°C. We also found that the partitioning of PFAS reaches equilibrium with 7 – 16 h, depending on whether the PFAS are present in single solutions or in a mixture. Based on the outcomes of the thermodynamics and kinetics studies, PFAS will adsorb PET microplastics in natural and engineered aquatic systems. PFCAs are likely to adsorb faster than their homologous PFSA, but more PFASs would adsorb at equilibrium due to their stronger hydrophobic and electrostatic interactions. Increase in water pH decreases adsorption of PFAS due to increased electrostatic repulsion while higher salinity favors PFAS adsorption due to charge screening. In addition, humic acid competes with PFAS for adsorption. These factors will drive more adsorption of PFAS in seawater, which typically have a high ionic strength and lower NOM concentration, relative to freshwater.

The partitioning of PFAS onto MPs in aquatic systems implies that organisms may be exposed to higher doses of PFAS than is present in water if they ingest PFAS-adsorbed MPs. Risk assessment of PFAS in aquatic systems should therefore consider their partitioning to MPs and other suspended solids in water. The importance of partitioning increases as the salinity of water increases and NOM concentration decreases. We however note that agglomeration of MPs will be important in saline waters (due to EDL compression, similar to nanomaterials);(Adeleye et al., 2019; Adeleye & Keller, 2014) but future studies should consider whether adsorbed PFAS can

enhance colloidal stability of MPs in water, e.g., via electrosteric repulsion.

## Supporting Information

Additional experimental details, materials and methods, and results, including figures and tables.

## Acknowledgements

The authors are grateful for support from Brown and Caldwell through the UCI Water-Energy Nexus Center. We also appreciate Lauren Nicole O'Brien, Natasha Thandi, Sarah Kadiri, Hugo Yao, Zachary William Wharton, and Ivan Doan for their help with blending the microplastics. The FTIR analysis was performed at UCI Laser Spectroscopy Labs while SEM was done at the UC Irvine Materials Research Institute (IMRI). IMRI is supported in part by the National Science Foundation through the UC Irvine Materials Research Science and Engineering Center (DMR-2011967).

## Chapter 5 Adsorption of PFAS onto aged secondary microplastics

### 5.1 Introduction

Microplastics (MPs) age and are transformed through various processes in natural and engineered aquatic environments including wastewater treatment systems. The surface morphology and textural properties of MPs change under the influence of light, temperature, microbes, chemical reactions, abundant or depleted oxygen content, and various aquatic conditions (Ding et al., 2020b; Hüffer et al., 2018b). For instance, MPs aging initiated by biofilm formation, sulfidation, adsorption of natural organic matter onto MPs (Lapointe et al., 2020), temperature fluctuation, and exposure to ultraviolet (UV) can result to changes in properties such as surface morphology, mechanical strength, hydrophobicity/hydrophilicity, surface charge, size (due to fragmentation into smaller particles), oxygen content, molecular weight, etc. (X. Liu et al., 2021). Also, polymer chains scission and oxidation during aging can result in the release of oligomers and oxygen-containing intermediates (X. Liu, Q. Deng, Y. Zheng, D. Wang, & B.-J. J. W. R. Ni, 2022). These physical and chemical changes in MPs as they age may influence their interactions, behavior, and fate. As such, understanding the effect of aging on MPs interactions with contaminants is vital to accurately assess their environmental fate.

MPs found in wastewater treatment plants (WWTPs) are mostly aged, with roughened surfaces and various oxygen-containing functional groups (i.e., carbonyl and hydroxyl)(Wu et al., 2022b). Aging could occur either within the treatment plant or during sewer transport. Although most aging

studies have focused on processes within WWTPs such as UV, H<sub>2</sub>O<sub>2</sub> exposure, and mechanical wear, MPs also experience complex transformations during sewer transport. Compared to pristine MPs, MPs aged in sewer pipe simulated conditions have altered physicochemical properties which could influence their fate and removal in subsequent treatment steps (Parashar & Hait, 2023). The anaerobic, oxygen-depleted sewer environment facilitates reactions with reductive compounds like hydrogen sulfide generated by microbial activities. Additionally, raw wastewater contains abundant natural organic matter (NOM) from sources like decomposing plant matter and food waste. NOM comprises hydrophobic and hydrophilic organic molecules, which can adsorb onto microplastic surfaces in sewers and primary treatment. This fouling coats microplastics with organic layers, increasing hydrophobicity. Elucidating the complex ageing processes of microplastics by exposure to Na<sub>2</sub>S and NOM interactions during sewer transport is crucial for understanding MPs interaction and fate in wastewater systems.

This study aimed to investigate the effect of aging on the adsorption behavior of microplastics in different aqueous environments. Two ageing conditions, exposure to Na<sub>2</sub>S and loading of microplastics with natural organic matter, were selected to simulate distinct environmental scenarios. In this study Na<sub>2</sub>S treatment represents a condition where MPs are exposed to sulfide-rich environments by the reaction of Na<sub>2</sub>S·9H<sub>2</sub>O with tromethamine, which can induce chemical modifications on their surfaces. Loading microplastics with natural organic matter replicates the process by which microplastics become coated or aggregated with organic substances present in the environment. To evaluate the adsorption behavior, experiments were conducted using deionized water and synthetic wastewater as aqueous matrices. Deionized water represented a

simplified and controlled environment, while synthetic wastewater aimed to simulate a more complex and realistic scenario where microplastics interact with various constituents typically found in wastewater.

## 5.2 Materials and Methods

### 5.2.1 Production of secondary MPs from PET bottles

We produced the secondary PET MPs used in this study according to the method described in the previous chapter.(Salawu & Adeleye, 2023) We rinsed 3.46 L PET water bottles with deionized (DI) water (18.2 MΩ cm, Milli-Q Ultrapure Water Systems) ten times, dried and cut the bottles into card-size pieces. Subsequently, we shredded the card-sized plastics to 0.5 × 4.0 cm strips using a paper shredder (Aurora, China). To further reduce the PET size, we cut the plastics into smaller pieces (~ 0.5 × 1.0 cm) and then poured 50 mg of the small plastic pieces in a glass beaker containing 300 mL water with 0.05% Bovine Serum Albumin (BSA, ≥99.0%, Fisher BioReagents, Fair Lawn, NJ). We added BSA to prevent the agglomeration of microplastics (MPs) while blending, following established methods. (Guo et al., 2022; Ji et al., 2020) We blended the small plastic pieces using hand blenders (Yissvic LB2108, Ningbo, China) for 30 seconds at a time, allowing them to cool down for 5 minutes between each blending cycle. In total, the blending process lasted 240 minutes. After blending, we isolated the MPs suspended in the solution by sieving using stacked sieves (Hogentogler, Gerwig Lane, DC). We specifically targeted MPs within the size range of 500 – 2000 μm, as against 53 – 250 μm used in the previous chapter. To remove the BSA from the surface of the MPs, we dialyzed the sieved MPs against DI water for 5

days, using a Spectra/Por 3 RC dialysis membrane with a molecular weight cutoff of 3,500 Da. Following the dialysis process, we dried the MPs in an oven at 50°C for 12 hours and stored them for future use.

### 5.2.2 Aging of secondary PET MPs by Na<sub>2</sub>S treatment and loading with natural organic matter

To perform Na<sub>2</sub>S treatment of the MPs, sodium sulfide (Na<sub>2</sub>S) was prepared by adding Tromethamine (Tris) buffer to sodium sulfide nonahydrate (Na<sub>2</sub>S.9H<sub>2</sub>O). Briefly, 2.5 M of Tris buffer at pH 7 was added to 100 mL of 6 mM Na<sub>2</sub>S.9H<sub>2</sub>O in drops. The pH of the mixture was adjusted to 8.5 using 1, 2, and 5 M HCl solution. Subsequently, 250 mg of secondary PET MPs was added to 20 mL of the Na<sub>2</sub>S solution and covered with aluminum foil to avoid light interference. The suspension was shaken on a rotary shaker for 48 h after which the Na<sub>2</sub>S treated PET MPs were recovered and rinsed ten times. The Na<sub>2</sub>S treated MPs were dried at 50°C.

Natural organic matter loading was done by adding 250 mg of the secondary PET MPs to synthetic wastewater produced according to the OECD guidelines (OECD, 2001) (See constituents of the synthetic wastewater in Table C1). For effect of NOM in deionized water, secondary PET MPs were added to a solution containing the organic constituents of the synthetic wastewater (peptone, meat extract, and urea) only. To avoid interference due to microorganisms, all the materials including tips, bottles, and filters (0.2 µm PES Thermo scientific Nalgene) used in the preparation of synthetic wastewater were autoclaved and the preparation done under a biosafety cabinet.

### 5.2.3 Characterization of PET MPs

We characterized the secondary PET MPs for textural and functional group properties. We utilized

a light microscope and ImageJ for particle size distribution. We compared the functional groups on the surface of the differently aged MPs to themselves and to that of the pristine (unaged) MPs via Fourier transformed infrared spectroscopy (FTIR) using a Jasco FT/IR-4700 spectrometer (Japan). We determined the surface elemental composition on the MPs via X-ray photoelectron spectroscopy (XPS) using a Kratos AXIS Supra spectrometer (Manchester, UK). We used Micromeritics 3Flex Surface Characterization Analyzer (Norcross, GA) to characterize the Brunauer-Emmett-Teller (BET) surface area of the MPs through nitrogen sorption and determined the surface topography of the MPs using atomic force microscopy (Anton Paar Tosca 400 AFM, Graz, Austria).

#### 5.2.4 PFAS adsorption studies

To investigate the adsorption of per- and polyfluoroalkyl substances (PFAS) onto secondary polyethylene terephthalate microplastics (PET MPs), we conducted batch experiments first in deionized water and then synthetic wastewater. In our study, we focused on six specific PFAS: perfluorobutanoic acid (PFBA), hexafluoropropylene oxide dimer acid (GenX), perfluorobutane sulfonic acid (PFBS), perfluorooctanoic acid (PFOA), perfluorooctane sulfonic acid (PFOS), and perfluorooctanesulfonamide (FOSA). For the batch experiments, we adopted the same method as described in the previous chapter. Briefly, we added 20 mg of PET MPs to 10 mL of each aqueous solution containing the respective PFAS at a concentration of 200  $\mu\text{g/L}$ . We prepared the mixtures in 15 mL polypropylene containers. To ensure accuracy, we performed all experiments in triplicates, including triplicate controls without MPs to quantify partitioning to the container. To determine the equilibrium concentrations of PFAS, we employed liquid chromatography with tandem mass spectrometry (LC-MS/MS) using an Agilent 6470 LC/TQ instrument (Santa Clara,

CA). Detailed information on determination of equilibrium PFAS concentration and LC-MS/MS analysis can be found in Section S2. We conducted adsorption kinetics experiments to determine the equilibrium adsorption time and maximum adsorption capacity of the MPs for each PFAS (200 µg/L). We determined MPs adsorption capacity ( $q_e$ ) for each PFAS, and fit classical models to the kinetics data as described in the previous chapter.

## 5.3 Results and Discussions

### 5.3.1 Characterization of secondary PET MPs

The particle size distribution of pristine, Na<sub>2</sub>S treated, and NOM-loaded MPs as shown in the histograms (Figure 5.1a-c), can be summarized as follows: Na<sub>2</sub>S treated MPs have the smallest particles (mean of 1201 µm and a median of 999 µm) and were distributed within 108 – 2627 µm, with about 85.8 % within 500 – 2000 µm. Pristine MPs have a slightly larger particle size (mean of 1350 µm and a median of 1060 µm) and were distributed within 253 – 3301 µm, with about 92.7 % within 500 – 2000 µm. MPs preloaded with natural organic matter have the largest particle size (1444 µm and a median of 1118 µm). The particle size distribution of NOM-preloaded MPs was 304 – 3386 µm, with about 92.4% of the particles within 500 – 2000 µm size range. The particle sizes obtained in this study are in good agreement with the target sizes, providing further validation that the production method used is suitable for producing secondary polyethylene terephthalate (PET) microplastics. We confirmed the irregular shapes, sizes, and surface roughness on the MPs using AFM analysis (Figure C1). Na<sub>2</sub>S treated MPs have the highest mean surface roughness followed by pristine MPs and then NOM-loaded MPs (Figure 5.1d). Na<sub>2</sub>S treated MPs had the highest BET surface area ( $0.76 \pm 0.03 \text{ m}^2/\text{g}$ ) followed by NOM-loaded ( $0.14 \pm 0.03 \text{ m}^2/\text{g}$ ) and pristine MPs ( $0.0919 \pm 0.02 \text{ m}^2/\text{g}$ ).



The increases in surface area and roughness coupled with decreases in particle size seen in the Na<sub>2</sub>S treated MPs compared to pristine microplastics can be attributed to chemical and physical changes occurring during the treatment process. Sulfur compounds like hydrogen sulfide and Na<sub>2</sub>S sulfuric acid can chemically weather and corrode the surface of plastic particles, making the MPs more brittle and fragmented (Li et al., 2021; Zhao et al., 2021). This oxidation-driven degradation creates additional surface area by forming cavities and pits within the plastic particles (Shao et al., 2020; Wu et al., 2020.). The fragmented and weakened polymer chains may also break apart more readily under mechanical stress, reducing the average particle size. Overall, the Na<sub>2</sub>S treatment appears to substantially alter the physical structure of the MPs through polymer oxidation reactions, resulting in a rougher and more porous surface, greater surface area, and smaller plastic particles compared to the smooth pristine MPs.

Preloading MPs with natural organic matter can have various complex effects on the surface of secondary MPs. Adsorption of organic substances like humic acids and proteins onto the microplastics increases the surface area by coating the particles. Based on the results of the particle size distribution and AFM analysis, we hypothesize that adsorption of NOM may have resulted in filling of the cracks and surface irregularities on the secondary PET MPs, creating a more smooth and uniform topography. In this aging process, NOM acts as a filler. Various studies have showed that NOM could adsorb on MPs surface forming a protein layer due to Van der Waals or hydrophobic interaction (Abdurahman et al., 2020; Ali et al., 2022; Li et al., 2019).

In addition, NOM can initially induce aggregation of plastic particles through bridge-forming

mechanisms, increasing average particle size. Hydrophobic regions of adsorbed NOM can bind and trap smaller microplastic fragments, preventing their loss from the surface and preserving the parent particle size (Ali et al., 2022). However, organic coatings can also act as steric barriers that disaggregate plastic particle clusters, counteracting this effect.

FTIR analysis shows similarity between the spectra of pristine and Na<sub>2</sub>S treated PET MPs (Figure 5.1 e). However, the spectrum of NOM-loaded MPs was different from that of the pristine and Na<sub>2</sub>S treated MPs. Additional peaks were observed at 3300 cm<sup>-1</sup>, 1623 cm<sup>-1</sup>, and 1408 cm<sup>-1</sup> which were also found in the FTIR spectrum of NOM (Figure C2). Stretching vibrations of OH and NH in proteins peptide bond formed from multiple linkage of amino acids was responsible for the peak at 3300 cm<sup>-1</sup>, while the peaks at 1623 cm<sup>-1</sup> was assigned to amide I band related to the C=O stretching vibration in peptide bonds of proteins and peptides (Barth, 2007; Eftekhari et al., 2021). The peak at 1408 cm<sup>-1</sup> can be attributed to the asymmetric COO<sup>-</sup> stretching vibration of carboxylate groups in amino acids and C-N stretching vibration in urea, which are both components of the natural organic matter prepared (Kong & Yu, 2007). Loading of NOM on MPs was also confirmed by determining change in residual concentration of peptone in NOM solution (Figure C3). PCA analysis further confirms no difference in the functional group between pristine and Na<sub>2</sub>S treated MPs but revealed differences between pristine and NOM-loaded MPs (Figure 5.1f). Determination of the wavenumber with highest square loadings reveals the difference between pristine and NOM-loaded MPs were as a result of increase in intensities of peaks attributed to OH/NH, COO<sup>-</sup>, and C=O formation.

XPS analysis shows that the chemical properties of the secondary MPs are altered after aging by Na<sub>2</sub>S treatment and NOM-loading (Figure 5.1 g-i and Table C2). The result shows that NOM-preloaded MPs had the highest carbon (74%) and oxygen (23%) content but the lowest nitrogen content (3%) of the three secondary PET MPs. The Na<sub>2</sub>S treated MPs had 61% C, 22% O, and 17% N while pristine MPs had 64% C, 22% O and 14% N. The O/C ratio is often used as a quantitative parameter to characterize the surface modification of microplastics(Liu et al., 2019). We observed an increase in the intensity of O/C ratio after aging with NOM-preloaded MPs having the highest O/C ratio of the three secondary MPs (Table C2). The increase in O/C ratio reveals oxidation of the secondary PET MPs after aging. This result is consistent with previous studies that have investigated sulfidation of PET microplastics.

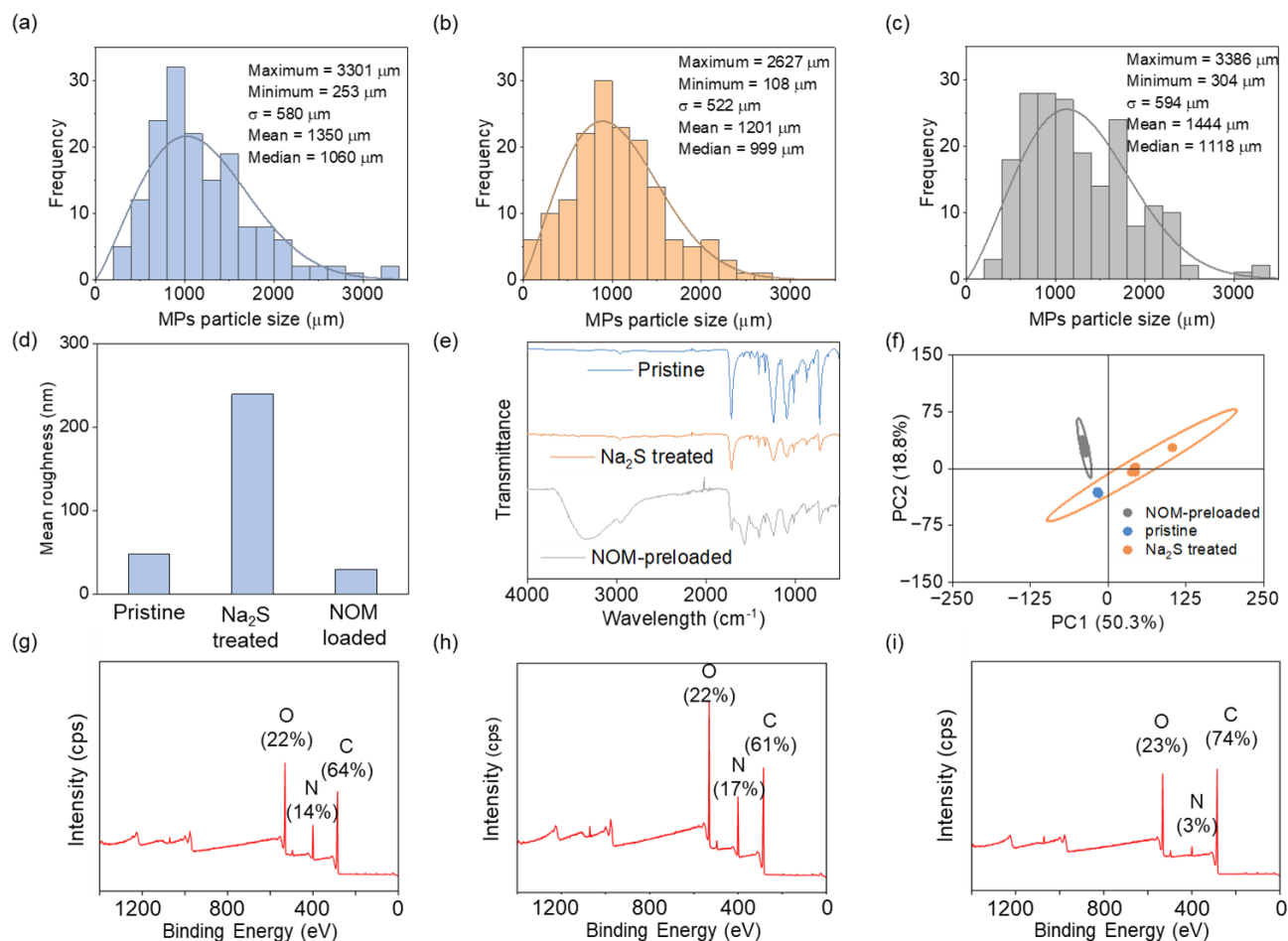


Figure 5.1 Particle size distribution of (a) pristine (b)  $\text{Na}_2\text{S}$  treated (c) NOM loaded MPs (d) mean surface roughness as obtained from AFM analysis. (e) FTIR spectra of pristine and aged MPs (f) PCA analysis showing the difference in the FTIR spectra of pristine and aged MPs. XPS survey spectra of (g) pristine (h)  $\text{Na}_2\text{S}$  treated (i) NOM loaded MPs.

### 5.3.2 Effect of aging on adsorption of PFAS in deionized water

#### 5.3.2.1 $\text{Na}_2\text{S}$ treatment

In the current study, adsorption of PFAS onto pristine MPs reached equilibrium after 16 h, which is slower compared to our previous study using smaller microplastics (53-250  $\mu\text{m}$ ) that

equilibrated faster. This slower equilibrium for the larger 500-2000  $\mu\text{m}$  microplastics may be attributed to their lower BET surface area (surface area of secondary PET MPs of size 500 – 2000 and 53 – 250  $\mu\text{m}$  are  $0.0919 \pm 0.02 \text{ m}^2/\text{g}$  and  $1.42 \text{ m}^2/\text{g} \pm 0.03 \text{ m}^2/\text{g}$ , respectively). Based on pseudo-first order rate constants, perfluoroalkyl carboxylic acids (PFCAs) adsorbed more rapidly to the secondary PET microplastics than perfluoroalkyl sulfonic acids (PFSA), consistent with the previous study.

For  $\text{Na}_2\text{S}$  treated MPs, adsorption equilibrium was achieved faster, in under 8 h. The PFO adsorption rate constants reveal PFCAs adsorbed faster overall than PFSA onto both pristine and  $\text{Na}_2\text{S}$  treated MPs. The  $k_1$  values (Table C3) for PFOA ( $2.39 \pm 0.88 \text{ min}^{-1}$ ) and PFBA ( $1.74 \pm 0.68 \text{ min}^{-1}$ ) were consistently higher than those for PFOS and PFBS. This trend was maintained after  $\text{Na}_2\text{S}$  treatment, although the  $k_1$  decreased for both classes of PFAS, reflective of the slower adsorption kinetics induced by the surface alterations from  $\text{Na}_2\text{S}$  treatment.

The adsorption capacity ( $q_e$ ) was consistently higher for the  $\text{Na}_2\text{S}$  treated MPs compared to the pristine MPs across all PFAS analytes. The  $q_e$  increased by 1.5 to 2.9 times, corresponding to 28 – 95 % (Figure 5.2a) increase after  $\text{Na}_2\text{S}$  treatment. This enhanced  $q_e$  of  $\text{Na}_2\text{S}$  treated MPs suggests oxidation, increase roughness, and surface area introduced by  $\text{Na}_2\text{S}$  treatment increased the affinity of the MPs for all the PFAS compounds, through mechanisms such as hydrophobic and electrostatic interactions. The sulfonate, PFOS generally displayed higher  $q_e$  values than the perfluoroalkyl carboxylates (PFCAs) like PFOA for both pristine and  $\text{Na}_2\text{S}$  treated MPs. The higher hydrophobicity of PFSA likely contributed to their greater adsorption out of the aqueous

solution onto the MPs surfaces (Deng et al., 2012). However, after Na<sub>2</sub>S treatment, the  $q_e$  difference between PFSAs and PFCAs was reduced, indicating the introduced oxygen content may have improved PFCA adsorption closer to PFSAs levels.

Based on the result, Na<sub>2</sub>S treatment improved adsorption capacity across all PFAS and enhanced adsorption kinetics (Figure 5.2b), although PFSAs displayed greater  $q_e$  while PFCAs showed faster  $k_1$  values. The results provide useful insights into how sewer-induced aging processes like Na<sub>2</sub>S treatment influence subsequent PFAS adsorption onto microplastics entering wastewater treatment plants.

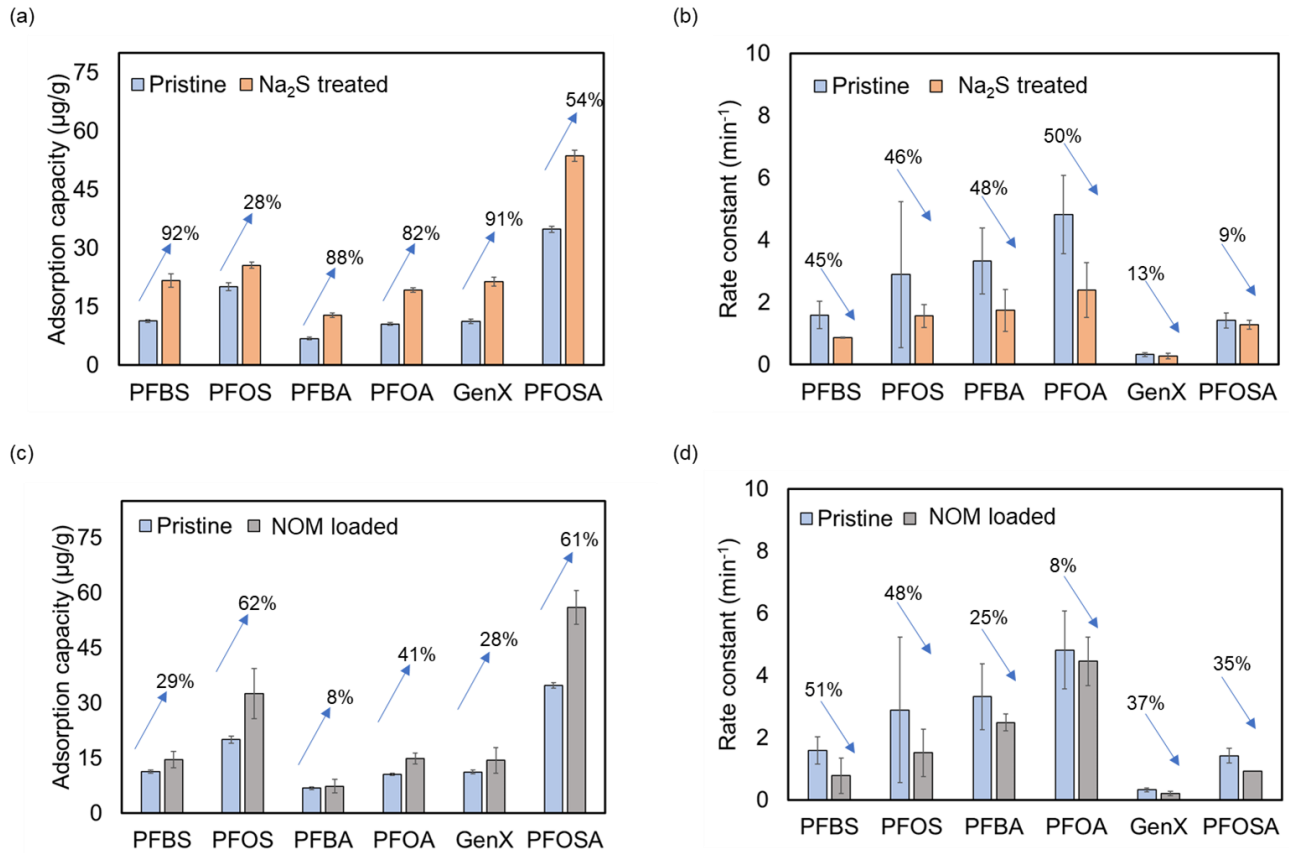


Figure 5.2. (a) Adsorption capacities and (b) rate constants of pristine and sulfided secondary PET MPs; (c) adsorption capacities (d) rate constants of pristine and NOM loaded MPs in deionized water. Initial concentration of each PFAS =  $200 \mu\text{g/L}$ , MP dose =  $2 \text{ g/L}$ , pH = 7, and shaker speed = 80 rpm.

### 5.3.2.2 Loading with NOM

Similar to the result obtained after  $\text{Na}_2\text{S}$  treatment, NOM loading increased the  $q_e$  for all PFAS analytes tested compared to the pristine microplastics but showed a decrease in  $k_l$  (Figure 5.2c and d). The  $q_e$  values were 1.2 to 1.6 times higher, which corresponds to 16 – 42 % increase in adsorption capacity after NOM loading. This enhanced adsorption capacity suggests the NOM on

the MPs provided additional sorption sites for the PFAS compounds, likely through hydrophobic partitioning. The NOM thus increased the affinity of the MPs for these PFAS. Also, PFASs maintained higher  $q_e$  values than PFCAs onto both MPs types, although the margin was reduced with NOM loading. As we observed in the effect of  $\text{Na}_2\text{S}$  treatment, the greater hydrophobicity of PFASs may have contributed to their higher adsorption from the aqueous solution. But NOM loading improved PFCA adsorption closer to PFASs through the added hydrophobic partitioning sites.

Hydrophobic natural organic matter (NOM) provides nonpolar sites that serve as partitioning surfaces enabling sorption of hydrophobic PFAS as well as other hydrophobic contaminants (Higgins & Luthy, 2006). The affinity for these NOM hydrophobic sorption sites has been reported to overcome the electrostatic repulsion between the negatively charged functional head groups of PFAS and negatively charged sites on organic matter surfaces that may limit the adsorption process (Delle Site, 2001; Joo et al., 2021b).

The increase in  $q_e$  observed contrasts with the result in our previous study where adsorption of PFAS decreased with an increase in humic acid concentration. However, (Ateia et al., 2020) reported similar result. The study reported that loading microplastics with NOM enhanced the adsorption of PFAS to microplastics with long-chain PFAS showing a significant increase in adsorption. However, no significant increase was observed for short-chain PFAS.



We attempt to explain the contrasting result obtained when MPs are loaded compared to when added to matrix at the same time with PFAS. Loading MPs with NOM can increase the adsorption of PFAS due to the formation of a complex between NOM and PFAS, co-sorption of NOM and PFAS, and an increase in the surface area of microplastics. However, adding NOM and PFAS at the same time can decrease the adsorption of PFAS on MPs due to competition for adsorption sites, blocking of adsorption sites, and reduction in the surface area available for PFAS adsorption. Our study highlights the importance of considering NOM loading when evaluating microplastics' sorption behavior, as neglecting this factor can result in a significant underestimation of their actual values.

### 5.3.3 Effect of aging on adsorption of PFAS in synthetic wastewater

#### 5.3.3.1 Na<sub>2</sub>S treatment

Similar to the trend we observed in deionized water, Na<sub>2</sub>S treatment of the MPs enhanced their adsorption capacity for all PFAS analytes. As shown in Figure 5.3a,  $q_e$  increased between 1.3 to 2.2 times after Na<sub>2</sub>S treatment. When comparing the effects of Na<sub>2</sub>S treatment on the adsorption capacity ( $q_e$ ) between deionized water and synthetic wastewater matrices, we noticed some differences depending on the PFAS compound. For PFOS, the increase in  $q_e$  with Na<sub>2</sub>S treatment was lower in synthetic wastewater compared to deionized water. This suggests that certain components in the synthetic wastewater matrix may have competed with PFOS for reactive adsorption sites or hindered access to sites on the Na<sub>2</sub>S treated MPs.

The decrease in PFOS adsorption capacity in synthetic wastewater implies complex matrix effects whereby the wastewater constituents interact with Na<sub>2</sub>S treated sites and influence PFOS removal to a greater extent than is observed in clean deionized water. Further work is needed to elucidate the specific molecular-level interactions contributing to this matrix-dependent behavior. Overall, the results reveal the complexity of factors governing PFAS adsorption in real water matrices, where organic and inorganic components can modulate adsorbent surface reactivity in ways that differ across PFAS analogues. The PFSAAs maintained higher  $q_e$  values than PFCAs for both pristine and Na<sub>2</sub>S treated MPs. The greater hydrophobicity of PFSAAs drove their preferential adsorption from the aqueous solution. But Na<sub>2</sub>S treatment reduced this margin between PFSAAs and PFCAs, improving adsorption of the more hydrophilic PFCAs. A consistent decrease in  $k_l$  was also observed for all the PFAS (Figure 5.3 b) when sulfided MPs are used to adsorb PFAS compared to pristine MPs.

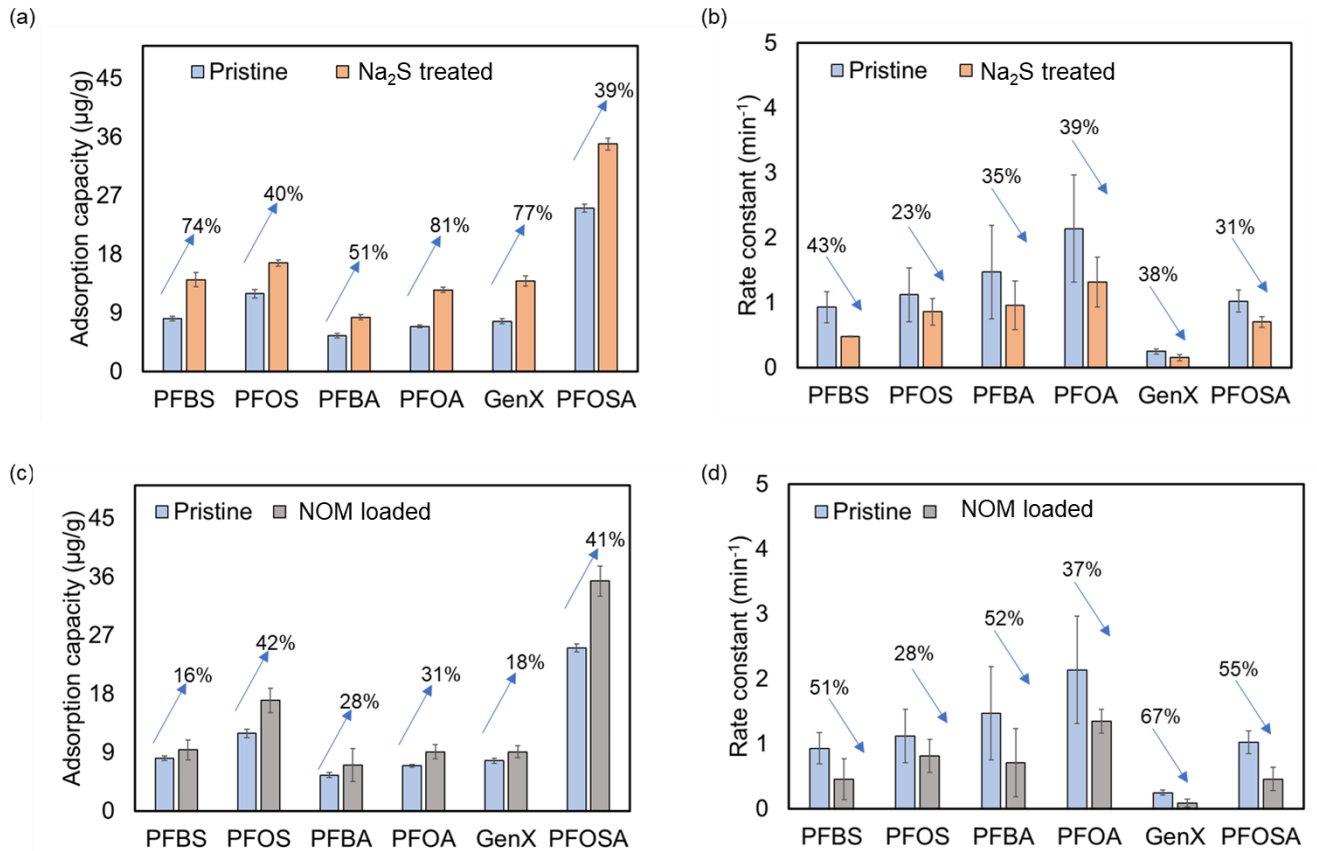


Figure 5.3. (a) Adsorption capacities and (b) rate constants of pristine and Na<sub>2</sub>S treated secondary PET MPs; (c) adsorption capacities (d) rate constants of pristine and NOM loaded MPs in synthetic wastewater. Initial concentration of each PFAS = 200 µg/L, MP dose = 2 g/L, pH = 7, and shaker speed = 80 rpm.

### 5.3.3.2 Loading with NOM

For each of the PFAS compounds under investigation, the equilibrium adsorption capacities ( $q_e$ ) exhibited notable increases when interacting with microplastics loaded with natural organic matter (NOM) in comparison to their interactions with pristine microplastics, as illustrated in the figure (Figure 5.3 c). The observed enhancements were particularly pronounced for FOSA, where the  $q_e$  increased from  $25.05 \pm 0.58$  µg/g in pristine microplastics to  $35.32 \pm 2.34$  µg/g in NOM-loaded

microplastics. Similarly, PFOS demonstrated a substantial increase in  $q_e$ , rising from  $11.92 \pm 0.67$   $\mu\text{g/g}$  in pristine microplastics to  $16.98 \pm 1.90$   $\mu\text{g/g}$  when interacting with NOM-loaded microplastics. This observed trend closely parallels the results obtained during the adsorption of PFAS to NOM-loaded microplastics in deionized water, demonstrating the consistent and significant impact of natural organic matter on the adsorption behavior of these PFAS compounds onto microplastics.

However,  $k_1$  showed a decrease for all PFAS (Figure 5.3 d). This decline in  $k_1$  values suggests a substantial alteration in the adsorption kinetics, predominantly attributed to the presence of the NOM coating on the microplastics. This reduction in  $k_1$  implies a potential hindrance in the adsorption process of PFAS molecules onto the microplastic surfaces. Several factors associated with the NOM coating may contribute to this hindrance, including the partial obstruction of available surface area on the microplastics, acting as a diffusion barrier that slows down the movement of PFAS molecules toward adsorption sites, creating competitive interactions for binding sites on the microplastic surface, and potentially forming complexes or aggregates in solution due to chemical interactions between NOM and PFAS compounds. In essence, while the NOM coating enhances the adsorption capacity of microplastics for PFAS, it simultaneously modifies the kinetics, introducing complexities and competitive dynamics to the adsorption process.

### 5.3.4 Conclusion, environmental implications, and limitations.

The results of this study reveal that aging processes including Na<sub>2</sub>S treatment and natural organic matter (NOM) fouling significantly alter the surface properties of microplastics, enhancing their adsorption capacity for perfluoroalkyl substances (PFAS) compounds. Across both deionized water and synthetic wastewater matrices, aged microplastics exhibited a markedly higher equilibrium adsorption capacity ( $q_e$ ) for all investigated PFAS compared to pristine microplastics. Na<sub>2</sub>S treatment increased  $q_e$  by 28-95%, while NOM fouling increased it by 16-42%, highlighting the dramatic impact of sewer-induced aging on subsequent contaminant uptake. Although sulfidation enhanced adsorption capacity in both water types, the increase was lower in wastewater for certain PFAS like PFOS, indicating potential competitive effects from wastewater constituents. Perfluoroalkyl sulfonic acids (PFSAs) displayed greater  $q_e$  than perfluoroalkyl carboxylic acids (PFCAs) on both pristine and aged microplastics, attributed to their higher hydrophobicity. However, aging processes improved PFCA adsorption closer to PFSAs levels by increasing surface polarity. Despite enhancing sorption capacity, NOM fouling hindered the adsorption kinetics ( $k_1$ ), likely due to surface blockage, competitive interactions, and complexation.

These findings emphasize that microplastics entering wastewater treatment plants have often undergone transformations that increase their affinity for hydrophobic organic contaminants like PFAS. Aged microplastics may provide a significant route for PFAS persistence and accumulation in the environment. Implementing technologies to remove microplastics early in wastewater treatment could help mitigate discharge of PFAS-loaded microplastics. This study also highlights the need to evaluate PFAS-microplastic interactions under realistic conditions, as aging processes

and water chemistry modulate behavior in complex ways. Further research is recommended to develop strategies for reducing microplastic-mediated PFAS pollution.

One limitation of this work is that it examined PFAS adsorption onto pristine and aged microplastics in controlled laboratory experiments with synthetic wastewater. While this allows close examination of how specific aging processes like  $\text{Na}_2\text{S}$  treatment and NOM fouling affect sorption capacity and kinetics, it does not fully capture the complexities of real wastewater matrices. Actual wastewater contains a diverse mixture of organic matter, suspended solids, and dissolved chemicals that may influence PFAS-microplastic interactions in ways not observed here. The use of synthetic wastewater also does not account for variability in wastewater composition across different sources and treatment stages. Testing aged microplastics spiked into real wastewater samples could provide additional insights by better representing competitive effects, variable fouling conditions, and water chemistry impacts. The controlled experiments here provide valuable fundamental adsorption data on pristine and aged microplastics, but further testing in real wastewater is needed to confirm behavior under field conditions. Additionally, only two model aging processes were evaluated, while other transformations like weathering, biofilm growth, and fragmentation may also modify microplastic surfaces and sorption capacity in wastewater systems.

## Chapter 6 Summary

This thesis provides valuable insights into the occurrence, behavior, and interactions of per- and polyfluoroalkyl substances (PFAS) across various aquatic environments. The work elucidates the presence of PFAS in wastewater sources, their partitioning tendencies, and the role of microplastics as potential sinks for these contaminants. Through multiple studies that covers PFAS sampling, detection, characterization, and sorption experiments, I generated key findings that advance current understanding of PFAS fate and transport pathways. The major conclusions arising from this body of research are:

### Project 1.

1. Nine different PFAS compounds were detected across all collected raw wastewater samples from the three sites. Of the 9 PFAS identified, 5 were carboxylates, 2 were sulfonates, and 2 were PFAS precursors.
2. Perfluorododecanoic acid (PFDOA) displayed the highest frequency, being present in all samples (DF = 100%). Perfluoropentanesulfonic acid (PFPeS) had the second highest detection frequency at 91%.
3. In contrast, the legacy PFAS compounds perfluorooctanoic acid (PFOA) and perfluorooctanesulfonic acid (PFOS) exhibited lower occurrence, with DFs of 14.3% and 0% respectively.
4. Two PFAS precursors were also found - 1H,1H,2H,2H-perfluorooctane sulfonate (6:2 FTS) (DF 52%) and perfluoro-1-octanesulfonamide (PFOSA) (DF 19%).

5. The concentration of 6:2 FTS (mean = 59.84 ng/L, median = 44.06 ng/L) was the highest of all the PFAS detected.
6. Four PFAS were detected in tap water collected from the sampling locations out of which 2 are PFAS precursors.
7. 6:2 FTS had the highest total concentration (38.60 ng/L) of the PFAS detected in tap water samples.
8. In wastewater samples, 6:2 FTS has the highest total concentration (658.25 ng/L) followed by PFDoA (618.44 ng/L).
9. PFOA (12.23 ng/L) had the lowest total concentrations of the 9 PFAS detected in wastewater.
10. PFAS profiles clustered distinctly from heavy metals, however PFOA was uniquely correlated with iron.

## Project 2.

1. PFAS adsorption reaches equilibrium with 7-16 hours, depending on whether the PFAS are present in single solutions or in a mixture.
2. The adsorption of PFAS onto secondary PET microplastics is spontaneous at 25°C.
3. PFCAs are likely to adsorb faster than their homologous PFSA, but more PFSA would adsorb at equilibrium due to their stronger hydrophobic and electrostatic interactions.
4. Surface roughness and/or the presence of additives in the commercial parent plastics can affect the uptake of PFAS by secondary microplastics.
5. Hydrophobic interaction is important in the partitioning of PFAS onto surfaces, but other interaction forces such as electrostatic interactions may also play important roles.



6. Water chemistry (pH, ionic strength, natural organic matter, and temperature) and PFAS chemistry (chain length and functionality) can affect PFAS partitioning from water to the surface of secondary microplastics.

### Project 3.

1. Aging processes like Na<sub>2</sub>S treatment and NOM loading significantly increased the adsorption capacity of microplastics for perfluoroalkyl substances compared to pristine microplastics.
2. Na<sub>2</sub>S treatment enhanced adsorption capacity by 28-95%, while NOM loading increased it by 16-42%, highlighting their impact on contaminant uptake.
3. Aged microplastics exhibited higher PFAS adsorption capacity consistently across deionized water and synthetic wastewater matrices.
4. Perfluoroalkyl sulfonic acids (PFSAs) displayed greater adsorption than perfluoroalkyl carboxylic acids (PFCAs) on both pristine and aged microplastics due to their higher hydrophobicity.
5. However, aging processes improved the adsorption of hydrophilic PFCAs relatively closer to the levels of hydrophobic PFSAs.
6. NOM loading increased adsorption capacity but hindered adsorption kinetics, likely due to surface blockage, competitive interactions, and complexation.
7. The results emphasize aged microplastics in wastewater can act as sinks for hydrophobic organic contaminants like PFAS and provide a route for their environmental persistence.
8. The study highlights the need to evaluate PFAS-microplastic interactions under realistic conditions, as aging and water chemistry influence behavior.

9. In summary, the major findings demonstrate aging processes transform microplastics to enhance sorption capacity for PFAS, and aged microplastics may facilitate PFAS accumulation in the environment.

This work significantly advances knowledge of per- and polyfluoroalkyl substances across aquatic systems. The work provides extensive new data on PFAS occurrence, speciation, and behavior in wastewater sources. Critical insights are gained into the interactions of PFAS with microplastics under various conditions. The research demonstrates that aged microplastics can act as sinks for PFAS persistence in the environment. Overall, this comprehensive study elucidates PFAS pathways from sources to sinks, while also revealing knowledge gaps that warrant further research. The outcomes present a foundation for developing more effective PFAS monitoring, control, and remediation strategies to reduce their proliferation.

## Chapter 7 Future perspectives

The findings from this work open multiple perspectives for further research to better understand and manage PFAS proliferation in aquatic environments. These perspectives include:

1. Additional wastewater sampling at finer spatial and temporal scales could provide more granular insights into PFAS sources, usage patterns, and fluctuation trends. Detailed investigation of household items leaching PFAS, and consumer product contents that could contain the contaminant would help trace detected PFAS to specific origins.
2. Expanded analysis of PFAS loading on microplastics sampled from real wastewater systems is needed to confirm laboratory results. Testing a wider range of aging processes and water chemistries would elucidate other factors influencing microplastic interactions.
3. Evaluating PFAS sorption by nanoplastics could reveal their role as potential vectors. Toxicity assays of PFAS-loaded microplastics on organisms at various trophic levels could clarify ecological risks. Pilot studies on mitigation technologies, including plastic removal and advanced treatment methods, are essential for developing effective solutions.
4. Overall, this work provides a critical and important knowledge baseline to guide future efforts toward reducing PFAS increase from sources to sinks in aquatic systems. The outcomes present further gap for the advanced research required to tackle this ubiquitous and complex contaminant threat.

## References

- Abdi, H., & Williams, L. J. (2010). Principal component analysis. *WIREs Computational Statistics*, 2(4), 433-459. <https://doi.org/https://doi.org/10.1002/wics.101>
- Abdurahman, A., Cui, K., Wu, J., Li, S., Gao, R., Dai, J., Liang, W., & Zeng, F. (2020). Adsorption of dissolved organic matter (DOM) on polystyrene microplastics in aquatic environments: Kinetic, isotherm and site energy distribution analysis. *Ecotoxicology and environmental safety*, 198, 110658.
- Adeleye, A. S., Ho, K. T., Zhang, M., Li, Y., & Burgess, R. M. (2019). Fate and transformation of graphene oxide in estuarine and marine waters. *Environmental science & technology*, 53(10), 5858-5867.
- Adeleye, A. S., & Keller, A. A. (2014). Long-term colloidal stability and metal leaching of single wall carbon nanotubes: effect of temperature and extracellular polymeric substances [Research Support, U.S. Gov't, Non-P.H.S.]. *Water Res*, 49(0), 236-250. <https://doi.org/10.1016/j.watres.2013.11.032>
- Adio, S. O., Basheer, C., Hussein, M. O., Siddiqui, M. N., & Tawabini, B. (2019). Comparative Evaluation of Biosynthesized Nanoscale Zerovalent Iron and Iron-Oxide Nanoparticles in Mercury Adsorption. *Journal of Environmental Engineering*, 145(7), 04019037. [https://doi.org/10.1061/\(ASCE\)EE.1943-7870.0001515](https://doi.org/10.1061/(ASCE)EE.1943-7870.0001515)
- Agency for Toxic, S., & Disease, R. (2018). Per-and polyfluoroalkyl substances (PFAS) and your health.
- Ali, I., Tan, X., Li, J., Peng, C., Naz, I., Duan, Z., & Ruan, Y. (2022). Interaction of microplastics and nanoplastics with natural organic matter (NOM) and the impact of NOM on the sorption behavior of anthropogenic contaminants—A critical review. *Journal of Cleaner Production*, 134314.
- Alimi, O. S., Farnar Budarz, J., Hernandez, L. M., & Tufenkji, N. (2018). Microplastics and Nanoplastics in Aquatic Environments: Aggregation, Deposition, and Enhanced Contaminant Transport. *Environmental Science & Technology*, 52(4), 1704-1724. <https://doi.org/10.1021/acs.est.7b05559>
- Allouzi, M. M. A., Tang, D. Y. Y., Chew, K. W., Rinklebe, J., Bolan, N., Allouzi, S. M. A., & Show, P. L. (2021). Micro (nano) plastic pollution: The ecological influence on soil-plant system and human health. *Science of the total environment*, 788, 147815.
- Alves, A. V., Tsianou, M., & Alexandridis, P. (2020). Fluorinated Surfactant Adsorption on Mineral Surfaces: Implications for PFAS Fate and Transport in the Environment. *Surfaces*, 3(4), 516-566.
- Amaral-Zettler, L. A., Zettler, E. R., & Mincer, T. J. (2020). Ecology of the plastisphere. *Nature Reviews Microbiology*, 18(3), 139-151.
- Andrady, A. L., & Koongolla, B. (2022). Degradation and Fragmentation of Microplastics. *Plastics and the Ocean: Origin, Characterization, Fate, and Impacts*, 227-268.
- Ankley, G. T., Cureton, P., Hoke, R. A., Houde, M., Kumar, A., Kurias, J., Lanno, R., McCarthy, C., Newsted, J., & Salice, C. J. (2021). Assessing the ecological risks of per-and polyfluoroalkyl substances: Current state-of-the science and a proposed path forward. *Environmental toxicology and chemistry*, 40(3), 564-605.
- Aonghusa, C. N., & Gray, N. F. (2002). Laundry detergents as a source of heavy metals in Irish domestic wastewater. *Journal of Environmental Science and Health, Part A*, 37(1), 1-6.
- Ateia, M., Zheng, T., Calace, S., Tharayil, N., Pilla, S., & Karanfil, T. (2020). Sorption behavior of real microplastics (MPs): insights for organic micropollutants adsorption on a large set of well-characterized MPs. *Science of the Total Environment*, 720, 137634.
- Atugoda, T., Vithanage, M., Wijesekara, H., Bolan, N., Sarmah, A. K., Bank, M. S., You, S., & Ok, Y. S. (2021). Interactions between microplastics, pharmaceuticals and personal care products: Implications for vector transport. *Environment International*, 149, 106367.
- Backe, W. J., Day, T. C., & Field, J. A. (2013). Zwitterionic, cationic, and anionic fluorinated chemicals in aqueous film forming foam formulations and groundwater from US military bases by nonaqueous large-volume injection HPLC-MS/MS. *Environmental science & technology*, 47(10), 5226-5234.

- Bamai, Y. A., Goudarzi, H., Araki, A., Okada, E., Kashino, I., Miyashita, C., & Kishi, R. (2020). Effect of prenatal exposure to per- and polyfluoroalkyl substances on childhood allergies and common infectious diseases in children up to age 7 years: The Hokkaido study on environment and children's health. *Environment international*, *143*, 105979.
- Barnes, D. K. A., Galgani, F., Thompson, R. C., & Barlaz, M. (2009). Accumulation and fragmentation of plastic debris in global environments. *Philosophical Transactions of the Royal Society B: Biological Sciences*, *364*(1526), 1985-1998. <https://doi.org/doi:10.1098/rstb.2008.0205>
- Barth, A. (2007). Infrared spectroscopy of proteins. *Biochimica et Biophysica Acta (BBA)-Bioenergetics*, *1767*(9), 1073-1101.
- Becker, A. M., Gerstmann, S., & Frank, H. (2008). Perfluorooctane surfactants in waste waters, the major source of river pollution. *Chemosphere*, *72*(1), 115-121.
- Benbrahim-Tallaa, L., Lauby-Secretan, B., Loomis, D., Guyton, K. Z., Grosse, Y., El Ghissassi, F., Bouvard, V., Guha, N., Mattock, H., & Straif, K. (2014). Carcinogenicity of perfluorooctanoic acid, tetrafluoroethylene, dichloromethane, 1, 2-dichloropropane, and 1, 3-propane sultone. *Lancet Oncology*, *15*(9), 924.
- Bentel, M. J., Yu, Y., Xu, L., Li, Z., Wong, B. M., Men, Y., & Liu, J. (2019). Defluorination of per- and polyfluoroalkyl substances (PFASs) with hydrated electrons: structural dependence and implications to PFAS remediation and management. *Environmental science & technology*, *53*(7), 3718-3728.
- Bhagat, K., Barrios, A. C., Rajwade, K., Kumar, A., Oswald, J., Apul, O., & Perreault, F. (2022). Aging of microplastics increases their adsorption affinity towards organic contaminants. *Chemosphere*, *298*, 134238.
- Bilela, L. L., Matijošytė, I., Krutkevičius, J., Alexandrino, D. A., Safarik, I., Burlakovs, J., Gaudêncio, S. P., & Carvalho, M. F. (2023). Impact of per- and polyfluorinated alkyl substances (PFAS) on the marine environment: Raising awareness, challenges, legislation, and mitigation approaches under the One Health concept. *Marine Pollution Bulletin*, *194*, 115309.
- Born, M. P., Brüll, C., & Schüttrumpf, H. (2023). Implications of a New Test Facility for Fragmentation Investigations on Virgin (Micro) plastics. *Environmental science & technology*, *57*(28), 10393-10403.
- Borthakur, A., Leonard, J., Koutnik, V. S., Ravi, S., & Mohanty, S. K. (2022). Inhalation risks of wind-blown dust from biosolid-applied agricultural lands: Are they enriched with microplastics and PFAS? *Current Opinion in Environmental Science & Health*, *25*, 100309.
- Brown, J. R. (2021). Dissolved organic carbon and the potential role to stream acidity in the Great Smoky Mountains National Park.
- Calafat, A. M., Wong, L.-Y., Kuklennyik, Z., Reidy, J. A., & Needham, L. L. (2007). Polyfluoroalkyl chemicals in the US population: data from the National Health and Nutrition Examination Survey (NHANES) 2003–2004 and comparisons with NHANES 1999–2000. *Environmental health perspectives*, *115*(11), 1596-1602.
- Campo, J., Masiá, A., Picó, Y., Farré, M., & Barceló, D. (2014). Distribution and fate of perfluoroalkyl substances in Mediterranean Spanish sewage treatment plants. *Science of the total environment*, *472*, 912-922.
- Cervantes-Avilés, P., Piñas, N. C., Ida, J., & Cuevas-Rodríguez, G. (2017). Influence of wastewater type on the impact generated by TiO<sub>2</sub> nanoparticles on the oxygen uptake rate in activated sludge process. *Journal of Environmental Management*, *190*, 35-44.
- Chen, C.-S., Le, C., Chiu, M.-H., & Chin, W.-C. (2018). The impact of nanoplastics on marine dissolved organic matter assembly. *Science of The Total Environment*, *634*, 316-320.

- Chen, C., Chen, L., Yao, Y., Artigas, F., Huang, Q., & Zhang, W. (2019). Organotin release from polyvinyl chloride microplastics and concurrent photodegradation in water: Impacts from salinity, dissolved organic matter, and light exposure. *Environmental science & technology*, 53(18), 10741-10752.
- Chen, X., Gu, X., Bao, L., Ma, S., & Mu, Y. (2021). Comparison of adsorption and desorption of triclosan between microplastics and soil particles. *Chemosphere*, 263, 127947.
- Cheng, Y., Mai, L., Lu, X., Li, Z., Guo, Y., Chen, D., & Wang, F. (2021). Occurrence and abundance of poly- and perfluoroalkyl substances (PFASs) on microplastics (MPs) in Pearl River Estuary (PRE) region: Spatial and temporal variations. *Environmental Pollution*, 281, 117025. <https://doi.org/https://doi.org/10.1016/j.envpol.2021.117025>
- Coggan, T. L., Moodie, D., Kolobaric, A., Szabo, D., Shimeta, J., Crosbie, N. D., Lee, E., Fernandes, M., & Clarke, B. O. (2019). An investigation into per-and polyfluoroalkyl substances (PFAS) in nineteen Australian wastewater treatment plants (WWTPs). *Heliyon*, 5(8), e02316.
- Coggan, T. L., Moodie, D., Kolobaric, A., Szabo, D., Shimeta, J., Crosbie, N. D., Lee, E., Fernandes, M., & Clarke, B. O. (2019). An investigation into per-and polyfluoroalkyl substances (PFAS) in nineteen Australian wastewater treatment plants (WWTPs). *Heliyon*, 5(8).
- Cole, M., Lindeque, P., Halsband, C., & Galloway, T. S. (2011). Microplastics as contaminants in the marine environment: a review. *Marine pollution bulletin*, 62(12), 2588-2597.
- Cousins, I. T., Goldenman, G., Herzke, D., Lohmann, R., Miller, M., Ng, C. A., Patton, S., Scheringer, M., Trier, X., & Vierke, L. (2019). The concept of essential use for determining when uses of PFASs can be phased out. *Environmental Science: Processes & Impacts*, 21(11), 1803-1815.
- Cui, D., Li, X., & Quinete, N. (2020). Occurrence, fate, sources and toxicity of PFAS: What we know so far in Florida and major gaps. *TrAC Trends in Analytical Chemistry*, 115976.
- da Costa, J. P., Santos, P. S. M., Duarte, A. C., & Rocha-Santos, T. (2016). (Nano)plastics in the environment – Sources, fates and effects. *Science of The Total Environment*, 566-567, 15-26. <https://doi.org/https://doi.org/10.1016/j.scitotenv.2016.05.041>
- Danmaliki, G. I., & Saleh, T. A. (2017). Effects of bimetallic Ce/Fe nanoparticles on the desulfurization of thiophenes using activated carbon. *Chemical Engineering Journal*, 307, 914-927.
- Delle Site, A. (2001). Factors affecting sorption of organic compounds in natural sorbent/water systems and sorption coefficients for selected pollutants. A review. *Journal of Physical and Chemical Reference Data*, 30(1), 187-439.
- Deng, S., Zhang, Q., Nie, Y., Wei, H., Wang, B., Huang, J., Yu, G., & Xing, B. (2012). Sorption mechanisms of perfluorinated compounds on carbon nanotubes. *Environmental pollution*, 168, 138-144.
- Dery, J. L., Gerrity, D., & Rock, C. M. (2019). Perfluoroalkyl and Polyfluoroalkyl Substances (PFAS): What consumers need to know. *University of Arizona Cooperative Extension*. az1794.
- Dey, S., Rout, A. K., Behera, B. K., & Ghosh, K. (2022). Plasticsphere community assemblage of aquatic environment: plastic-microbe interaction, role in degradation and characterization technologies. *Environmental Microbiome*, 17(1), 1-21.
- Dignac, M. F., Ginestet, P., Rybacki, D., Bruchet, A., Urbain, V., & Scribe, P. (2000). Fate of wastewater organic pollution during activated sludge treatment: nature of residual organic matter. *Water research*, 34(17), 4185-4194.
- Ding, L., Mao, R., Ma, S., Guo, X., & Zhu, L. (2020a). High temperature depended on the ageing mechanism of microplastics under different environmental conditions and its effect on the distribution of organic pollutants. *Water Research*, 174, 115634.
- Ding, L., Mao, R., Ma, S., Guo, X., & Zhu, L. J. W. R. (2020b). High temperature depended on the ageing mechanism of microplastics under different environmental conditions and its effect on the distribution of organic pollutants. 174, 115634.

- Ding, L., Yu, X., Guo, X., Zhang, Y., Ouyang, Z., Liu, P., Zhang, C., Wang, T., Jia, H., & Zhu, L. (2022). The photodegradation processes and mechanisms of polyvinyl chloride and polyethylene terephthalate microplastic in aquatic environments: Important role of clay minerals. *Water Research*, 208, 117879.
- Ding, R., Tong, L., & Zhang, W. (2021). Microplastics in freshwater environments: sources, fates and toxicity. *Water, Air, & Soil Pollution*, 232, 1-19.
- Dixit, F., Barbeau, B., Mostafavi, S. G., & Mohseni, M. (2019). PFOA and PFOS removal by ion exchange for water reuse and drinking applications: role of organic matter characteristics. *Environmental Science: Water Research & Technology*, 5(10), 1782-1795.
- Dong, Q., Min, X., Huo, J., & Wang, Y. (2021). Efficient sorption of perfluoroalkyl acids by ionic liquid-modified natural clay. *Chemical Engineering Journal Advances*, 7, 100135.
- Du, Z., Deng, S., Bei, Y., Huang, Q., Wang, B., Huang, J., & Yu, G. (2014). Adsorption behavior and mechanism of perfluorinated compounds on various adsorbents—A review. *Journal of hazardous materials*, 274, 443-454.
- Duan, L., Qin, Y., Meng, X., Liu, Y., Zhang, T., & Chen, W. (2023). Sulfide-and UV-induced aging differentially affect contaminant-binding properties of microplastics derived from commercial plastic products. *Science of the Total Environment*, 869, 161800.
- Eftekhari, S., Gugtapeh, H. S., & Rezaei, M. (2021). Effect of meat extract as an eco-friendly inhibitor on corrosion behavior of mild steel: Electrochemical noise analysis based on shot noise and stochastic theory. *Construction and Building Materials*, 292, 123423.
- Elhacham, E., Ben-Uri, L., Grozovski, J., Bar-On, Y. M., & Milo, R. (2020). Global human-made mass exceeds all living biomass. *Nature*, 588(7838), 442-444. <https://doi.org/10.1038/s41586-020-3010-5>
- Elias, S. A. (2018). Plastics in the Ocean. In D. A. Dellasala & M. I. Goldstein (Eds.), *Encyclopedia of the Anthropocene* (pp. 133-149). Elsevier. <https://doi.org/https://doi.org/10.1016/B978-0-12-809665-9.10514-2>
- Elimelech, M., Williams, R., Gregory, J., & X, J. (1998). *Particle Deposition and Aggregation*. Butterworth-Heinemann.
- Enyoh, C. E., Wang, Q., Wang, W., Chowdhury, T., Rabin, M. H., Islam, R., Yue, G., Yichun, L., & Xiao, K. (2022). Sorption of Per-and Polyfluoroalkyl Substances (PFAS) using Polyethylene (PE) microplastics as adsorbent: Grand Canonical Monte Carlo and Molecular Dynamics (GCMC-MD) studies. *International Journal of Environmental Analytical Chemistry*, 1-17.
- Er, C. T. X., Sen, L. Z., Srinophakun, P., & Wei, O. C. J. B. T. (2023). Recent advances and challenges in sustainable management of plastic waste using biodegradation approach. 128772.
- Essien, J. P., Benson, N. U., & Antai, S. P. (2008). Seasonal dynamics of physicochemical properties and heavy metal burdens in Mangrove sediments and surface water of the brackish Qua Iboe Estuary, Nigeria. *Toxicological and Environ Chemistry*, 90(2), 259-273.
- Europe, P. J. P. (2022). Plastics—the facts 2022. 1, 1-81.
- Evans, C. D., Monteith, D. T., & Cooper, D. M. (2005). Long-term increases in surface water dissolved organic carbon: observations, possible causes and environmental impacts. *Environmental pollution*, 137(1), 55-71.
- Fan, X., Zou, Y., Geng, N., Liu, J., Hou, J., Li, D., Yang, C., & Li, Y. (2021). Investigation on the adsorption and desorption behaviors of antibiotics by degradable MPs with or without UV ageing process. *Journal of Hazardous Materials*, 401, 123363.
- Febrianto, J., Kosasih, A. N., Sunarso, J., Ju, Y.-H., Indraswati, N., & Ismadji, S. (2009). Equilibrium and kinetic studies in adsorption of heavy metals using biosorbent: a summary of recent studies. *Journal of hazardous materials*, 162(2-3), 616-645.

- Flury, M., Narayan, R. J. C. O. i. G., & Chemistry, S. (2021). Biodegradable plastic as an integral part of the solution to plastic waste pollution of the environment. *30*, 100490.
- Frias, J. P., & Nash, R. J. M. p. b. (2019). Microplastics: Finding a consensus on the definition. *138*, 145-147.
- Fu, L., Li, J., Wang, G., Luan, Y., & Dai, W. (2021). Adsorption behavior of organic pollutants on microplastics. *Ecotoxicology and Environmental Safety*, *217*, 112207.
- Fu, Q., Tan, X., Ye, S., Ma, L., Gu, Y., Zhang, P., Chen, Q., Yang, Y., & Tang, Y. (2021). Mechanism analysis of heavy metal lead captured by natural-aged microplastics. *Chemosphere*, *270*, 128624.
- Gagliano, E., Sgroi, M., Falciglia, P. P., Vagliasindi, F. G. A., & Roccaro, P. (2020). Removal of poly-and perfluoroalkyl substances (PFAS) from water by adsorption: Role of PFAS chain length, effect of organic matter and challenges in adsorbent regeneration. *Water research*, *171*, 115381.
- Gaines, L. G. (2023). Historical and current usage of per-and polyfluoroalkyl substances (PFAS): A literature review. *American Journal of Industrial Medicine*, *66*(5), 353-378.
- Gewert, B., Plassmann, M. M., & MacLeod, M. (2015). Pathways for degradation of plastic polymers floating in the marine environment. *Environmental science: processes & impacts*, *17*(9), 1513-1521.
- Geyer, R., Jambeck, J. R., & Law, K. L. (2017a). Production, use, and fate of all plastics ever made. *Science Advances*, *3*(7), e1700782. <https://doi.org/doi:10.1126/sciadv.1700782>
- Geyer, R., Jambeck, J. R., & Law, K. L. J. S. a. (2017b). Production, use, and fate of all plastics ever made. *3*(7), e1700782.
- Gianico, A., Braguglia, C. M., Gallipoli, A., Montecchio, D., & Mininni, G. (2021). Land application of biosolids in Europe: possibilities, con-straints and future perspectives. *Water*, *13*(1), 103.
- Glüge, J., Scheringer, M., Cousins, I. T., DeWitt, J. C., Goldenman, G., Herzke, D., Lohmann, R., Ng, C. A., Trier, X., & Wang, Z. (2020). An overview of the uses of per-and polyfluoroalkyl substances (PFAS). *Environmental Science: Processes & Impacts*, *22*(12), 2345-2373.
- Guelfo, J. L., Korzeniowski, S., Mills, M. A., Anderson, J., Anderson, R. H., Arblaster, J. A., Conder, J. M., Cousins, I. T., Dasu, K., & Henry, B. J. (2021). Environmental Sources, Chemistry, Fate, and Transport of Per-and Polyfluoroalkyl Substances: State of the Science, Key Knowledge Gaps, and Recommendations Presented at the August 2019 SETAC Focus Topic Meeting. *Environmental toxicology and chemistry*, *40*(12), 3234-3260.
- Guo, X., Lv, M., Li, J., Ding, J., Wang, Y., Fu, L., Sun, X., Han, X., & Chen, L. (2022). The distinct toxicity effects between commercial and realistic polystyrene microplastics on microbiome and histopathology of gut in zebrafish. *Journal of Hazardous Materials*, *434*, 128874.
- Halsband, C. (2021). Effects of Biofouling on the Sinking Behavior of Microplastics in Aquatic Environments. In *Handbook of Microplastics in the Environment* (pp. 1-13). Springer.
- Han, Z., Salawu, O. A., Zenobio, J. E., Zhao, Y., & Adeleye, A. S. (2021). Emerging investigator series: immobilization of arsenic in soil by nanoscale zerovalent iron: role of sulfidation and application of machine learning. *Environmental Science: Nano*, *8*(3), 619-633.
- Hansen, M. C., Børresen, M. H., Schlabach, M., & Cornelissen, G. (2010). Sorption of perfluorinated compounds from contaminated water to activated carbon. *Journal of Soils and Sediments*, *10*(2), 179-185.
- Hanun, J. N., Hassan, F., Theresia, L., Chao, H.-R., Bu, H. M., Rajendran, S., Kataria, N., Yeh, C.-F., Show, P. L., & Khoo, K. S. (2023). Weathering effect triggers the sorption enhancement of microplastics against oxybenzone. *Environmental Technology & Innovation*, 103112.
- Harley-Nyang, D., Memon, F. A., Jones, N., & Galloway, T. (2022). Investigation and analysis of microplastics in sewage sludge and biosolids: A case study from one wastewater treatment works in the UK. *Science of the Total Environment*, *823*, 153735.



- Hellsing, M. S., Josefsson, S., Hughes, A. V., & Ahrens, L. (2016). Sorption of perfluoroalkyl substances to two types of minerals. *Chemosphere*, *159*, 385-391.
- Higgins, C. P., & Luthy, R. G. (2006). Sorption of perfluorinated surfactants on sediments. *Environmental science & technology*, *40*(23), 7251-7256.
- Ho, Y.-S., & McKay, G. (1998). Sorption of dye from aqueous solution by peat. *Chemical Engineering Journal*, *70*(2), 115-124.
- Hüffer, T., Weniger, A.-K., & Hofmann, T. (2018a). Sorption of organic compounds by aged polystyrene microplastic particles. *Environmental pollution*, *236*, 218-225.
- Hüffer, T., Weniger, A.-K., & Hofmann, T. J. E. P. (2018b). Sorption of organic compounds by aged polystyrene microplastic particles. *236*, 218-225.
- Jambeck, J. R., Geyer, R., Wilcox, C., Siegler, T. R., Perryman, M., Andrady, A., Narayan, R., & Law, K. L. (2015). Plastic waste inputs from land into the ocean. *Science*, *347*(6223), 768-771. <https://doi.org/doi:10.1126/science.1260352>
- Jaubet, M. L., Hines, E., Elías, R., & Garaffo, G. V. (2021). Factors driving the abundance and distribution of microplastics on sandy beaches in a Southwest Atlantic seaside resort. *Marine Environmental Research*, *171*, 105472.
- Jessieleena, A., Rathinavelu, S., Velmaiel, K. E., John, A. A., Nambi, I. M. J. E. S., & Research, P. (2023). Residential houses—a major point source of microplastic pollution: insights on the various sources, their transport, transformation, and toxicity behaviour. 1-22.
- Ji, Y., Wang, C., Wang, Y., Fu, L., Man, M., & Chen, L. (2020). Realistic polyethylene terephthalate nanoplastics and the size-and surface coating-dependent toxicological impacts on zebrafish embryos. *Environmental Science: Nano*, *7*(8), 2313-2324.
- Jia, C., You, C., & Pan, G. (2010). Effect of temperature on the sorption and desorption of perfluorooctane sulfonate on humic acid. *Journal of Environmental Sciences*, *22*(3), 355-361.
- Jiang, Z., Guo, Z., Zhang, Z., Qi, Y., Pu, C., Wang, Q., Jia, Z., & Xiao, C. (2019). Preparation and properties of bottle-recycled polyethylene terephthalate (PET) filaments. *Textile Research Journal*, *89*(7), 1207-1214.
- Johnson, R. L., Anschutz, A. J., Smolen, J. M., Simcik, M. F., & Penn, R. L. (2007). The adsorption of perfluorooctane sulfonate onto sand, clay, and iron oxide surfaces. *Journal of Chemical & Engineering Data*, *52*(4), 1165-1170.
- Joo, S. H., Liang, Y., Kim, M., Byun, J., & Choi, H. (2021a). Microplastics with adsorbed contaminants: Mechanisms and Treatment. *Environmental Challenges*, 100042.
- Joo, S. H., Liang, Y., Kim, M., Byun, J., & Choi, H. (2021b). Microplastics with adsorbed contaminants: Mechanisms and Treatment. *Environmental Challenges*, *3*, 100042.
- Kameda, Y., Yamada, N., & Fujita, E. (2021). Source-and polymer-specific size distributions of fine microplastics in surface water in an urban river. *Environmental pollution*, *284*, 117516.
- Karapanagioti, H. K., & Werner, D. (2018). Sorption of hydrophobic organic compounds to plastics in the marine environment: sorption and desorption kinetics. In *Hazardous chemicals associated with plastics in the marine environment* (pp. 205-219). Springer.
- Keller, A. A., Wang, H., Zhou, D., Lenihan, H. S., Cherr, G., Cardinale, B. J., Miller, R., & Ji, Z. (2010). Stability and Aggregation of Metal Oxide Nanoparticles in Natural Aqueous Matrices. *Environmental Science & Technology*, *44*(6), 1962-1967. <https://doi.org/10.1021/es902987d>
- Kershaw, P. (2016). *Marine plastic debris and microplastics—Global lessons and research to inspire action and guide policy change*. United Nations Environment Programme.
- Khan, F. R., Patsiou, D., & Catarino, A. I. (2022). Pollutants bioavailability and toxicological risk from microplastics. In *Handbook of Microplastics in the Environment* (pp. 697-736). Springer.
- Khumalo, S. M., Lasich, M., Bakare, B. F., & Rathilal, S. (2022). Sorption of Perfluorinated and Pharmaceutical Compounds in Plastics: A Molecular Simulation Study. *Water*, *14*(12), 1951.

- Klungness, G. D., & Byrne, R. H. (2000). Comparative hydrolysis behavior of the rare earths and yttrium: the influence of temperature and ionic strength. *Polyhedron*, *19*(1), 99-107.
- Knepper, T. P., & Lange, F. T. (2011). *Polyfluorinated chemicals and transformation products* (Vol. 17). Springer Science & Business Media.
- Koelmans, A. A., Bakir, A., Burton, G. A., & Janssen, C. R. (2016). Microplastic as a Vector for Chemicals in the Aquatic Environment: Critical Review and Model-Supported Reinterpretation of Empirical Studies. *Environmental Science & Technology*, *50*(7), 3315-3326. <https://doi.org/10.1021/acs.est.5b06069>
- Kokalj, A. J., Kuehnel, D., Puntar, B., Gotvajn, A. Ž., & Kalčíkova, G. (2019). An exploratory ecotoxicity study of primary microplastics versus aged in natural waters and wastewaters. *Environmental pollution*, *254*, 112980.
- Kong, J., & Yu, S. (2007). Fourier transform infrared spectroscopic analysis of protein secondary structures. *Acta biochimica et biophysica Sinica*, *39*(8), 549-559.
- Kumar, R., Sharma, P., Verma, A., Jha, P. K., Singh, P., Gupta, P. K., Chandra, R., & Prasad, P. V. (2021). Effect of physical characteristics and hydrodynamic conditions on transport and deposition of microplastics in riverine ecosystem. *Water*, *13*(19), 2710.
- Lang, M., Yu, X., Liu, J., Xia, T., Wang, T., Jia, H., & Guo, X. (2020). Fenton aging significantly affects the heavy metal adsorption capacity of polystyrene microplastics. *Science of the Total Environment*, *722*, 137762.
- Lapointe, M., Farner, J. M., Hernandez, L. M., Tufenkji, N. J. E. s., & technology. (2020). Understanding and improving microplastic removal during water treatment: impact of coagulation and flocculation. *54*(14), 8719-8727.
- Lenka, S. P., Kah, M., & Padhye, L. P. (2022). Occurrence and fate of poly-and perfluoroalkyl substances (PFAS) in urban waters of New Zealand. *Journal of hazardous materials*, *428*, 128257.
- Lewis, R. C., Johns, L. E., & Meeker, J. D. (2015). Serum biomarkers of exposure to perfluoroalkyl substances in relation to serum testosterone and measures of thyroid function among adults and adolescents from NHANES 2011–2012. *International journal of environmental research and public health*, *12*(6), 6098-6114.
- Li, X., Li, M., Mei, Q., Niu, S., Wang, X., Xu, H., Dong, B., Dai, X., & Zhou, J. L. (2021). Aging microplastics in wastewater pipeline networks and treatment processes: Physicochemical characteristics and Cd adsorption. *Science of the Total Environment*, *797*, 148940.
- Li, Y., Wang, X., Fu, W., Xia, X., Liu, C., Min, J., Zhang, W., & Crittenden, J. C. (2019). Interactions between nano/micro plastics and suspended sediment in water: Implications on aggregation and settling. *Water Research*, *161*, 486-495.
- Li, Z., Hu, X., Qin, L., & Yin, D. (2020). Evaluating the effect of different modified microplastics on the availability of polycyclic aromatic hydrocarbons. *Water Research*, *170*, 115290.
- Liang, J., Chen, R., Gu, J.-n., Li, J., Shi, F., Xue, Y., Huang, B., Guo, M., Jia, J., & Li, K. (2023). Selective and efficient removal of emerging contaminants by sponge-like manganese ferrite synthesized using a solvent-free method: Crucial role of the three-dimensional porous structure. *Water Research*, *232*, 119685.
- Limbach, L. K., Bereiter, R., Müller, E., Krebs, R., Gälli, R., & Stark, W. J. (2008). Removal of oxide nanoparticles in a model wastewater treatment plant: influence of agglomeration and surfactants on clearing efficiency. *Environmental science & technology*, *42*(15), 5828-5833.
- Liu, P., Li, H., Wu, J., Wu, X., Shi, Y., Yang, Z., Huang, K., Guo, X., & Gao, S. (2022). Polystyrene microplastics accelerated photodegradation of co-existed polypropylene via photosensitization of polymer itself and released organic compounds. *Water Research*, *214*, 118209.

- Liu, P., Lu, K., Li, J., Wu, X., Qian, L., Wang, M., & Gao, S. (2020). Effect of aging on adsorption behavior of polystyrene microplastics for pharmaceuticals: Adsorption mechanism and role of aging intermediates. *Journal of Hazardous Materials*, 384, 121193.
- Liu, P., Qian, L., Wang, H., Zhan, X., Lu, K., Gu, C., & Gao, S. (2019). New insights into the aging behavior of microplastics accelerated by advanced oxidation processes. *Environmental science & technology*, 53(7), 3579-3588.
- Liu, S., Huang, Y., Luo, D., Wang, X., Wang, Z., Ji, X., Chen, Z., Dahlgren, R. A., Zhang, M., & Shang, X. (2022). Integrated effects of polymer type, size and shape on the sinking dynamics of biofouled microplastics. *Water Research*, 220, 118656.
- Liu, X., Deng, Q., Zheng, Y., Wang, D., & Ni, B.-J. (2022). Microplastics aging in wastewater treatment plants: Focusing on physicochemical characteristics changes and corresponding environmental risks. *Water Research*, 221, 118780.
- Liu, X., Deng, Q., Zheng, Y., Wang, D., & Ni, B.-J. J. W. R. (2022). Microplastics aging in wastewater treatment plants: Focusing on physicochemical characteristics changes and corresponding environmental risks. 221, 118780.
- Liu, X., Sun, P., Qu, G., Jing, J., Zhang, T., Shi, H., & Zhao, Y. J. J. o. H. M. (2021). Insight into the characteristics and sorption behaviors of aged polystyrene microplastics through three type of accelerated oxidation processes. 407, 124836.
- Liu, Z., Adyel, T. M., Miao, L., You, G., Liu, S., & Hou, J. J. E. P. (2021). Biofilm influenced metal accumulation onto plastic debris in different freshwaters. 285, 117646.
- Llorca, M., Schirinzi, G., Martínez, M., Barceló, D., & Farré, M. (2018). Adsorption of perfluoroalkyl substances on microplastics under environmental conditions. *Environmental pollution*, 235, 680-691.
- Lohmann, R. (2012). Critical review of low-density polyethylene's partitioning and diffusion coefficients for trace organic contaminants and implications for its use as a passive sampler. *Environmental science & technology*, 46(2), 606-618.
- Lu, D., Sha, S., Luo, J., Huang, Z., & Jackie, X. Z. (2020). Treatment train approaches for the remediation of per-and polyfluoroalkyl substances (PFAS): A critical review. *Journal of hazardous materials*, 386, 121963.
- Luo, H., Liu, C., He, D., Xu, J., Sun, J., Li, J., & Pan, X. (2022). Environmental behaviors of microplastics in aquatic systems: a systematic review on degradation, adsorption, toxicity and biofilm under aging conditions. *Journal of Hazardous Materials*, 423, 126915.
- Luo, H., Tu, C., He, D., Zhang, A., Sun, J., Li, J., Xu, J., & Pan, X. (2023). Interactions between microplastics and contaminants: A review focusing on the effect of aging process. *Science of the Total Environment*, 165615.
- Malygina, N., Mitrofanova, E., Kuryatnikova, N., Biryukov, R., Zolotov, D., Pershin, D., & Chernykh, D. (2021). Microplastic Pollution in the Surface Waters from Plain and Mountainous Lakes in Siberia, Russia. *Water*, 13(16), 2287. <https://www.mdpi.com/2073-4441/13/16/2287>
- Mao, R., Lang, M., Yu, X., Wu, R., Yang, X., & Guo, X. (2020). Aging mechanism of microplastics with UV irradiation and its effects on the adsorption of heavy metals. *Journal of Hazardous Materials*, 393, 122515.
- Mattsson, K., Björkroth, F., Karlsson, T., & Hassellöv, M. (2021). Nanofragmentation of expanded polystyrene under simulated environmental weathering (thermooxidative degradation and hydrodynamic turbulence). *Frontiers in Marine Science*, 7, 578178.
- McCormick, A. R., Hoellein, T. J., London, M. G., Hittie, J., Scott, J. W., & Kelly, J. J. (2016). Microplastic in surface waters of urban rivers: concentration, sources, and associated bacterial assemblages. *Ecosphere*, 7(11), e01556.

- McDonough, L. K., Santos, I. R., Andersen, M. S., O'Carroll, D. M., Rutledge, H., Meredith, K., Oudone, P., Bridgeman, J., Goody, D. C., & Sorensen, J. P. R. (2020). Changes in global groundwater organic carbon driven by climate change and urbanization. *Nature Communications*, *11*(1), 1279.
- McGuinty, E., & Walker, T. R. (2023). Solutions, approaches and mitigation strategies for plastic waste management. In *Plastic pollution in the global ocean* (pp. 375-398).
- Meegoda, J. N., Kewalramani, J. A., Li, B., & Marsh, R. W. (2020). A review of the applications, environmental release, and remediation technologies of per-and polyfluoroalkyl substances. *International journal of environmental research and public health*, *17*(21), 8117.
- Mejías, C., Martín, J., Santos, J. L., Aparicio, I., & Alonso, E. (2023). Adsorption of perfluoroalkyl substances on polyamide microplastics: Effect of sorbent and influence of environmental factors. *Environmental Research*, *216*, 114834.
- Meng, L., Tian, H., Lv, J., Wang, Y., & Jiang, G. (2023). Influence of microplastics on the photodegradation of perfluorooctane sulfonamide (FOSA). *Journal of Environmental Sciences*, *127*, 791-798.
- Müller, A., Becker, R., Dorgerloh, U., Simon, F.-G., & Braun, U. (2018). The effect of polymer aging on the uptake of fuel aromatics and ethers by microplastics. *Environmental pollution*, *240*, 639-646.
- Neale, P. A., Antony, A., Gernjak, W., Leslie, G., & Escher, B. I. (2011). Natural versus wastewater derived dissolved organic carbon: Implications for the environmental fate of organic micropollutants. *Water research*, *45*(14), 4227-4237.
- Nguyen, H. T., Kaserzon, S. L., Thai, P. K., Vijayasathy, S., Bräunig, J., Crosbie, N. D., Bignert, A., & Mueller, J. F. (2019). Temporal trends of per-and polyfluoroalkyl substances (PFAS) in the influent of two of the largest wastewater treatment plants in Australia. *Emerging Contaminants*, *5*, 211-218.
- Nguyen, H. T., McLachlan, M. S., Tschärke, B., Thai, P., Braeunig, J., Kaserzon, S., O'Brien, J. W., & Mueller, J. F. (2022). Background release and potential point sources of per-and polyfluoroalkyl substances to municipal wastewater treatment plants across Australia. *Chemosphere*, *293*, 133657.
- Nguyen, T. M. H., Bräunig, J., Thompson, K., Thompson, J., Kabiri, S., Navarro, D. A., Kookana, R. S., Grimison, C., Barnes, C. M., & Higgins, C. P. (2020). Influences of chemical properties, soil properties, and solution pH on soil–water partitioning coefficients of per-and polyfluoroalkyl substances (PFASs). *Environmental science & technology*, *54*(24), 15883-15892.
- Noyma, N. P., de Magalhaes, L., Furtado, L. L., Mucci, M., van Oosterhout, F., Huszar, V. L. M., Marinho, M. M., & Lüring, M. (2016). Controlling cyanobacterial blooms through effective flocculation and sedimentation with combined use of flocculants and phosphorus adsorbing natural soil and modified clay. *Water Research*, *97*, 26-38.
- OECD. (2001). Organization of the Economic Collaboration and Development. Guideline for the testing of chemicals 303 A, Simulation Test - Aerobic Sewage Treatment Activated Sludge Unit; . OECD: Paris, 2001,
- OECD. (2018). Toward a New Comprehensive Global Database of Per-and Polyfluoroalkyl Substances (PFASs): Summary Report on Updating the OECD 2007 List of Per and Polyfluoroalkyl Substances (PFASs).
- Olsson, M. (2014). *The Cost of Inaction: A Socioeconomic analysis of costs linked to effects of endocrine disrupting substances on male reproductive health*. Nordic Council of Ministers.
- Ouyang, Z., Zhang, Z., Jing, Y., Bai, L., Zhao, M., Hao, X., Li, X., & Guo, X. (2022). The photo-aging of polyvinyl chloride microplastics under different UV irradiations. *Gondwana Research*, *108*, 72-80.
- Parashar, N., & Hait, S. (2023). Recent advances on microplastics pollution and removal from wastewater systems: A critical review. *Journal of Environmental Management*, *340*, 118014.
- Parashar, N., Mahanty, B., & Hait, S. (2023). Microplastics as carriers of per-and polyfluoroalkyl substances (PFAS) in aquatic environment: interactions and ecotoxicological effects.

- Park, M., Wu, S., Lopez, I. J., Chang, J. Y., Karanfil, T., & Snyder, S. A. (2020). Adsorption of perfluoroalkyl substances (PFAS) in groundwater by granular activated carbons: Roles of hydrophobicity of PFAS and carbon characteristics. *Water research*, *170*, 115364.
- Petroody, S. S. A., Hashemi, S. H., & van Gestel, C. A. M. (2020). Factors affecting microplastic retention and emission by a wastewater treatment plant on the southern coast of Caspian Sea. *Chemosphere*, *261*, 128179.
- Podder, A., Sadmani, A. A., Reinhart, D., Chang, N.-B., & Goel, R. (2021). Per and poly-fluoroalkyl substances (PFAS) as a contaminant of emerging concern in surface water: a transboundary review of their occurrences and toxicity effects. *Journal of hazardous materials*, *419*, 126361.
- Popa, P., Timofti, M., Voiculescu, M., Dragan, S., Trif, C., & Georgescu, L. P. (2012). Study of physico-chemical characteristics of wastewater in an urban agglomeration in Romania. *The Scientific World Journal*, *2012*.
- Powell, B. A., Miller, T., & Kaplan, D. I. (2015). On the influence of ionic strength on radium and strontium sorption to sandy loam soils. *Journal of the South Carolina Academy of Science*, *13*(1), 4.
- Pozzebon, E. A., & Seifert, L. (2023). Emerging environmental health risks associated with the land application of biosolids: a scoping review. *Environmental Health*, *22*(1), 1-15.
- Priya, K., Renjith, K., Joseph, C. J., Indu, M., Srinivas, R., & Haddout, S. (2022). Fate, transport and degradation pathway of microplastics in aquatic environment—A critical review. *Regional Studies in Marine Science*, 102647.
- Prot, T., Korving, L., & van Loosdrecht, M. (2020). Ionic strength of the liquid phase of different sludge streams in a wastewater treatment plant.
- Rahman, M. F., Peldszus, S., & Anderson, W. B. (2014). Behaviour and fate of perfluoroalkyl and polyfluoroalkyl substances (PFASs) in drinking water treatment: A review. *Water Research*, *50*, 318-340.
- Rangel-Buitrago, N., Ochoa, F. L., Rodríguez, R. D. B., Moreno, J. B., Trilleras, J., Arana, V. A., & Neal, W. J. (2023). Decoding plastic pollution in the geological record: A baseline study on the Caribbean Coast of Colombia, north South America. *Marine Pollution Bulletin*, *192*, 114993.
- Regan, S., Hynds, P., & Flynn, R. (2017). An overview of dissolved organic carbon in groundwater and implications for drinking water safety. *Hydrogeology Journal*, *25*(4), 959.
- Rochman, C. M., Tahir, A., Williams, S. L., Baxa, D. V., Lam, R., Miller, J. T., Teh, F.-C., Werorilangi, S., & Teh, S. J. (2015). Anthropogenic debris in seafood: Plastic debris and fibers from textiles in fish and bivalves sold for human consumption. *Scientific reports*, *5*(1), 1-10.
- Rummel, C. D., Jahnke, A., Gorokhova, E., Kühnel, D., & Schmitt-Jansen, M. (2017). Impacts of biofilm formation on the fate and potential effects of microplastic in the aquatic environment. *Environmental science & technology letters*, *4*(7), 258-267.
- Saalidong, B. M., Aram, S. A., Otu, S., & Lartey, P. O. (2022). Examining the dynamics of the relationship between water pH and other water quality parameters in ground and surface water systems. *PloS one*, *17*(1), e0262117.
- Sacks, V. P., & Lohmann, R. (2011). Development and use of polyethylene passive samplers to detect triclosans and alkylphenols in an urban estuary. *Environmental science & technology*, *45*(6), 2270-2277.
- Sait, S. T., Sørensen, L., Kubowicz, S., Vike-Jonas, K., Gonzalez, S. V., Asimakopoulos, A. G., & Booth, A. M. (2021). Microplastic fibres from synthetic textiles: Environmental degradation and additive chemical content. *Environmental pollution*, *268*, 115745.
- Salawu, O., & Adeleye, A. S. (2023). Adsorption of PFAS onto secondary microplastics: A mechanistic study.

- Salawu, O. A., Han, Z., & Adeleye, A. S. (2022). Shrimp Waste-derived Porous Carbon Adsorbent: Performance, Mechanism, and Application of Machine Learning. *Journal of hazardous materials*, 129266.
- Saleh, T. A. (2015). Isotherm, kinetic, and thermodynamic studies on Hg (II) adsorption from aqueous solution by silica-multiwall carbon nanotubes. *Environmental Science and Pollution Research*, 22(21), 16721-16731.
- Satpathy, K. K., Mohanty, A. K., Natesan, U., Prasad, M. V. R., & Sarkar, S. K. (2010). Seasonal variation in physicochemical properties of coastal waters of Kalpakkam, east coast of India with special emphasis on nutrients. *Environmental monitoring and assessment*, 164, 153-171.
- Schaidler, L. A., Balan, S. A., Blum, A., Andrews, D. Q., Strynar, M. J., Dickinson, M. E., Lunderberg, D. M., Lang, J. R., & Peaslee, G. F. (2017). Fluorinated compounds in US fast food packaging. *Environmental science & technology letters*, 4(3), 105-111.
- Schultz, M. M., Higgins, C. P., Huset, C. A., Luthy, R. G., Barofsky, D. F., & Field, J. A. (2006). Fluorochemical mass flows in a municipal wastewater treatment facility. *Environmental science & technology*, 40(23), 7350-7357.
- Scott, J. W., Gunderson, K. G., Green, L. A., Rediske, R. R., & Steinman, A. D. (2021). Perfluoroalkylated substances (Pfas) associated with microplastics in a lake environment. *Toxics*, 9(5), 106.
- Senevirathna, S., Tanaka, S., Fujii, S., Kunacheva, C., Harada, H., Shivakoti, B. R., & Okamoto, R. (2010). A comparative study of adsorption of perfluorooctane sulfonate (PFOS) onto granular activated carbon, ion-exchange polymers and non-ion-exchange polymers. *Chemosphere*, 80(6), 647-651.
- Shah, F., & Wu, W. J. A. i. a. (2020). Use of plastic mulch in agriculture and strategies to mitigate the associated environmental concerns. *164*, 231-287.
- Shams, M., Alam, I., & Chowdhury, I. (2021). Interactions of nanoscale plastics with natural organic matter and silica surfaces using a quartz crystal microbalance. *Water Research*, 197, 117066.
- Shao, Y., Zhou, X., Liu, X., & Wang, L. (2020). Pre-oxidation-induced change of physicochemical characteristics and removal behaviours in conventional drinking water treatment processes for polyethylene microplastics. *RSC advances*, 10(68), 41488-41494.
- Shi, Y., Liu, P., Wu, X., Shi, H., Huang, H., Wang, H., & Gao, S. (2021). Insight into chain scission and release profiles from photodegradation of polycarbonate microplastics. *Water Research*, 195, 116980.
- Shih, K., & Wang, F. (2013). Adsorption behavior of perfluorochemicals (PFCs) on boehmite: influence of solution chemistry. *Procedia Environmental Sciences*, 18, 106-113.
- Shim, W. J., Hong, S. H., & Eo, S. (2018). Chapter 1 - Marine Microplastics: Abundance, Distribution, and Composition. In E. Y. Zeng (Ed.), *Microplastic Contamination in Aquatic Environments* (pp. 1-26). Elsevier. <https://doi.org/https://doi.org/10.1016/B978-0-12-813747-5.00001-1>
- Siriwardena, D. P., Crimi, M., Holsen, T. M., Bellona, C., Divine, C., & Dickenson, E. (2019). Influence of groundwater conditions and co-contaminants on sorption of perfluoroalkyl compounds on granular activated carbon. *Remediation Journal*, 29(3), 5-15.
- Smalling, K. L., Romanok, K. M., Bradley, P. M., Morriss, M. C., Gray, J. L., Kanagy, L. K., Gordon, S. E., Williams, B. M., Breitmeyer, S. E., & Jones, D. K. (2023). Per-and polyfluoroalkyl substances (PFAS) in United States tapwater: Comparison of underserved private-well and public-supply exposures and associated health implications. *Environment International*, 108033.
- Song, Y. K., Hong, S. H., Jang, M., Han, G. M., Jung, S. W., & Shim, W. J. (2017). Combined effects of UV exposure duration and mechanical abrasion on microplastic fragmentation by polymer type. *Environmental Science & Technology*, 51(8), 4368-4376.
- Suja, F., Pramanik, B. K., & Zain, S. M. (2009). Contamination, bioaccumulation and toxic effects of perfluorinated chemicals (PFCs) in the water environment: a review paper. *Water Science and Technology*, 60(6), 1533-1544.

- Sun, J., Dai, X., Wang, Q., van Loosdrecht, M. C. M., & Ni, B.-J. (2019). Microplastics in wastewater treatment plants: Detection, occurrence and removal. *Water Research*, *152*, 21-37.
- Sunderland, E. M., Hu, X. C., Dassuncao, C., Tokranov, A. K., Wagner, C. C., & Allen, J. G. (2019). A review of the pathways of human exposure to poly-and perfluoroalkyl substances (PFASs) and present understanding of health effects. *Journal of exposure science & environmental epidemiology*, *29*(2), 131-147.
- Talvitie, J., Mikola, A., Koistinen, A., & Setälä, O. (2017). Solutions to microplastic pollution—Removal of microplastics from wastewater effluent with advanced wastewater treatment technologies. *Water research*, *123*, 401-407.
- Tang, H. L., & Chen, H. (2015). Nitrification at full-scale municipal wastewater treatment plants: Evaluation of inhibition and bioaugmentation of nitrifiers. *Bioresource technology*, *190*, 76-81.
- Tarapore, P., & Ouyang, B. (2021). Perfluoroalkyl Chemicals and Male Reproductive Health: Do PFOA and PFOS Increase Risk for Male Infertility? *International Journal of Environmental Research and Public Health*, *18*(7), 3794.
- Tavasoli, E., Luek, J. L., Malley, J. P., & Mouser, P. J. (2021). Distribution and fate of per-and polyfluoroalkyl substances (PFAS) in wastewater treatment facilities. *Environmental Science: Processes & Impacts*, *23*(6), 903-913.
- Ter Halle, A., Jeanneau, L., Martignac, M., Jardé, E., Pedrono, B., Brach, L., & Gigault, J. (2017). Nanoplastic in the North Atlantic Subtropical Gyre. *Environmental Science & Technology*, *51*(23), 13689-13697. <https://doi.org/10.1021/acs.est.7b03667>
- Thompson, R. C., Moore, C. J., Vom Saal, F. S., & Swan, S. H. (2009). Plastics, the environment and human health: current consensus and future trends. *Philosophical transactions of the royal society B: biological sciences*, *364*(1526), 2153-2166.
- Uurasjärvi, E., Hartikainen, S., Setälä, O., Lehtiniemi, M., & Koistinen, A. (2020). Microplastic concentrations, size distribution, and polymer types in the surface waters of a northern European lake. *Water Environment Research*, *92*(1), 149-156.
- Vieira, Y., Lima, E. C., Foletto, E. L., & Dotto, G. L. (2021). Microplastics physicochemical properties, specific adsorption modeling and their interaction with pharmaceuticals and other emerging contaminants. *Science of the total environment*, *753*, 141981.
- Vivekanand, A. C., Mohapatra, S., & Tyagi, V. K. J. C. (2021). Microplastics in aquatic environment: Challenges and perspectives. *282*, 131151.
- Waldschläger, K., & Schüttrumpf, H. (2019). Effects of particle properties on the settling and rise velocities of microplastics in freshwater under laboratory conditions. *Environmental science & technology*, *53*(4), 1958-1966.
- Wang, C., Xian, Z., Jin, X., Liang, S., Chen, Z., Pan, B., Wu, B., Ok, Y. S., & Gu, C. (2020). Photo-aging of polyvinyl chloride microplastic in the presence of natural organic acids. *Water Research*, *183*, 116082.
- Wang, F., & Shih, K. (2011). Adsorption of perfluorooctanesulfonate (PFOS) and perfluorooctanoate (PFOA) on alumina: Influence of solution pH and cations. *Water Research*, *45*(9), 2925-2930.
- Wang, F., Shih, K. M., & Li, X. Y. (2015). The partition behavior of perfluorooctanesulfonate (PFOS) and perfluorooctanesulfonamide (FOSA) on microplastics. *Chemosphere*, *119*, 841-847.
- Wang, F., Zhang, M., Sha, W., Wang, Y., Hao, H., Dou, Y., & Li, Y. (2020). Sorption Behavior and Mechanisms of Organic Contaminants to Nano and Microplastics. *Molecules*, *25*(8), 1827. <https://www.mdpi.com/1420-3049/25/8/1827>
- Wang, H., Adeleye, A. S., Huang, Y., Li, F., & Keller, A. A. (2015). Heteroaggregation of nanoparticles with biocolloids and geocolloids [Review]. *Adv Colloid Interface Sci*, *226*(Pt A), 24-36. <https://doi.org/10.1016/j.cis.2015.07.002>

- Wang, T., Yu, C., Chu, Q., Wang, F., Lan, T., & Wang, J. (2020). Adsorption behavior and mechanism of five pesticides on microplastics from agricultural polyethylene films. *Chemosphere*, 244, 125491.
- Wang, Z., DeWitt, J. C., Higgins, C. P., & Cousins, I. T. (2017). A never-ending story of per-and polyfluoroalkyl substances (PFASs)? In: ACS Publications.
- Wang, Z., Ding, J., Razanajatovo, R. M., Huang, J., Zheng, L., Zou, H., Wang, Z., & Liu, J. (2022). Sorption of selected pharmaceutical compounds on polyethylene microplastics: Roles of pH, aging, and competitive sorption. *Chemosphere*, 307, 135561.
- Wei, C., Yin, S., Fu, H., Qu, X., Mitch, W. A., & Zhu, D. (2020). Sulfide-induced reduction of nitrobenzene mediated by different size fractions of rice straw-derived black carbon: A key role played by reactive polysulfide species. *Science of the Total Environment*, 748, 141365.
- Weinstein, J. E., Crocker, B. K., & Gray, A. D. (2016). From macroplastic to microplastic: Degradation of high-density polyethylene, polypropylene, and polystyrene in a salt marsh habitat. *Environmental toxicology and chemistry*, 35(7), 1632-1640.
- Windsor, F. M., Durance, I., Horton, A. A., Thompson, R. C., Tyler, C. R., & Ormerod, S. J. (2019). A catchment-scale perspective of plastic pollution. *Global Change Biology*, 25(4), 1207-1221.
- Wong, J. K. H., Lee, K. K., Tang, K. H. D., & Yap, P.-S. (2020). Microplastics in the freshwater and terrestrial environments: Prevalence, fates, impacts and sustainable solutions. *Science of the Total Environment*, 719, 137512.
- Wu, X., Liu, P., Huang, H., & Gao, S. (2020). Adsorption of triclosan onto different aged polypropylene microplastics: critical effect of cations. *Science of the Total Environment*, 717, 137033.
- Wu, X., Zhao, X., Chen, R., Liu, P., Liang, W., Wang, J., Teng, M., Wang, X., & Gao, S. (2022a). Wastewater treatment plants act as essential sources of microplastic formation in aquatic environments: A critical review. *Water Research*, 221, 118825.
- Wu, X., Zhao, X., Chen, R., Liu, P., Liang, W., Wang, J., Teng, M., Wang, X., & Gao, S. J. W. R. (2022b). Wastewater treatment plants act as essential sources of microplastic formation in aquatic environments: A critical review. 221, 118825.
- Xiao, F., Zhang, X., Penn, L., Gulliver, J. S., & Simcik, M. F. (2011). Effects of monovalent cations on the competitive adsorption of perfluoroalkyl acids by kaolinite: experimental studies and modeling. *Environmental science & technology*, 45(23), 10028-10035.
- Xu, C., Chen, H., & Jiang, F. (2015). Adsorption of perfluorooctane sulfonate (PFOS) and perfluorooctanoate (PFOA) on polyaniline nanotubes. *Colloids and Surfaces A: Physicochemical and Engineering Aspects*, 479, 60-67.
- Xu, X., Jian, Y., Xue, Y., Hou, Q., & Wang, L. (2019). Microplastics in the wastewater treatment plants (WWTPs): occurrence and removal. *Chemosphere*, 235, 1089-1096.
- Yan, T., Chen, H., Jiang, F., & Wang, X. (2014). Adsorption of perfluorooctane sulfonate and perfluorooctanoic acid on magnetic mesoporous carbon nitride. *Journal of Chemical & Engineering Data*, 59(2), 508-515.
- Yao, J., Wen, J., Li, H., & Yang, Y. (2022). Surface functional groups determine adsorption of pharmaceuticals and personal care products on polypropylene microplastics. *Journal of hazardous materials*, 423, 127131.
- Ying, J., Qin, X., Wen, D., Huang, F., & Liu, F. (2022). Water with low ionic strength recovers the passivated birnessite-coated sand reactivity towards lincomycin removal. *Environmental pollution*, 315, 120306.
- You, C., Jia, C., & Pan, G. (2010). Effect of salinity and sediment characteristics on the sorption and desorption of perfluorooctane sulfonate at sediment-water interface. *Environmental pollution*, 158(5), 1343-1347.



- Yu, F., Li, Y., Huang, G., Yang, C., Chen, C., Zhou, T., Zhao, Y., & Ma, J. (2020). Adsorption behavior of the antibiotic levofloxacin on microplastics in the presence of different heavy metals in an aqueous solution. *Chemosphere*, *260*, 127650.
- Yu, Q., Zhang, R., Deng, S., Huang, J., & Yu, G. (2009). Sorption of perfluorooctane sulfonate and perfluorooctanoate on activated carbons and resin: Kinetic and isotherm study. *Water research*, *43*(4), 1150-1158.
- Zenobio, J. E., Salawu, O. A., Han, Z., & Adeleye, A. S. (2022a). Adsorption of per- and polyfluoroalkyl substances (PFAS) to containers. *Journal of Hazardous Materials Advances*, *7*, 100130. <https://doi.org/https://doi.org/10.1016/j.hazadv.2022.100130>
- Zenobio, J. E., Salawu, O. A., Han, Z., & Adeleye, A. S. (2022b). Adsorption of per-and polyfluoroalkyl substances (PFAS) to containers. *Journal of Hazardous Materials Advances*, *7*, 100130.
- Zha, F., Shang, M., Ouyang, Z., & Guo, X. (2022). The aging behaviors and release of microplastics: A review. *Gondwana Research*, *108*, 60-71.
- Zhan, Z., Wang, J., Peng, J., Xie, Q., Huang, Y., & Gao, Y. (2016). Sorption of 3, 3', 4, 4'-tetrachlorobiphenyl by microplastics: a case study of polypropylene. *Marine pollution bulletin*, *110*(1), 559-563.
- Zhang, B., Song, X., Zhang, Y., Han, D., Tang, C., Yu, Y., & Ma, Y. (2012). Hydrochemical characteristics and water quality assessment of surface water and groundwater in Songnen plain, Northeast China. *Water research*, *46*(8), 2737-2748.
- Zhang, D. Q., Zhang, W. L., & Liang, Y. N. (2019). Adsorption of perfluoroalkyl and polyfluoroalkyl substances (PFASs) from aqueous solution-A review. *Science of the total environment*, *694*, 133606.
- Zhang, H., Wang, J., Zhou, B., Zhou, Y., Dai, Z., Zhou, Q., Christie, P., & Luo, Y. (2018). Enhanced adsorption of oxytetracycline to weathered microplastic polystyrene: kinetics, isotherms and influencing factors. *Environmental pollution*, *243*, 1550-1557.
- Zhang, K., Hamidian, A. H., Tubić, A., Zhang, Y., Fang, J. K., Wu, C., & Lam, P. K. (2021a). Understanding plastic degradation and microplastic formation in the environment: A review. *Environmental pollution*, *274*, 116554.
- Zhang, K., Hamidian, A. H., Tubić, A., Zhang, Y., Fang, J. K. H., Wu, C., & Lam, P. K. S. (2021b). Understanding plastic degradation and microplastic formation in the environment: A review. *Environmental pollution*, *274*, 116554.
- Zhang, R., Yan, W., & Jing, C. (2014). Mechanistic study of PFOS adsorption on kaolinite and montmorillonite. *Colloids and Surfaces A: Physicochemical and Engineering Aspects*, *462*, 252-258.
- Zhao, L., Bian, J., Zhang, Y., Zhu, L., & Liu, Z. (2014). Comparison of the sorption behaviors and mechanisms of perfluorosulfonates and perfluorocarboxylic acids on three kinds of clay minerals. *Chemosphere*, *114*, 51-58.
- Zhao, M., Zhang, T., Yang, X., Liu, X., Zhu, D., & Chen, W. (2021). Sulfide induces physical damages and chemical transformation of microplastics via radical oxidation and sulfide addition. *Water Research*, *197*, 117100.
- Ziajahromi, S., Neale, P. A., Rintoul, L., & Leusch, F. D. L. (2017). Wastewater treatment plants as a pathway for microplastics: development of a new approach to sample wastewater-based microplastics. *Water research*, *112*, 93-99.

Appendix

Supplementary materials for chapter 3

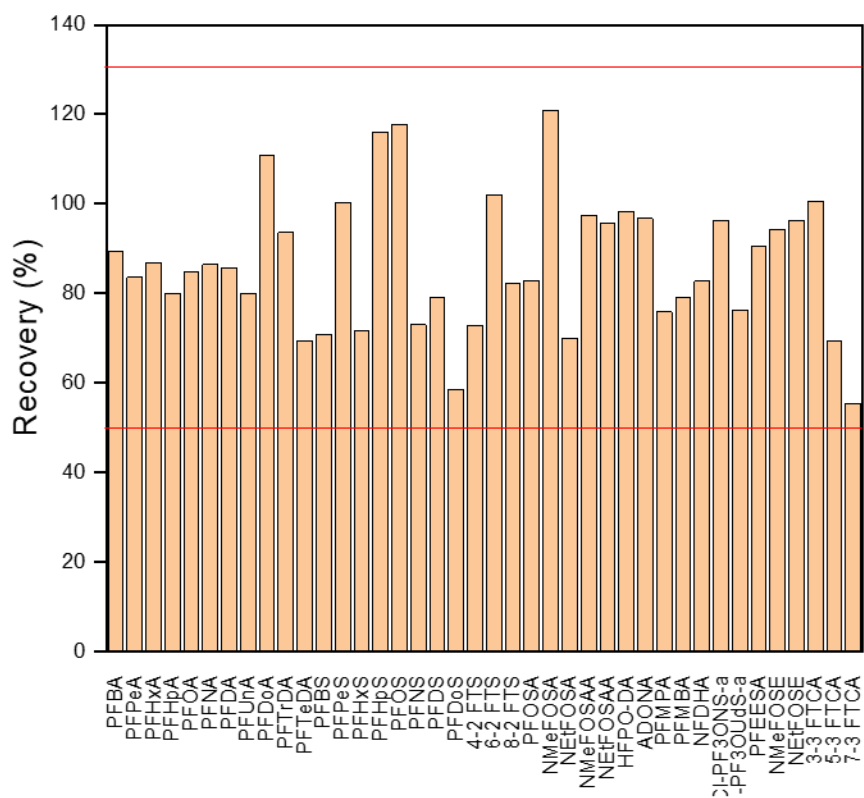


Figure A1. Recovery of target analyte from laboratory blanks

Table A1. List of 40 analytes analyzed in this study.

Analyte Name	Acronym	CAS Number	Chemical Formula	Molecular Weight (g/mol)	Chain Length	Quantification reference
Perfluoroalkyl Carboxylic Acids (PFCAs)						
Perfluorobutanoic acid	PFBA	375-22-4	C <sub>4</sub> HF <sub>7</sub> O <sub>2</sub>	214.03	C4	<sup>13</sup> C <sub>4</sub> -PFBA
Perfluoropentanoic acid	PFPeA	2706-90-3	C <sub>5</sub> HF <sub>9</sub> O <sub>2</sub>	264.05	C5	<sup>13</sup> C <sub>5</sub> -PFPeA
Perfluorohexanoic acid	PFHxA	307-24-4	C <sub>6</sub> HF <sub>11</sub> O <sub>2</sub>	314.05	C6	<sup>13</sup> C <sub>5</sub> -PFHxA
Perfluoroheptanoic acid	PFHpA	375-85-9	C <sub>7</sub> HF <sub>13</sub> O <sub>2</sub>	364.06	C7	<sup>13</sup> C <sub>4</sub> -PFHpA
Perfluorooctanoic acid	PFOA	335-67-1	C <sub>8</sub> HF <sub>15</sub> O <sub>2</sub>	414.07	C8	<sup>13</sup> C <sub>8</sub> -PFOA
Perfluorononanoic acid	PFNA	375-95-1	C <sub>9</sub> HF <sub>17</sub> O <sub>2</sub>	464.08	C9	<sup>13</sup> C <sub>9</sub> -PFNA
Perfluorodecanoic acid	PFDA	335-76-2	C <sub>10</sub> HF <sub>19</sub> O <sub>2</sub>	514.08	C10	<sup>13</sup> C <sub>6</sub> -PFDA
Perfluoroundecanoic acid	PFUnA	2058-94-8	C <sub>11</sub> HF <sub>21</sub> O <sub>2</sub>	564.09	C11	<sup>13</sup> C <sub>7</sub> -PFUnA
Perfluorododecanoic acid	PFDoA	307-55-1	C <sub>12</sub> HF <sub>23</sub> O <sub>2</sub>	614.1	C12	<sup>13</sup> C <sub>2</sub> -PFDoA
Perfluorotridecanoic acid	PFTTrDA	72629-94-8	C <sub>13</sub> HF <sub>25</sub> O <sub>2</sub>	664.1	C13	<sup>13</sup> C <sub>2</sub> -PFDoA
Perfluorotetradecanoic acid	PFTeDA	376-06-7	C <sub>14</sub> HO <sub>2</sub> F <sub>27</sub>	714.11	C14	<sup>13</sup> C <sub>2</sub> -PFTeDA
Pefluorinated Sulfonic Acids						
Perfluorobutanesulfonic acid	PFBS	375-73-5	C <sub>4</sub> HF <sub>9</sub> O <sub>3</sub> S	300.1	C4	<sup>13</sup> C <sub>3</sub> -PFBS
Perfluoropentanesulfonic acid	PFPeS	2706-91-4	C <sub>5</sub> H <sub>12</sub> O <sub>3</sub> S	152.211	C5	<sup>13</sup> C <sub>3</sub> -PFHxS
Perfluorohexanesulfonic acid	PFHxS	355-46-4	C <sub>6</sub> H <sub>14</sub> O <sub>3</sub> S	166.24	C6	<sup>13</sup> C <sub>3</sub> -PFHxS
Perfluoroheptanesulfonic acid	PFHpS	375-92-8	C <sub>7</sub> H <sub>16</sub> O <sub>3</sub> S	180.26	C7	<sup>13</sup> C <sub>8</sub> -PFOS
Perfluorooctanesulfonic acid	PFOS	1763-23-1	C <sub>8</sub> HF <sub>17</sub> O <sub>3</sub> S	500.13	C8	<sup>13</sup> C <sub>8</sub> -PFOS
Perfluorononanesulfonic acid	PFNS	68259-12-1	C <sub>9</sub> HF <sub>19</sub> O <sub>3</sub> S	550.14	C9	<sup>13</sup> C <sub>8</sub> -PFOS

Perfluorodecanesulfonic acid	PFDS	335-77-3	C <sub>10</sub> HF <sub>21</sub> O <sub>3</sub> S	600.15	C10	<sup>13</sup> C <sub>8</sub> -PFOS
Perfluorododecanesulfonic acid	PFDoS	79780-39-5	C <sub>12</sub> HF <sub>23</sub> O <sub>3</sub> S	700.16	C12	<sup>13</sup> C <sub>8</sub> -PFOS
Fluorotelomer carboxylic acids						
3-Perfluoropropyl propanoic acid	3:3 FTCA	356-02-5	C <sub>6</sub> H <sub>5</sub> F <sub>7</sub> O <sub>2</sub>	242.09	C6	<sup>13</sup> C <sub>5</sub> -PFPeA
2H,2H,3H,3H-Perfluorooctanoic acid	5:3 FTCA	914637-49-3	C <sub>8</sub> H <sub>5</sub> F <sub>11</sub> O <sub>2</sub>	342.11	C8	<sup>13</sup> C <sub>5</sub> -PFHxA
3-Perfluoroheptyl propanoic acid	7:3 FTCA	812-70-4	C <sub>10</sub> H <sub>5</sub> F <sub>15</sub> O <sub>2</sub>	442.13	C10	<sup>13</sup> C <sub>5</sub> -PFHxA
Perfluorooctane Sulfonamides and Derivatives						
Perfluoro-1-octanesulfonamide	PFOSA	754-91-6	C <sub>8</sub> H <sub>2</sub> F <sub>17</sub> NO <sub>2</sub> S	499.15	C8	<sup>13</sup> C <sub>8</sub> -PFOSA
N-Ethylperfluoro-1-octanesulfonamide	N-EtFOSA	4151-50-2	C <sub>12</sub> H <sub>8</sub> F <sub>17</sub> NO <sub>4</sub> S	585.23	C12	D <sub>5</sub> -NEtFOSA
N-Methylperfluoro octanesulfonamide	N-MeFOSA	31506-32-8	C <sub>11</sub> H <sub>6</sub> F <sub>17</sub> NO <sub>4</sub> S	571.21	C11	D <sub>3</sub> -NMeFOSA
Perfluorooctane sulfonamidoacetic acids						
N-ethylperfluoro-1-octanesulfonamidoacetic acid	NEtFOSAA	2991-50-6	C <sub>12</sub> H <sub>8</sub> F <sub>17</sub> NO <sub>4</sub> S	585.23	C12	D <sub>5</sub> -N-EtFOSAA
N-methylperfluoro-1-octanesulfonamidoacetic acid	NMeFOSAA	2355-31-9	C <sub>11</sub> H <sub>6</sub> F <sub>17</sub> NO <sub>4</sub> S	571.21	C11	D <sub>3</sub> -NMeFOSAA
Perfluorooctane sulfonamide ethanols						
N-ethylperfluorooctane sulfonamidoethanol	NEtFOSE	1691-99-2	C <sub>12</sub> H <sub>10</sub> F <sub>17</sub> NO <sub>3</sub> S	571.25	C12	D <sub>9</sub> -NEtFOSE
N-methylperfluorooctane sulfonamidoethanol	NMeFOSE	24448-09-7	C <sub>11</sub> H <sub>8</sub> F <sub>17</sub> NO <sub>3</sub> S	557.23	C11	D <sub>7</sub> -NMeFOSE
Per- and Polyfluoroalkyl Ether Carboxylic Acids (PFECA)						
Perfluoro-3-methoxypropanoic acid (PF4OPeA)	PFMPA	377-73-1	C <sub>4</sub> HF <sub>7</sub> O <sub>3</sub>	230.04	C4	<sup>13</sup> C <sub>5</sub> -PFPeA
Perfluoro-4-methoxybutanoic acid (PF5OHxA)	PFMBA	8603903-89-5	C <sub>5</sub> HF <sub>9</sub> O <sub>3</sub>	280.04	C5	<sup>13</sup> C <sub>5</sub> -PFPeA
Hexafluoropropylene oxide dimer acid (GenX)	HFPO-DA	13252-13-6	C <sub>6</sub> HF <sub>11</sub> O <sub>3</sub>	330.05	C6	<sup>13</sup> C <sub>3</sub> -HFPO-DA
Perfluoro-3,6-dioxahexanoic acid (3,6-OPHpA)	NFDHA	151772-58-6	C <sub>5</sub> HF <sub>9</sub> O <sub>4</sub>	296.04	C5	<sup>13</sup> C <sub>5</sub> -PFHxA
4,8-Dioxa-3H-perfluorononanoic acid	ADONA	919005-14-4	C <sub>7</sub> H <sub>2</sub> F <sub>12</sub> O <sub>4</sub>	378.07	C7	<sup>13</sup> C <sub>3</sub> -HFPO-DA
Chlorinated Polyfluoroalkyl Ether Sulfonic Acids (Cl-PFESAs)						
Perfluoro(2-ethoxyethane)sulfonic acid	PFEESA	117205-07-9	C <sub>4</sub> F <sub>9</sub> KO <sub>4</sub> S	354.19	C4	<sup>13</sup> C <sub>5</sub> -PFHxA
9-Chlorohexadecafluoro-3-oxanone-1-sulfonic acid	9Cl-PF3ONS	756426-58-1*	C <sub>8</sub> F <sub>16</sub> ClSO <sub>4</sub>	532.58	C8	<sup>13</sup> C <sub>3</sub> -HFPO-DA

11-Chloroeicosafluoro-3-oxaundecane-1-sulfonic acid	11Cl-PF3OUdS Fluorotelomer Sulfonates (FTS)	763051-92-9	$C_{10}F_{20}ClSO_4$	632.6	C10	$^{13}C_3$ -HFPO-DA
1H,1H,2H,2H-perfluorohexane sulfonate (4:2)	4:2 FTS	757124-72-4	$C_6H_5F_9O_3S$	328.15	C6	$^{13}C_2$ -4:2 FTS
1H,1H,2H,2H-perfluorooctane sulfonate (6:2)	6:2 FTS	27619-97-2	$C_8H_5F_{13}O_3S$	428.17	C8	$^{13}C_2$ -6:2 FTS
1H,1H,2H,2H-perfluorodecane sulfonate (8:2)	8:2 FTS	39108-34-4	$C_{10}H_5F_{17}O_3S$	528.18	C10	$^{13}C_2$ -8:2 FTS

Table A2. Physical and chemical properties of raw wastewater

Days	Temperature		pH		Conductivity (mS/cm)		NH3 - N		COD	
	Average	SD	Average	SD	Average	SD	Average	SD	Average	SD
Site A										
1	16.3	6.84	8.37	0.05	1.55	0.02				
2	15.8	6.06	7.94	0.04	1.29	0.01				
3	16.43	6.7	8.33	0.1	1.32	0.01				
4	13.7	5.28	8.39	0.04	1.19	0	48.86	10.67	680	56.03
5	15.63	3.75	8.4	0.04	1.35	0.01				
6	11.17	5.08	8	0.1	1.21	0.01				
7	15.07	3.78	8.39	0.07	1.28	0.01				
Site B										
1	12.73	0.38	8.24	0.05	0.46	0.05				
2	8.47	0.06	8.16	0.06	0.93	0.01				
3	13.57	0.21	8.22	0.03	1.02	0				
4	5.5	0.4	8	0.02	0.95	0.02	50.86	5.01	172.67	51.43
5	11.9	0.1	7.39	0.01	1.11	0.01				
6	11.7	0.2	7.64	0.09	0.95	0				
7	13.27	0.12	7.55	0.21	1	0.01				
Site C										
1	14.47	0.4	8.3	0.02	0.91	0.35				
2	5.13	0.4	8.57	0.12	0.58	0.3				
3	5.53	0.55	8.17	0.12	0.82	0				
4	12.87	0.81	7.94	0.01	1.01	0	54.57	8.3	324	40.45
5	14.63	0.4	7.87	0	1.01	0				
6	13.83	0.35	7.63	0.14	1.09	0.02				
7	11.77	0.12	7.91	0.19	0.99	0.01				

Table A3. Showing mean, median, and range of PFAS in raw wastewater.

PFAS	Mean	Median	Range
		ng/L	
PFPeA	27.83	26.11	20.25 - 40.53
PFHxA	4.67	4.48	1.32 - 8.42
PFOA	4.08	2.92	1.21 - 8.10
PFDoA	29.45	28.53	9.42 - 48.85
PFTTrDA	12.26	12.22	12.03 - 12.52
PFPeS	19.22	18.62	4.14 - 43.41
PFNS	9.53	9.53	9.07 - 10.0
6:2 FTS	59.84	44.06	6.81 - 128.71
PFOSA	9.78	9.79	8.87 - 10.65



## Supplementary materials for chapter 3

### S1 PFAS stock preparation

Stock solutions of the studied PFAS—perfluorooctanoic acid (PFOA; 95%, Alfa Aesar, Haverhill, MA), perfluorooctane sulfonate (PFOS; 98%, Matrix Scientific, Columbia, SC), perfluorobutanoic acid (PFBA; > 98%, Oakwood Chemical, Estill, SC), perfluorobutane sulfonate (PFBS; Tokyo Chemical Industry, Tokyo, Japan), and hexafluoropropylene oxide dimer acid (GenX, C<sub>6</sub>H<sub>4</sub>F<sub>11</sub>NO<sub>3</sub>, 98%, Sigma-Aldrich)—were prepared by dissolving the PFAS powder in LCMS-grade methanol (Thermo Scientific, Waltham, MA) followed by 1 min vortex before diluting to 200 µg/g for the batch adsorption experiments.

### S2 Determination of PFAS equilibrium concentration of PFAS and LC-MS/MS analysis

At the end of the batch adsorption studies, 2 mL aliquots were carefully transferred to microcentrifuges tube and centrifuged (21,130 g, 15 min; Southwest Science SC1024R, Trenton, NJ). The supernatant (1 mL) was collected using a syringe and needle and centrifuged again (21,130 g, 15 min). After centrifugation, 50 µL of the supernatant were diluted with 60 % methanol:water, spiked with isotopically mass-labeled PFAS mix (MPFAC-MXA, Wellington Laboratories, Overland Park, KS) to correct for variation during mass spectrometric analysis (Zenobio et al., 2022b).

Liquid chromatography with tandem mass spectrometry (LC-MS/MS, Agilent 6470 LC/TQ, Santa Clara, CA) in negative electrospray ionization mode was used to determine equilibrium PFAS concentration after batch adsorption. Separation of the analytes was achieved using an Agilent

ZORBAX RRHD Eclipse Plus reversed phase C18 column. The mobile phases were made up of 100% acetonitrile (eluent A) and 2 mM ammonium acetate (eluent B). The injection volume was 2.0  $\mu\text{L}$ . Analysis was done with a 7-point standard calibration for each PFAS with concentration range from 10  $\mu\text{g/L}$  to 0.0137  $\mu\text{L}$ .

### S3 Adsorption kinetics, isotherm, and effect of aqueous chemistry studies

Adsorption kinetics and isotherm studies were conducted at pH 7 and at 20°C in DI water. The effect of aqueous phase chemistry was investigated by varying ionic strength (0 – 100 mM NaCl), pH (3 – 11), temperature (25 – 50°C), and natural organic matter (0 – 100 mg/L), summarized in Table S1, using humic acid. These ranges cover what is expected in most engineered and natural aquatic systems. For each batch adsorption experiment, 20 mg of PET secondary MPs was combined with 10 mL of 200  $\mu\text{g/L}$  PFAS. The PFAS-MPs suspension was shaken for the desired time on a New Brunswick Innova 2100 orbital shaker (150 rpm).

### S4 Calculations of adsorption capacities

Adsorption capacity is used to determine the quantity of an adsorbent required for quantitative enrichment of adsorbates from given solutions (Danmaliki & Saleh, 2017). The amount of PFAS adsorbed per unit mass of adsorbents (adsorption capacity) at equilibrium ( $q_e$ ), at a specific time ( $q_t$ ), and percent adsorption ( $E$ ) were calculated after each adsorption process using the relations below:

$$\text{Adsorption capacity at equilibrium, } q_e = \frac{C_i - C_e}{M} \times V \quad (1)$$

$$\text{Adsorption capacity at a specific time, } q_t = \frac{C_i - C_e}{M} \times V \quad (2)$$

$$\text{Percent adsorption, } E = \frac{C_i - C_e}{C_i} \times 100 \quad (3)$$

where  $q_e$  is the adsorption capacity or the amount of solute (PFAS) adsorbed on adsorbent at equilibrium all through the article, except otherwise specified ( $\mu\text{g/g}$ ),  $C_i$  is the initial concentration of solute ( $\text{mg/L}$  or  $\mu\text{g/L}$ ),  $C_e$  is the equilibrium concentration of solute remaining in solution ( $\text{mg/L}$  or  $\mu\text{g/L}$ ),  $V$  is the volume of the solution, and  $E$  is the percent adsorption expressed in %.

## S5 Experimental models

### *Adsorption kinetics*

Adsorption kinetics study is important to understand the uptake rate of PFAS by secondary MPs and is used to determine equilibrium time of adsorption. The determined equilibrium time was used in subsequent studies, including isotherm and studies on the effect of water chemistry. Kinetics equations fitted to the experimental data also helps to evaluate percent adsorption of PFAS to secondary MPs, rate limiting steps, and mechanisms (Febrianto et al., 2009).

Obtained data was fitted to three adsorption kinetic models, including pseudo first order (PFO; Eq. 4), pseudo second order (PSO; Eq. 5), and Webber and Morris intraparticle diffusion model (Eq. 6). PFO and PSO kinetics models are influenced by surface reactions while intraparticle diffusion model is controlled by diffusion processes (Vieira et al., 2021). These models were chosen because they best describe the uptake of contaminants in aqueous solution and have been used to study the adsorption of different contaminants to microplastics (Chen et al., 2021; Karapanagioti & Werner, 2018; Yao et al., 2022; Yu et al., 2020; Zhan et al., 2016).

$$\frac{dq_t}{dt} = k (q_e - q_t) \quad (4)$$

$$\frac{dq_t}{dt} = k (q_e - q_t)^2 \quad (5)$$

$$q_t = K_{id}t^{1/2} \quad (6)$$

where  $q_t$  is adsorption capacity at specific time (mins),  $k_1$ (1/min),  $k_2$  (g/(mg·min)), and  $k_{id}$  (mg/(g·h<sup>1/2</sup>)) are PFO, PSO, and intraparticle diffusion rate constants, respectively.

### *Adsorption isotherm*

Adsorption isotherms are characterized by constant values that express the affinity and surface properties of the adsorbent (Danmaliki & Saleh, 2017). Langmuir (Eq. 7) and Freundlich (Eq. 8) isotherm models were used in this study. Langmuir and Freundlich isotherm were selected because they are the most used models to understand the properties of an adsorption process and preliminary studies reveals that the Flory-Huggins' isotherm is not appropriate for describing the adsorption of PFAS by the secondary PET MPs (Adio et al., 2019; Danmaliki & Saleh, 2017; Ho & McKay, 1998). Langmuir adsorption isotherm assumes monolayer and uniform adsorption at a finite number of localized sites with no interactions nor transmigration between molecules adsorbed on neighboring sites on the adsorbent surface (Adio et al., 2019; Han et al., 2021; Saleh, 2015). Freundlich isotherm assumes that adsorption could occur on multilayer surfaces with non-uniform distribution of energy (Adio et al., 2019).

$$q_e = \frac{kq_m^o C_e}{1 + K_L C_e} \quad (7)$$

$$q_e = K_F \cdot C_e^{1/n} \quad (8)$$

where  $K_L$  is Langmuir adsorption constant (L/mg),  $q_m$  is maximum adsorption capacity,  $K_F$  is Freundlich isotherm constant and indicates adsorption capacity  $((\text{mg/g})(\text{L/mg})^{1/n})$  and  $1/n$  indicates adsorption intensity.

#### S6 Density Functional Theory (DFT) method and result of FUKUI analysis

DFT calculations were carried out to investigate the chemical properties and interaction between the selected PFAS and MPs. All calculations were run using gaussian 16. Chemical structures were drawn using GaussView 5.0 software. One polyethylene terephthalate monomer was used to represent the PET MPs, to reduce computation cost. Geometry optimizations, vibration frequency analysis, energy calculations and Fukui analysis were carried out using the hybrid Becke 3-parameter (Exchange) and Lee, Yang and Parr. (B3LYP) functionals and 6-31+G (d,p) basis set. The basis sets were selected based on their ability to produce results that conforms with experimental data at minimal computational cost. Local reactivity sites were determined by the condensed Fukui functions. UCA-FUKUI v.1.0 software was used to calculate the FUKUI condensed functions using a finite difference approximation method. The finite difference approximation method provides the three Fukui functions,  $f_k^+$ ,  $f_k^-$ ,  $f_k^0$ , and that represents atomic sites prone to nucleophilic, electrophilic, and radical attacks respectively. These functions help to predict the most electrophilic and nucleophilic atoms on a molecule and where interaction are more likely <sup>2</sup>. Quantum chemical descriptors such as total electronic energy of molecules (E), energies of the highest occupied and lowest unoccupied molecular orbitals ( $E_{HOMO}$  and  $E_{LUMO}$  respectively), band gap ( $\Delta E$ ) electronegativity ( $\chi$ ), global hardness ( $\eta$ ), and dipole moment ( $\mu$ ), were computed according to the DFT-Koopman's ionization theorem.<sup>3</sup> Adsorption energies were calculated based on the relation;

$$E_{adsorption} = -[E_{complex} - (E_{PFAS} + E_{microplastics})] \quad (10)$$

where  $E_{adsorption}$ ,  $E_{PFAS}$ , and  $E_{microplastics}$  represent the Gibbs free energies of PFAS-microplastics complex, isolated PFAS and isolated microplastics respectively.

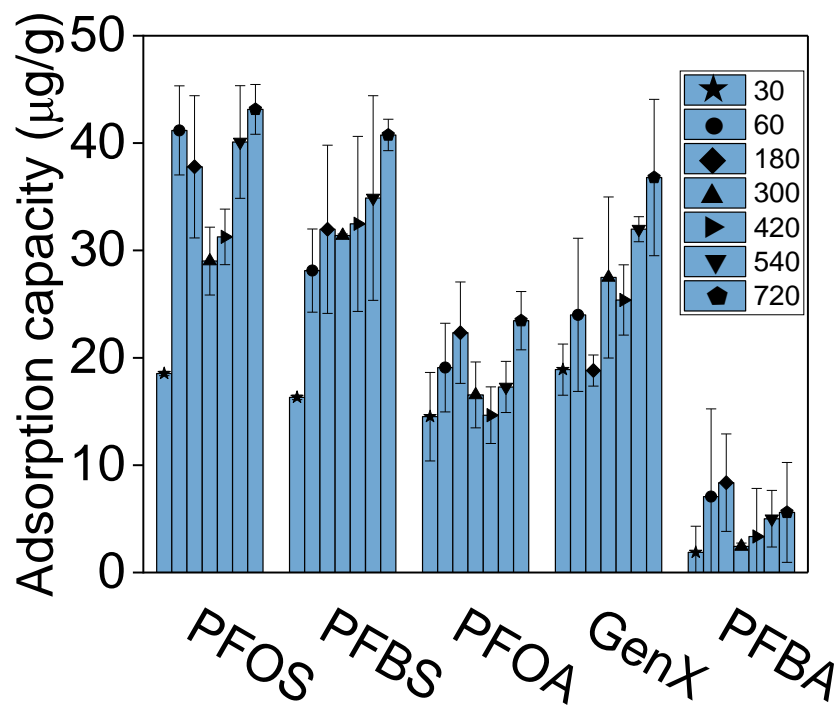


Figure B1. Adsorption capacity at different times ( $q_t$ ) of the secondary PET MPs for PFAS in single-PFAS systems.

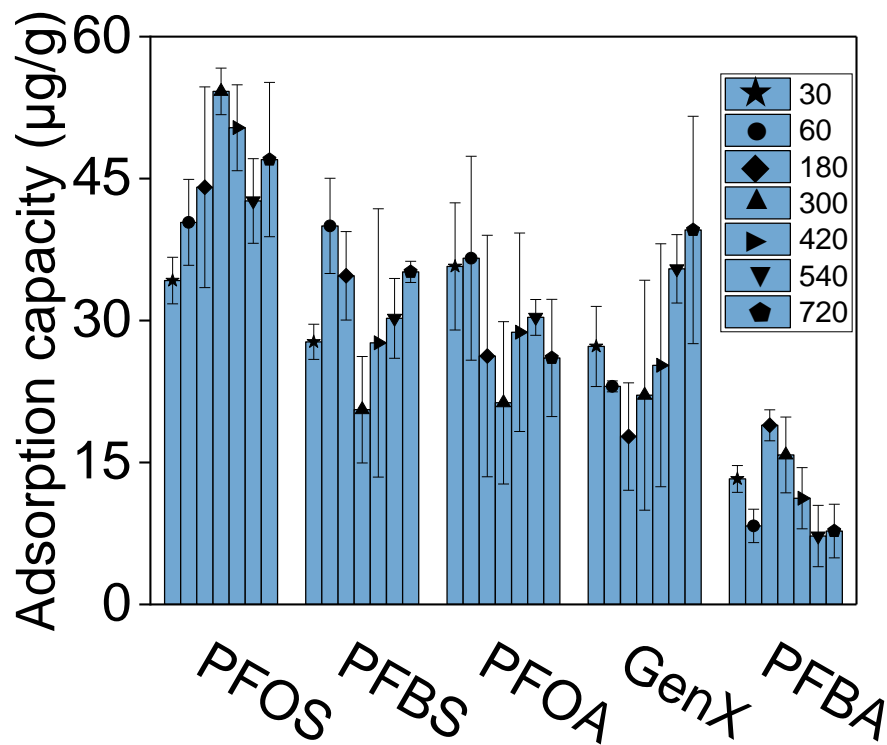


Figure B2. Adsorption capacity at different times ( $q_t$ ) of the secondary PET MPs for PFAS in mixed-PFAS system.



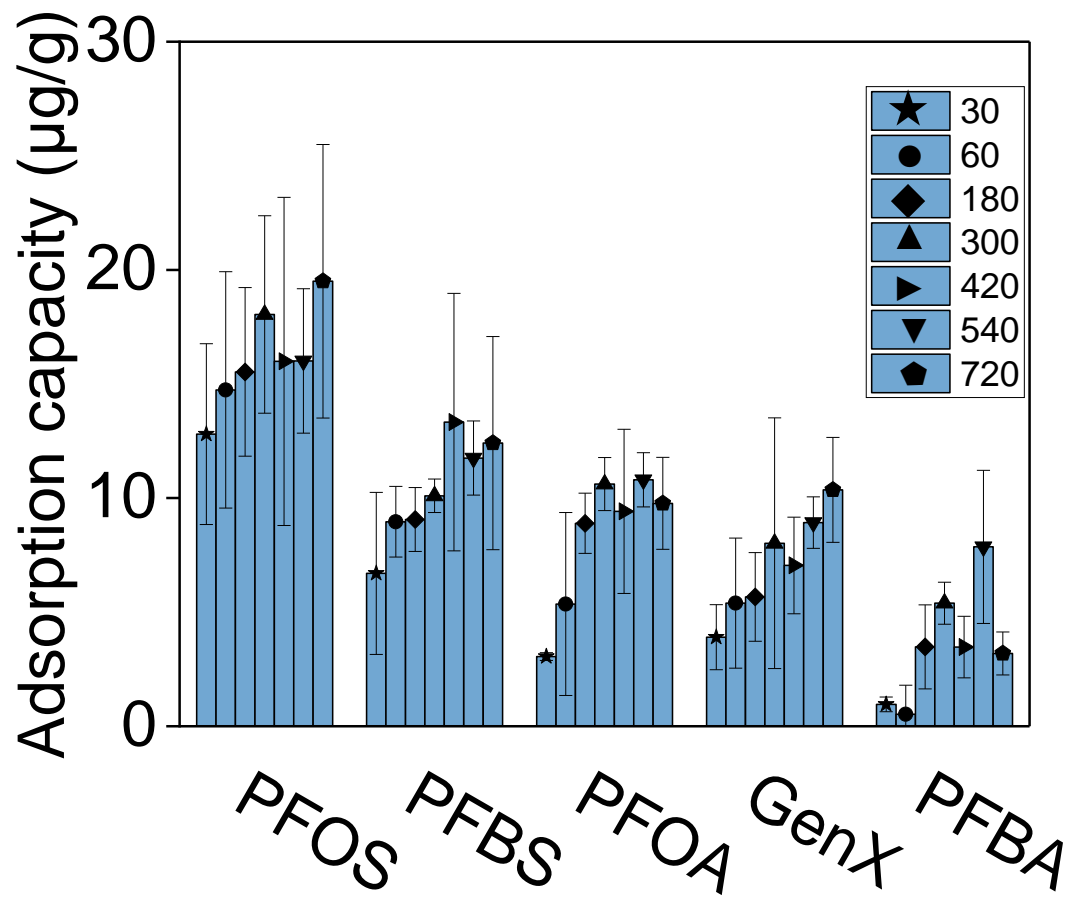


Figure B3. Adsorption capacity at different times ( $q_t$ ) of the commercial PET MPs for PFAS in single-PFAS system.

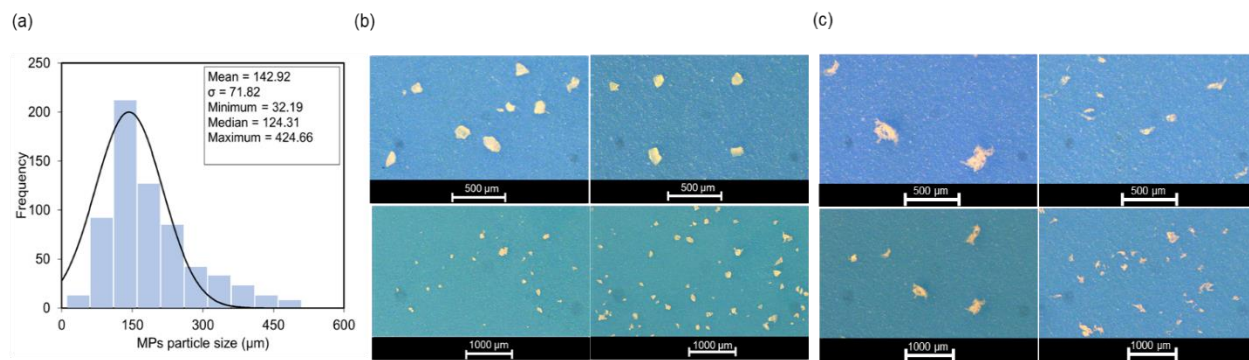


Figure B4. (a) Particle size distribution and (b) surface morphology of commercial PET MPs; (c) surface morphology of secondary PET MPs. Surface morphology was viewed under light microscope.

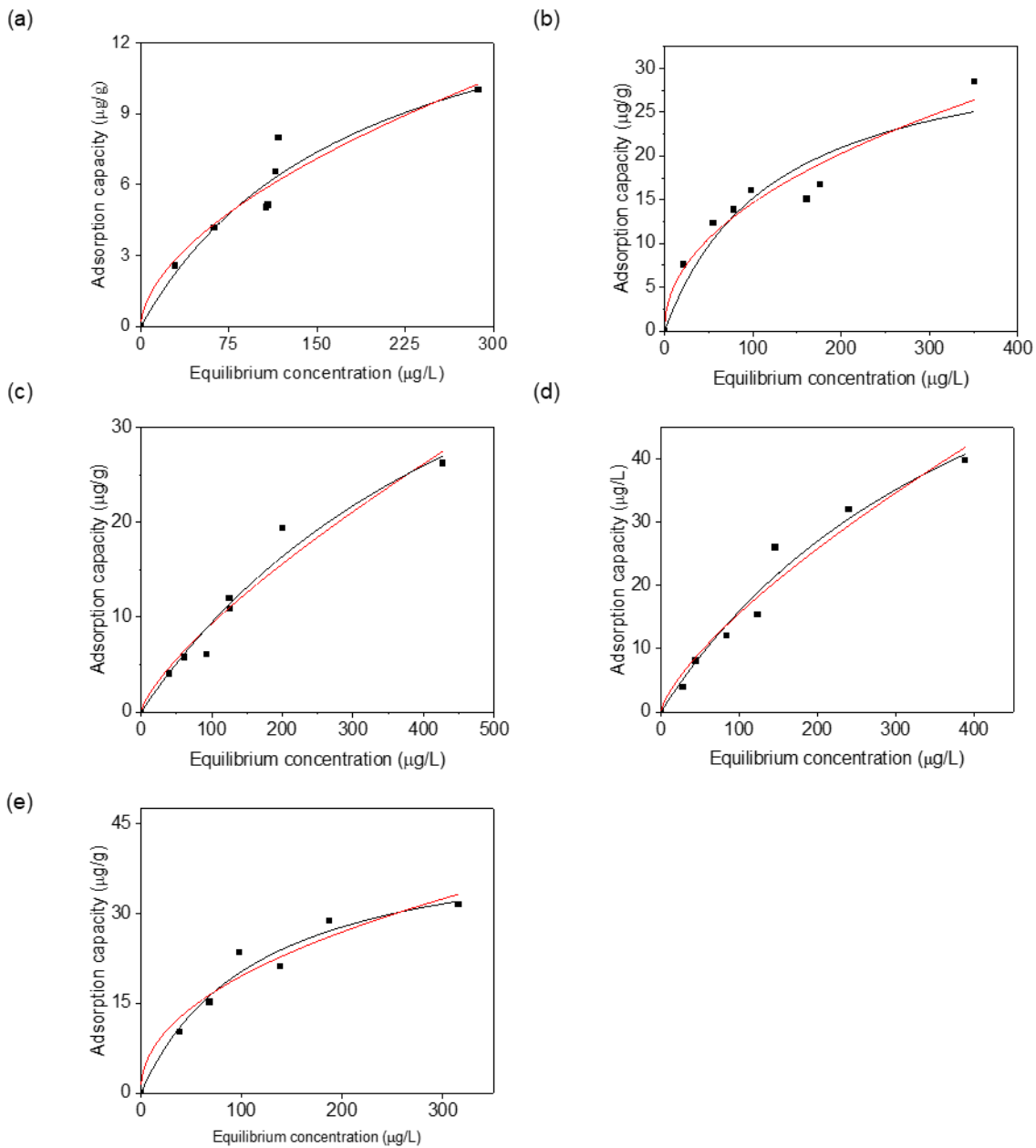


Figure B5. Non-linear Langmuir (red lines) and Freundlich (black lines) isotherms fitting of the experimental data for the adsorption of (a) PFBA, (b) PFOA, (c) GenX, (d) PFBS, and (e) PFOS by the secondary PET microplastics.

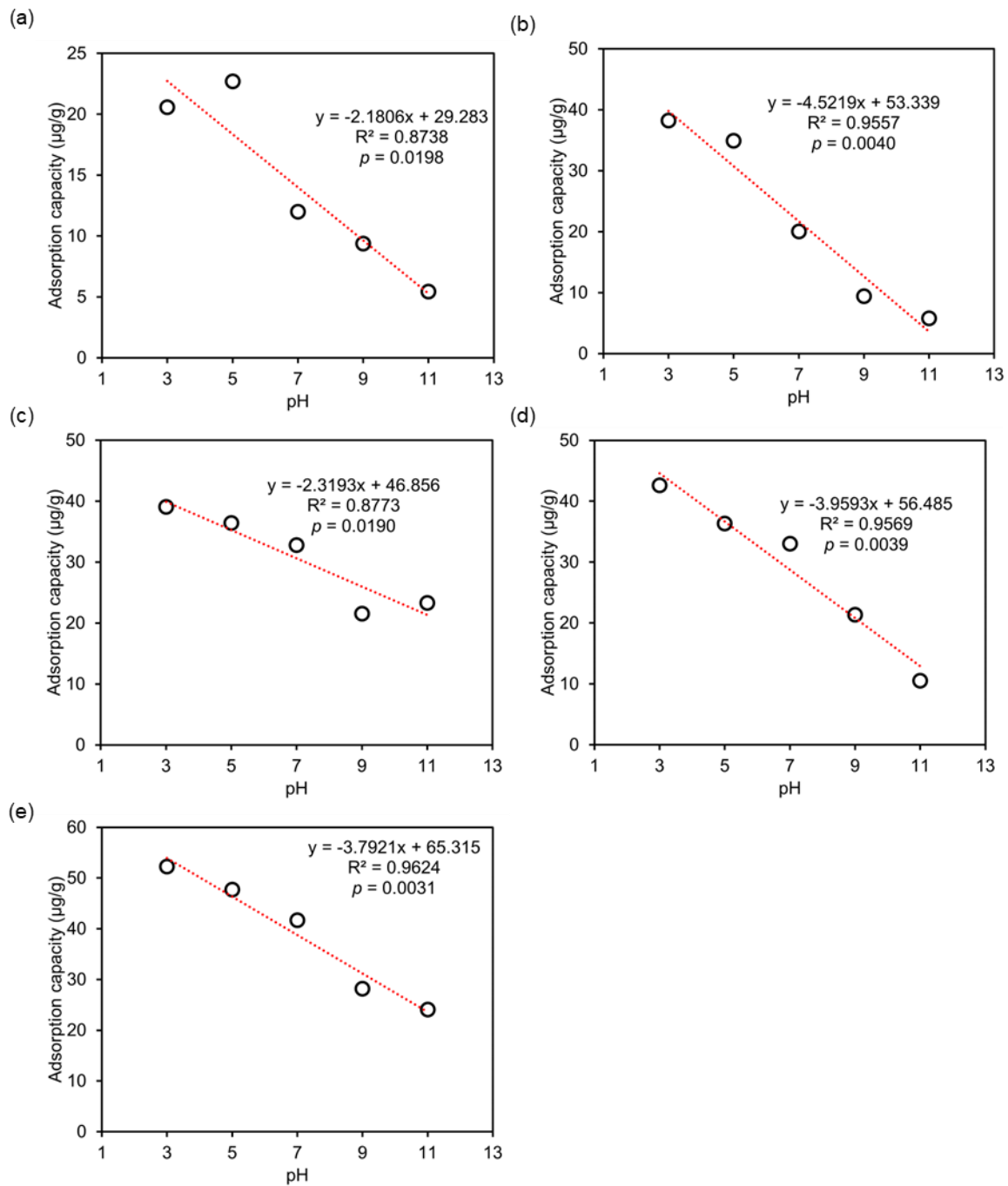


Figure B6. Correlation between pH and the adsorption capacity of secondary PET MPs for PFAS.

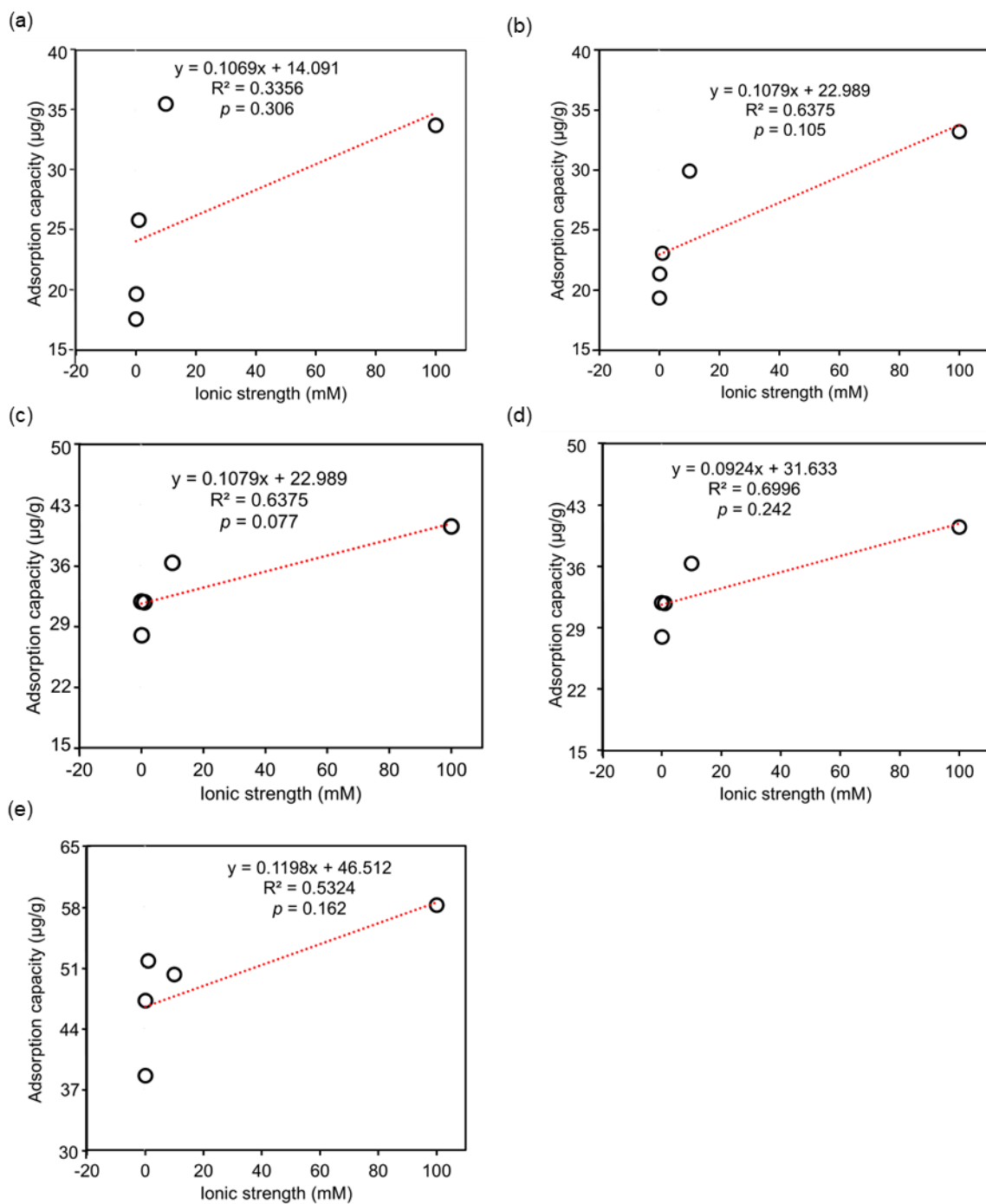


Figure B7. Correlation between ionic strength and the adsorption capacity of secondary PET MPs for PFAS.



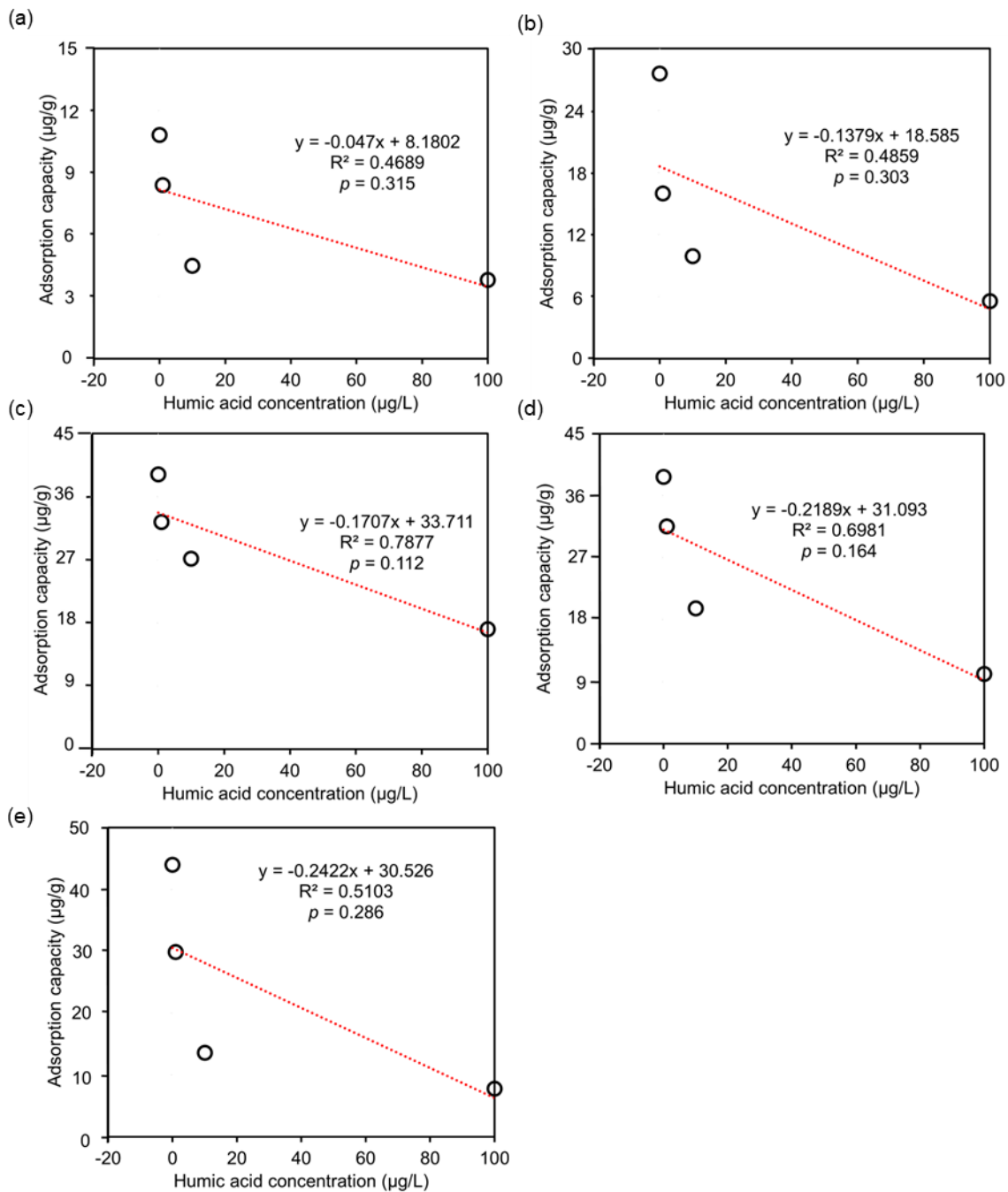


Figure B8. Correlation between humic acid concentration and the adsorption capacity of secondary PET MPs for PFAS.

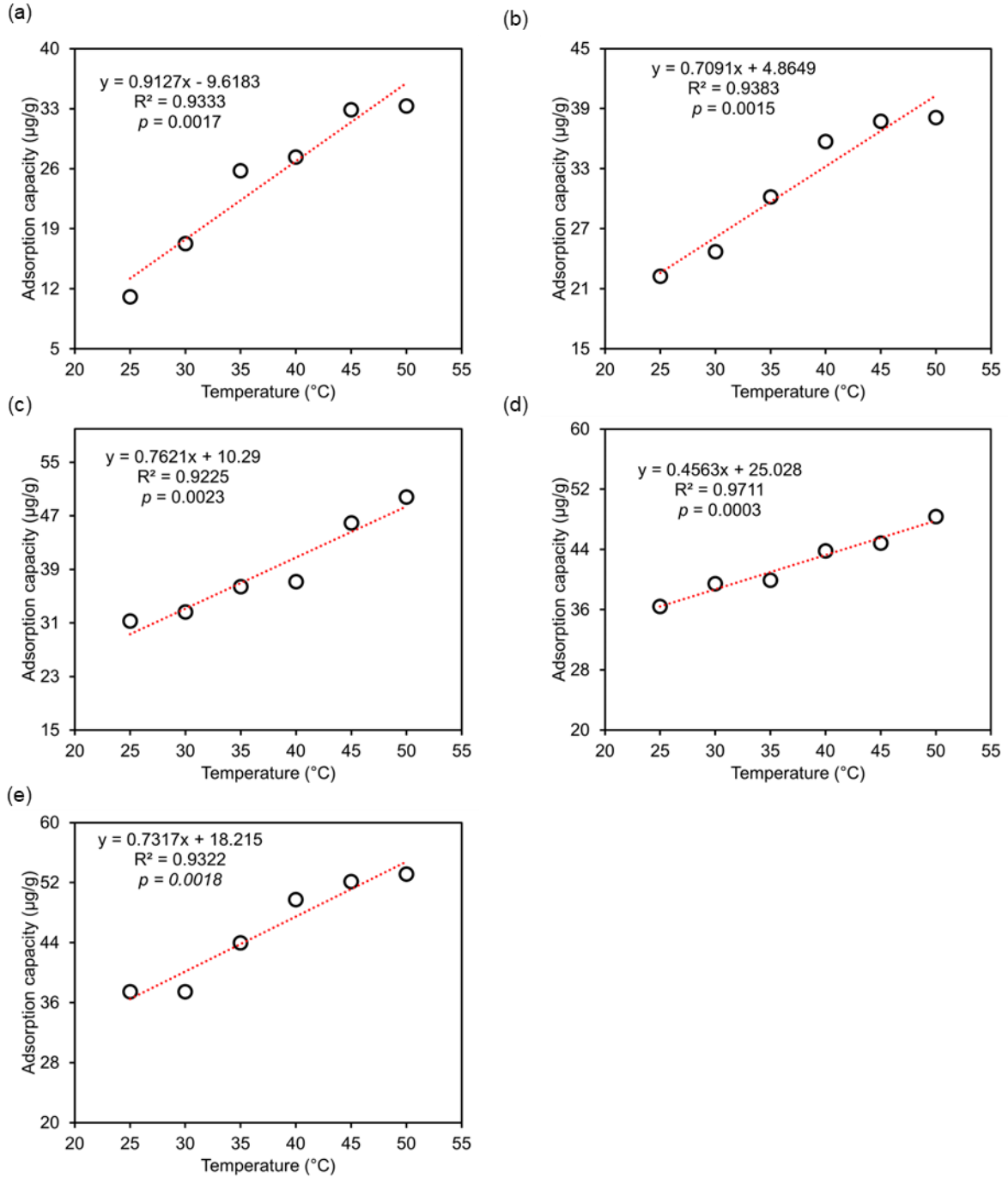


Figure B9. Correlation between temperature and the adsorption capacity of secondary PET MPs for PFAS.



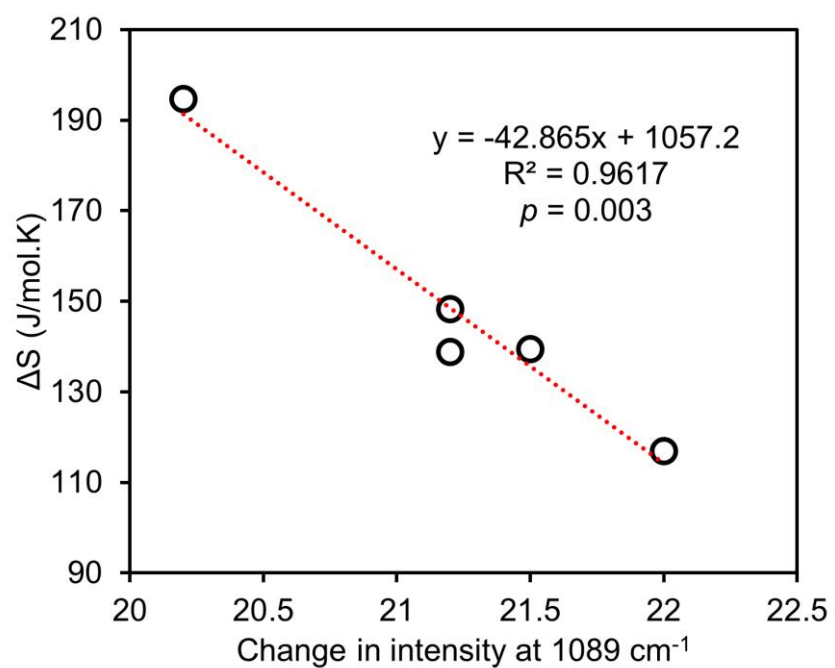


Figure B10. Correlation between  $\Delta S$  and change in the intensity of the peak at  $1089 \text{ cm}^{-1}$  (which represents stretching vibration of the C-O of PET's ester group).

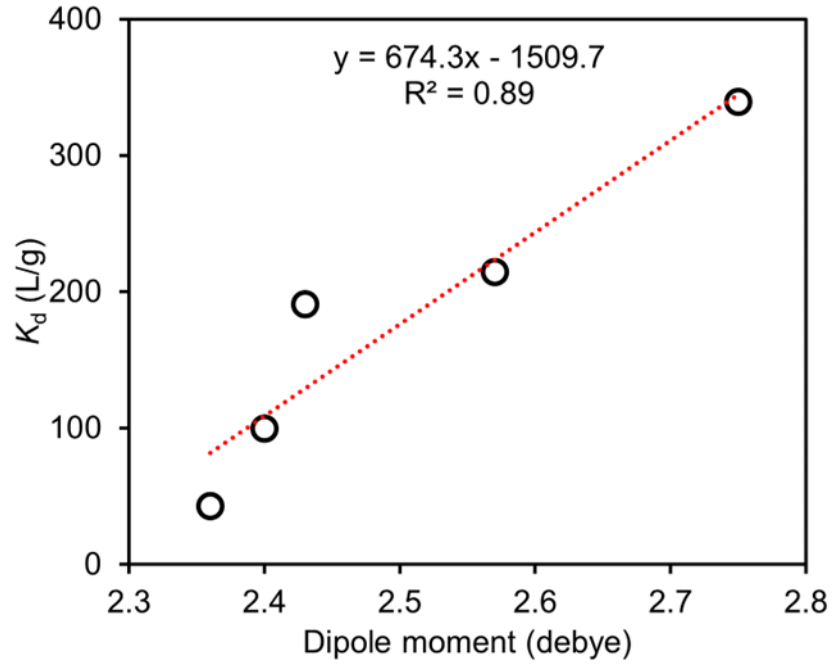


Figure B11. Correlation between the distribution coefficient ( $K_d$ ) of the secondary PET MPs for PFAS and the dipole moment of the PFAS.

Table B1. Ranges of water chemistry parameters studied.

Water chemistry conditions	Range covered in this study	Conditions in different environmental aquatic media		
		Surface water	Wastewater	Groundwater
pH	3, 5, 7, 9, and 11	6.8 – 9.4 (Essien et al., 2008; Satpathy et al., 2010; Zhang et al., 2012)	6.5 – 8.0(Popa et al., 2012; Tang & Chen, 2015)	5.2 – 8.8 (Saalidong et al., 2022; Zhang et al., 2012)
Ionic strength (mM)	0, 0.1, 1, 10, and 100	0 - 700(Klungnes & Byrne, 2000)	3 - 41(Cervantes-Avilés et al., 2017; Prot et al., 2020)	10.80 – 100 (Powell et al., 2015; Ying et al., 2022)
Natural organic matter (mg/L) <sup>1</sup>	0, 1, 10, and 100	< 1 - 100(Brown, 2021; Evans et al., 2005)	9 - 82(Dignac et al., 2000; Neale et al., 2011)	0 – 5(McDonough et al., 2020; Regan et al., 2017)
Temperature (°C)	25, 30, 35, 40, 45, 50	-	-	-

<sup>1</sup> Studied as dissolved fraction of humic acid.

Table B2. Kinetics parameters derived from non-linear pseudo first order (PFO), pseudo second order, and intraparticle diffusion models fitting for single-PFAS and mixed-PFAS systems.

Parameter		PFBS	PFOS	PFBA	PFOA	GenX
<i>Single-PFAS system</i>						
		Average $\pm$ SD	Average $\pm$ SD	Average $\pm$ SD	Average $\pm$ SD	Average $\pm$ SD
Pseudo first order	$q_e$ ( $\mu\text{g/g}$ )	$35.57 \pm 1.66$	$36.71 \pm 2.94$	$5.17 \pm 0.99$	$18.98 \pm 1.37$	$28.37 \pm 2.51$
	$k_1$ (1/min)	$0.023 \pm 0.005$	$0.036 \pm 0.015$	$0.038 \pm 0.022$	$0.052 \pm 0.027$	$0.036 \pm 0.011$
	$R^2$	0.94	0.82	0.46	0.84	0.79
Pseudo second order	$q_e$ ( $\mu\text{g/g}$ )	$38.92 \pm 2.18$	$38.45 \pm 4.07$	$5.24 \pm 1.27$	$19.33 \pm 1.73$	$30.05 \pm 0.05$
	$k_2$ (g/(mg.min))	$0.00 \pm 0.00$	$0.00 \pm 0.00$	$0.02 \pm 0.01$	$0.01 \pm 0.01$	$0.00 \pm 0.00$
	$R^2$	0.96	0.79	0.41	0.82	0.83
Intraparticle diffusion	$k_{ID} \times 10^3$ ( $\text{mg} \cdot \text{g}^{-1} \text{min}^{-(1/2)}$ )	$1.29 \pm 0.25$	$1.14 \pm 0.44$	$0.12 \pm 0.11$	$0.52 \pm 0.24$	$1.11 \pm 0.20$
	$C \times 10^3$	$9.03 \pm 4.22$	$13.57 \pm 7.29$	$2.52 \pm 1.89$	$8.62 \pm 3.97$	$6.53 \pm 3.42$
	$R^2$	0.82	0.53	0.16	0.44	0.83
<i>Mixed-PFAS system</i>						
Pseudo first order	$q_e$ ( $\mu\text{g/g}$ )	$31.21 \pm 2.62$	$47.26 \pm 2.96$	$11.82 \pm 1.66$	$29.29 \pm 2.07$	$27.21 \pm 2.92$
	$k_1$ (1/min)	$0.013 \pm 0.003$	$0.020 \pm 0.00$	$0.025 \pm 0.00$	$0.025 \pm 0.00$	$0.026 \pm 0.00$
	$R^2$	0.78	0.84	0.52	0.81	0.64
	$q_e$ ( $\mu\text{g/g}$ )	$30.87 \pm 4.42$	$47.26 \pm 5.54$	$11.82 \pm 1.70$	$29.29 \pm 2.35$	$29.00 \pm 3.84$
	$k_2$ (g/(mg.min))	$0.00 \pm 0.00$	$0.01 \pm 0.00$	$0.00 \pm 0.00$	$0.00 \pm 0.00$	$0.01 \pm 0.00$

Pseudo second order	$R^2$	0.77	0.84	0.52	0.81	0.67
Intraparticle diffusion	$k_{ID} \times 10^3$ (mg g <sup>-1</sup> min <sup>-(1/2)</sup> )	0.44 ± 0.35	0.47 ± 0.54	0.03 ± 0.18	0.26 ± 0.34	0.75 ± 0.22
	$C \times 10^3$	19.59 ± 7.22	33.35 ± 11.23	9.81 ± 3.80	21.23 ± 7.22	11.04 ± 4.52
	$R^2$	0.21	0.11	0.01	0.09	0.67
<i>Commercial Single-PFAS system</i>						
		Average ± SD	Average ± SD	Average ± SD	Average ± SD	Average ± SD
Pseudo first order	$q_e$ (µg/g)	11.37 ± 0.63	16.92 ± 0.64	4.25 ± 1.31	9.46 ± 0.73	8.25 ± 0.68
	$k_1$ (1/min)	1.62 ± 0.46	2.59 ± 0.61	0.36 ± 0.30	0.85 ± 0.30	0.95 ± 0.36
	$R^2$	0.91	0.95	0.67	0.88	0.84
Pseudo second order	$q_e$ (µg/g)	12.36 ± 0.71	17.64 ± 0.70	4.69 ± 2.83	10.74 ± 1.23	9.47 ± 0.88
	$k_2$ (g/(mg.min))	0.18 ± 0.07	0.28 ± 0.11	0.05 ± 0.08	0.09 ± 0.06	0.11 ± 0.06
	$R^2$	0.94	0.96	0.65	0.86	0.90
Intraparticle diffusion	$k_{ID} \times 10^3$ (mg·g <sup>-1</sup> min <sup>-(1/2)</sup> )	3.13 ± 0.65	4.01 ± 1.22	1.68 ± 0.58	2.79 ± 0.66	2.56 ± 0.33
	$C \times 10^3$	3.26 ± 1.41	6.67 ± 2.65	0.00 ± 1.24	1.71 ± 1.44	1.43 ± 0.71
	$R^2$	0.79	0.64	0.59	0.75	0.91

Table B3. Summary of parameters obtained from fitting experimental data to Langmuir and Freundlich adsorption isotherms for adsorption of PFAS onto PET MPs

Isotherm parameters	PFBS	PFOS	PFBA	PFOA	GenX
	Langmuir				
	Average $\pm$ SD	Average $\pm$ SD	Average $\pm$ SD	Average $\pm$ SD	Average $\pm$ SD
Maximum adsorption capacity, $q_{\max}$ ( $\mu\text{g/g}$ )	$37.77 \pm 1.87$	$45.12 \pm 2.92$	$16.54 \pm 4.17$	$25.63 \pm 5.107$	$62.76 \pm 1.85$
Adsorption affinity, $b$ (L/mg)	$37.42 \pm 1.25$	$2.14 \pm 0.18$	$5.37 \pm 2.39$	$145.18 \pm 39.73$	$1.77 \pm 0.08$
Correlation coefficient ( $R^2$ )	0.53	0.91	0.88	0.58	0.95
	Freundlich				
Empirical constant ( $n$ )	$1.05 \pm 0.07$	$0.78 \pm 0.15$	$0.57 \pm 0.10$	$0.47 \pm 0.08$	$0.75 \pm 0.09$
Freundlich constant, $K_F$ ( $\text{mg/g} \cdot (\text{L}/(\text{mg})(1/n)) \times 10^{-4}$ )	$0.74 \pm 0.30$	$2.18 \pm 1.47$	$4.19 \pm 2.15$	$1.67 \pm 0.64$	$3.01 \pm 1.59$
Correlation coefficient ( $R^2$ )	0.98	0.93	0.90	0.87	0.87

Table B4. Effect of pH on the adsorption capacity of the secondary PET MPs for PFAS

pH	PFBA	PFOA	GenX	PFBS	PFOS
	Mean ± SD ( $\mu\text{g}/\text{m}^2$ )	Mean ± SD ( $\mu\text{g}/\text{m}^2$ )	Mean ± SD ( $\mu\text{g}/\text{m}^2$ )	Mean ± SD ( $\mu\text{g}/\text{m}^2$ )	Mean ± SD ( $\mu\text{g}/\text{m}^2$ )
3	5.39 ± 0.20 <sup>a</sup>	10.01 ± 1.36 <sup>d</sup>	10.22 ± 0.32 <sup>g</sup>	11.16 ± 0.68 <sup>i</sup>	13.67 ± 0.64 <sup>m</sup>
5	5.94 ± 0.71 <sup>a</sup>	9.15 ± 1.12 <sup>d</sup>	9.54 ± 0.89 <sup>g</sup>	9.51 ± 0.24 <sup>ij</sup>	12.49 ± 0.64 <sup>mn</sup>
7	3.14 ± 0.24 <sup>b</sup>	5.25 ± 0.84 <sup>c</sup>	8.58 ± 1.19 <sup>g</sup>	8.65 ± 0.27 <sup>j</sup>	10.90 ± 0.89 <sup>n</sup>
9	2.45 ± 0.28 <sup>bc</sup>	2.46 ± 0.61 <sup>f</sup>	5.64 ± 0.70 <sup>gh</sup>	5.59 ± 1.46 <sup>k</sup>	7.37 ± 0.63 <sup>o</sup>
11	1.42 ± 0.54 <sup>c</sup>	1.51 ± 0.44 <sup>f</sup>	6.10 ± 0.59 <sup>gh</sup>	2.75 ± 1.19 <sup>l</sup>	6.31 ± 0.90 <sup>o</sup>

pH	PFBA	PFOA	GenX	PFBS	PFOS
	Mean ± SD ( $\mu\text{g}/\text{g}$ )	Mean ± SD ( $\mu\text{g}/\text{g}$ )	Mean ± SD ( $\mu\text{g}/\text{g}$ )	Mean ± SD ( $\mu\text{g}/\text{g}$ )	Mean ± SD ( $\mu\text{g}/\text{g}$ )
3	20.58 ± 0.75 <sup>a</sup>	38.24 ± 5.21 <sup>d</sup>	39.04 ± 1.23 <sup>g</sup>	42.62 ± 2.60 <sup>i</sup>	52.24 ± 2.45 <sup>m</sup>
5	22.70 ± 2.73 <sup>a</sup>	34.94 ± 4.28 <sup>d</sup>	36.44 ± 3.42 <sup>g</sup>	36.34 ± 0.93 <sup>ij</sup>	47.71 ± 2.45 <sup>mn</sup>
7	12.00 ± 0.91 <sup>b</sup>	20.05 ± 3.21 <sup>e</sup>	32.77 ± 4.53 <sup>g</sup>	33.02 ± 1.02 <sup>j</sup>	41.66 ± 3.39 <sup>n</sup>
9	9.38 ± 1.08 <sup>bc</sup>	9.41 ± 2.31 <sup>f</sup>	21.56 ± 2.68 <sup>gh</sup>	21.35 ± 5.56 <sup>k</sup>	28.16 ± 2.41 <sup>o</sup>
11	5.44 ± 2.08 <sup>c</sup>	5.78 ± 1.69 <sup>f</sup>	23.29 ± 2.24 <sup>gh</sup>	10.52 ± 4.54 <sup>l</sup>	24.09 ± 3.45 <sup>o</sup>

Table B5. Effect of ionic strength on the adsorption capacity of the secondary PET MPs for PFAS

Ionic strength (mM)	PFBA	PFOA	GenX	PFBS	PFOS
	Mean $\pm$ SD ( $\mu\text{g}/\text{m}^2$ )	Mean $\pm$ SD ( $\mu\text{g}/\text{m}^2$ )	Mean $\pm$ SD ( $\mu\text{g}/\text{m}^2$ )	Mean $\pm$ SD ( $\mu\text{g}/\text{m}^2$ )	Mean $\pm$ SD ( $\mu\text{g}/\text{m}^2$ )
0	1.98 $\pm$ 0.24 <sup>a</sup>	5.07 $\pm$ 0.12 <sup>d</sup>	8.34 $\pm$ 1.58 <sup>e</sup>	8.40 $\pm$ 1.09 <sup>f</sup>	10.09 $\pm$ 1.26 <sup>i</sup>
0.1	2.53 $\pm$ 0.58 <sup>ab</sup>	5.59 $\pm$ 0.95 <sup>d</sup>	7.32 $\pm$ 0.93 <sup>e</sup>	9.66 $\pm$ 1.05 <sup>fg</sup>	12.35 $\pm$ 3.21 <sup>i</sup>
1	4.14 $\pm$ 1.66 <sup>abc</sup>	6.04 $\pm$ 1.38 <sup>d</sup>	8.32 $\pm$ 1.74 <sup>e</sup>	11.77 $\pm$ 0.67 <sup>gh</sup>	13.55 $\pm$ 1.12 <sup>i</sup>
10	6.68 $\pm$ 2.11 <sup>bc</sup>	7.83 $\pm$ 0.84 <sup>d</sup>	9.51 $\pm$ 1.94 <sup>e</sup>	11.80 $\pm$ 0.65 <sup>gh</sup>	13.14 $\pm$ 0.87 <sup>i</sup>
100	6.21 $\pm$ 2.00 <sup>c</sup>	8.69 $\pm$ 0.71 <sup>d</sup>	10.60 $\pm$ 0.15 <sup>e</sup>	12.81 $\pm$ 2.05 <sup>h</sup>	15.23 $\pm$ 2.34 <sup>i</sup>

Ionic strength (mM)	PFBA	PFOA	GenX	PFBS	PFOS
	Mean $\pm$ SD ( $\mu\text{g}/\text{g}$ )	Mean $\pm$ SD ( $\mu\text{g}/\text{g}$ )	Mean $\pm$ SD ( $\mu\text{g}/\text{g}$ )	Mean $\pm$ SD ( $\mu\text{g}/\text{g}$ )	Mean $\pm$ SD ( $\mu\text{g}/\text{g}$ )
0	7.58 $\pm$ 0.91 <sup>a</sup>	19.36 $\pm$ 0.47 <sup>d</sup>	31.85 $\pm$ 6.02 <sup>e</sup>	32.08 $\pm$ 4.15 <sup>f</sup>	38.55 $\pm$ 4.81 <sup>i</sup>
0.1	9.68 $\pm$ 2.20 <sup>ab</sup>	21.36 $\pm$ 3.64 <sup>d</sup>	27.97 $\pm$ 3.56 <sup>e</sup>	36.92 $\pm$ 4.00 <sup>fg</sup>	47.18 $\pm$ 12.27 <sup>i</sup>
1	15.83 $\pm$ 6.35 <sup>abc</sup>	23.09 $\pm$ 5.28 <sup>d</sup>	31.79 $\pm$ 6.64 <sup>e</sup>	44.95 $\pm$ 2.55 <sup>gh</sup>	51.76 $\pm$ 4.26 <sup>i</sup>
10	25.51 $\pm$ 8.04 <sup>bc</sup>	29.93 $\pm$ 3.22 <sup>d</sup>	36.33 $\pm$ 7.40 <sup>e</sup>	45.06 $\pm$ 2.49 <sup>gh</sup>	50.18 $\pm$ 3.31 <sup>i</sup>
100	23.74 $\pm$ 7.64 <sup>c</sup>	33.19 $\pm$ 2.70 <sup>d</sup>	40.49 $\pm$ 0.56 <sup>e</sup>	48.95 $\pm$ 7.82 <sup>h</sup>	58.19 $\pm$ 8.94 <sup>i</sup>



Table B6. Effect of humic acid concentration on the adsorption capacity of the secondary PET MPs for PFAS

Humic acid (mg/L)	PFBA Mean $\pm$ SD ( $\mu\text{g}/\text{m}^2$ )	PFOA Mean $\pm$ SD ( $\mu\text{g}/\text{m}^2$ )	GenX Mean $\pm$ SD ( $\mu\text{g}/\text{m}^2$ )	PFBS Mean $\pm$ SD ( $\mu\text{g}/\text{m}^2$ )	PFOS Mean $\pm$ SD ( $\mu\text{g}/\text{m}^2$ )
0	2.83 $\pm$ 0.32 <sup>a</sup>	7.23 $\pm$ 0.68 <sup>c</sup>	10.26 $\pm$ 0.75 <sup>f</sup>	10.14 $\pm$ 1.70 <sup>i</sup>	11.52 $\pm$ 0.74 <sup>m</sup>
1	2.20 $\pm$ 0.63 <sup>ab</sup>	4.18 $\pm$ 0.80 <sup>d</sup>	8.48 $\pm$ 0.59 <sup>fg</sup>	8.26 $\pm$ 1.20 <sup>ij</sup>	7.82 $\pm$ 0.80 <sup>n</sup>
10	1.17 $\pm$ 0.76 <sup>b</sup>	2.59 $\pm$ 0.73 <sup>de</sup>	7.11 $\pm$ 0.74 <sup>g</sup>	5.14 $\pm$ 1.57 <sup>jk</sup>	3.55 $\pm$ 0.80 <sup>p</sup>
100	1.00 $\pm$ 0.53 <sup>b</sup>	1.45 $\pm$ 0.58 <sup>e</sup>	4.49 $\pm$ 1.37 <sup>h</sup>	2.65 $\pm$ 1.14 <sup>l</sup>	2.03 $\pm$ 0.61 <sup>p</sup>

Humic acid (mg/L)	PFBA Mean $\pm$ SD ( $\mu\text{g}/\text{g}$ )	PFOA Mean $\pm$ SD ( $\mu\text{g}/\text{g}$ )	GenX Mean $\pm$ SD ( $\mu\text{g}/\text{g}$ )	PFBS Mean $\pm$ SD ( $\mu\text{g}/\text{g}$ )	PFOS Mean $\pm$ SD ( $\mu\text{g}/\text{g}$ )
0	10.82 $\pm$ 1.23 <sup>a</sup>	27.60 $\pm$ 2.59 <sup>c</sup>	39.20 $\pm$ 2.86 <sup>f</sup>	38.74 $\pm$ 6.49 <sup>i</sup>	44.00 $\pm$ 2.84 <sup>m</sup>
1	8.39 $\pm$ 2.39 <sup>ab</sup>	15.98 $\pm$ 3.05 <sup>d</sup>	32.41 $\pm$ 2.24 <sup>fg</sup>	31.56 $\pm$ 4.57 <sup>ij</sup>	29.88 $\pm$ 3.05 <sup>n</sup>
10	4.49 $\pm$ 2.89 <sup>b</sup>	9.91 $\pm$ 2.78 <sup>de</sup>	27.16 $\pm$ 2.82 <sup>g</sup>	19.65 $\pm$ 5.99 <sup>jk</sup>	13.57 $\pm$ 3.05 <sup>p</sup>
100	3.80 $\pm$ 2.02 <sup>b</sup>	5.55 $\pm$ 2.23 <sup>e</sup>	17.14 $\pm$ 5.24 <sup>h</sup>	10.12 $\pm$ 4.35 <sup>l</sup>	7.77 $\pm$ 2.34 <sup>p</sup>

Table B7. Effect of temperature on the adsorption capacity of the secondary PET MPs for PFAS

Temperature (°C)	PFBA Mean ± SD (µg/m <sup>2</sup> )	PFOA Mean ± SD (µg/m <sup>2</sup> )	GenX Mean ± SD (µg/m <sup>2</sup> )	PFBS Mean ± SD (µg/m <sup>2</sup> )	PFOS Mean ± SD (µg/m <sup>2</sup> )
25	2.90 ± 1.13 <sup>a</sup>	5.82 ± 0.68 <sup>c</sup>	8.19 ± 1.27 <sup>e</sup>	9.54 ± 0.58 <sup>g</sup>	9.81 ± 0.15 <sup>i</sup>
30	4.52 ± 1.68 <sup>ab</sup>	6.47 ± 0.49 <sup>c</sup>	8.54 ± 2.37 <sup>e</sup>	10.32 ± 0.60 <sup>gh</sup>	9.81 ± 0.42 <sup>i</sup>
35	6.74 ± 0.95 <sup>ab</sup>	7.90 ± 1.40 <sup>cd</sup>	9.53 ± 1.57 <sup>ef</sup>	10.45 ± 1.35 <sup>gh</sup>	11.51 ± 2.08 <sup>i</sup>
40	7.16 ± 1.31 <sup>ab</sup>	9.35 ± 0.42 <sup>d</sup>	9.72 ± 1.06 <sup>ef</sup>	11.47 ± 1.49 <sup>gh</sup>	13.02 ± 2.61 <sup>i</sup>
45	8.60 ± 1.53 <sup>b</sup>	9.88 ± 1.30 <sup>d</sup>	12.02 ± 1.68 <sup>ef</sup>	11.74 ± 0.91 <sup>gh</sup>	13.65 ± 1.28 <sup>i</sup>
50	8.72 ± 2.90 <sup>b</sup>	9.98 ± 0.50 <sup>d</sup>	13.04 ± 0.74 <sup>f</sup>	12.66 ± 1.04 <sup>h</sup>	13.91 ± 0.90 <sup>i</sup>

Temperature (°C)	PFBA Mean ± SD (µg/g)	PFOA Mean ± SD (µg/g)	GenX Mean ± SD (µg/g)	PFBS Mean ± SD (µg/g)	PFOS Mean ± SD (µg/g)
25	11.06 ± 4.32 <sup>a</sup>	22.23 ± 2.59 <sup>c</sup>	31.27 ± 4.84 <sup>e</sup>	36.43 ± 2.21 <sup>g</sup>	37.47 ± 0.57 <sup>i</sup>
30	17.27 ± 6.40 <sup>ab</sup>	24.71 ± 1.85 <sup>c</sup>	32.63 ± 9.04 <sup>e</sup>	39.44 ± 2.27 <sup>gh</sup>	37.47 ± 1.61 <sup>i</sup>
35	25.76 ± 3.63 <sup>ab</sup>	30.18 ± 5.36 <sup>cd</sup>	36.41 ± 5.99 <sup>ef</sup>	39.92 ± 5.17 <sup>gh</sup>	43.98 ± 7.95 <sup>i</sup>
40	27.37 ± 5.00 <sup>ab</sup>	35.73 ± 1.60 <sup>d</sup>	37.14 ± 4.03 <sup>ef</sup>	43.80 ± 5.69 <sup>gh</sup>	49.73 ± 9.96 <sup>i</sup>
45	32.87 ± 5.85 <sup>b</sup>	37.75 ± 4.95 <sup>d</sup>	45.93 ± 6.41 <sup>ef</sup>	44.86 ± 3.47 <sup>gh</sup>	52.15 ± 4.89 <sup>i</sup>
50	33.33 ± 11.07 <sup>b</sup>	38.12 ± 1.90 <sup>d</sup>	49.82 ± 2.83 <sup>f</sup>	48.38 ± 3.99 <sup>h</sup>	53.13 ± 3.44 <sup>i</sup>

Table B8. Summary of the thermodynamics parameters for PFAS adsorption onto the secondary PET MPs.

Temperature (K)	$\Delta G$ (kJ/mol)					$\Delta H$ (kJ/mol)					$\Delta S$ (J/mol.K)				
	PFBA	PFOA	GenX	PFBS	PFOS	PFOA	PFBA	GenX	PFOS	PFBS	PFOA	PFBA	GenX	PFOS	PFBS
25	-16.44	-20.04	-20.36	-20.93	-22.52	24.04	41.04	21.41	18.96	13.97	148.23	194.64	139.47	138.80	116.87
30	-20.77	-18.10	-20.62	-22.88	-21.49										
35	-21.74	-19.52	-21.50	-23.76	-21.91										
40	-22.62	-19.93	-22.21	-24.52	-22.54										
45	-23.08	-21.05	-23.03	-25.46	-23.09										
50	-23.65	-21.34	-23.66	-25.68	-23.94										

Table B9. Change in the change in the intensity of the FTIR peak at  $1089\text{ cm}^{-1}$  (which represents stretching vibration of the C-O of PET's ester group after the adsorption of each PFAS).

	$I_{1089, \text{PET}} - I_{1089, \text{PET+PFAS}}$
PFBA	$20.2 \times 10^{-3}$
PFBS	$22.0 \times 10^{-3}$
PFOA	$21.2 \times 10^{-3}$
PFOS	$21.2 \times 10^{-3}$
GenX	$21.5 \times 10^{-3}$

Table B10. Molecular descriptors obtained from quantum calculations of each PFAS.

<b>Molecule</b>	<b>EHOM O (au)</b>	<b>ELUM O (au)</b>	<b>EHOM O (eV)</b>	<b>ELUM O (eV)</b>	<b><math>\Delta E</math> (eV)</b>	<b>I</b>	<b>A</b>	<b><math>\chi</math> (eV)</b>	<b><math>\eta</math> (eV)</b>	<b><math>\mu^2</math></b>	<b><math>2*\eta</math></b>	<b><math>\omega</math> (eV)</b>	<b>EB3LYP</b>
PFBA	-0.34	-0.07	-9.21	-1.92	7.29	9.21	1.92	5.57	3.65	31.00	7.29	4.25	-1002.68
PFOA	-0.34	-0.07	-9.19	-1.99	7.20	9.19	1.99	5.59	3.60	31.28	7.20	4.34	-1954.10
PFBS	-0.36	-0.05	-9.86	-1.43	8.43	9.86	1.43	5.64	4.22	31.86	8.43	3.78	-1675.78
PFOS	-0.36	-0.06	-9.75	-1.75	7.99	9.75	1.75	5.75	4.00	33.04	7.99	4.13	-2627.20
GenX	-0.33	-0.05	-8.95	-1.48	7.47	8.95	1.48	5.22	3.74	27.21	7.47	3.64	-1553.60

Table B11. Condensed FUKUI analysis of PFBS and PFBA

PFBS				PFBA			
Atoms	$f_k^-$	$f_k^+$	$f_k^0$	Atoms	$f_k^-$	$f_k^+$	$f_k^0$
C1	0.002	0.017	0.010	C1	0.010	0.038	0.024
C2	0.021	0.060	0.040	C2	0.021	0.039	0.030
C3	0.020	0.032	0.026	C3	0.045	0.079	0.062
C4	0.076	0.081	0.079	C4	0.015	0.259	0.137
S5	-0.039	0.197	0.079	O5	0.117	0.098	0.107
O6	0.088	0.108	0.098	O7	0.393	0.181	0.287
O8	0.194	0.067	0.131	F8	0.051	0.030	0.040
O9	0.198	0.092	0.145	F9	0.035	0.017	0.026
F10	0.055	0.031	0.043	F10	0.033	0.018	0.026
F11	0.036	0.014	0.025	F11	0.043	0.027	0.035
F12	0.059	0.042	0.050	F12	0.051	0.023	0.037
F13	0.044	0.023	0.033	F13	0.057	0.037	0.047
F14	0.019	0.012	0.015	F14	0.095	0.061	0.078
F15	0.034	0.021	0.027				
F16	0.015	0.006	0.010				
F17	0.076	0.034	0.055				
F18	0.081	0.031	0.056				

Table B12. Condensed FUKUI analysis of PFOS and PFOA

PFOS				PFOA			
Atoms	$f_k^-$	$f_k^+$	$f_k^0$	Atoms	$f_k^-$	$f_k^+$	$f_k^0$
C1	0.006	0.017	0.011	C1	0.006	0.028	0.017
C2	0.017	0.035	0.026	C2	0.017	0.036	0.027
C3	0.016	0.043	0.029	C3	0.016	0.042	0.029
C4	0.017	0.051	0.034	C4	0.019	0.048	0.033
C5	0.018	0.050	0.034	C5	0.018	0.047	0.032
C6	0.018	0.056	0.037	C6	0.016	0.034	0.025
C7	0.015	0.043	0.029	C7	0.030	0.040	0.035
C8	0.052	0.038	0.045	F8	0.018	0.011	0.014
S9	-0.022	0.090	0.034	F9	0.027	0.020	0.024
O11	0.014	0.048	0.031	F10	0.020	0.010	0.015
O12	0.117	0.045	0.081	F11	0.034	0.016	0.025
O13	0.131	0.072	0.101	F12	0.029	0.022	0.026
F14	0.028	0.020	0.024	F13	0.034	0.022	0.028
F15	0.032	0.016	0.024	F14	0.037	0.018	0.027
F16	0.017	0.011	0.014	F15	0.036	0.021	0.028
F17	0.020	0.011	0.015	F16	0.034	0.024	0.029
F18	0.026	0.021	0.023	F17	0.037	0.019	0.028
F19	0.032	0.022	0.027	F18	0.034	0.023	0.028
F20	0.035	0.019	0.027	F19	0.033	0.022	0.028
F21	0.033	0.025	0.029	F20	0.031	0.023	0.027
F22	0.035	0.021	0.028	F21	0.062	0.043	0.053
F23	0.031	0.024	0.028	F22	0.036	0.030	0.033
F24	0.034	0.024	0.029	C23	0.013	0.154	0.083
F25	0.031	0.025	0.028	O24	0.262	0.150	0.206
F26	0.033	0.026	0.029	O25	0.076	0.061	0.068
F27	0.030	0.020	0.025	C1	0.006	0.028	0.017
F28	0.034	0.027	0.030				
F29	0.050	0.026	0.038				
F30	0.049	0.025	0.037				

Supplementary for chapter 5

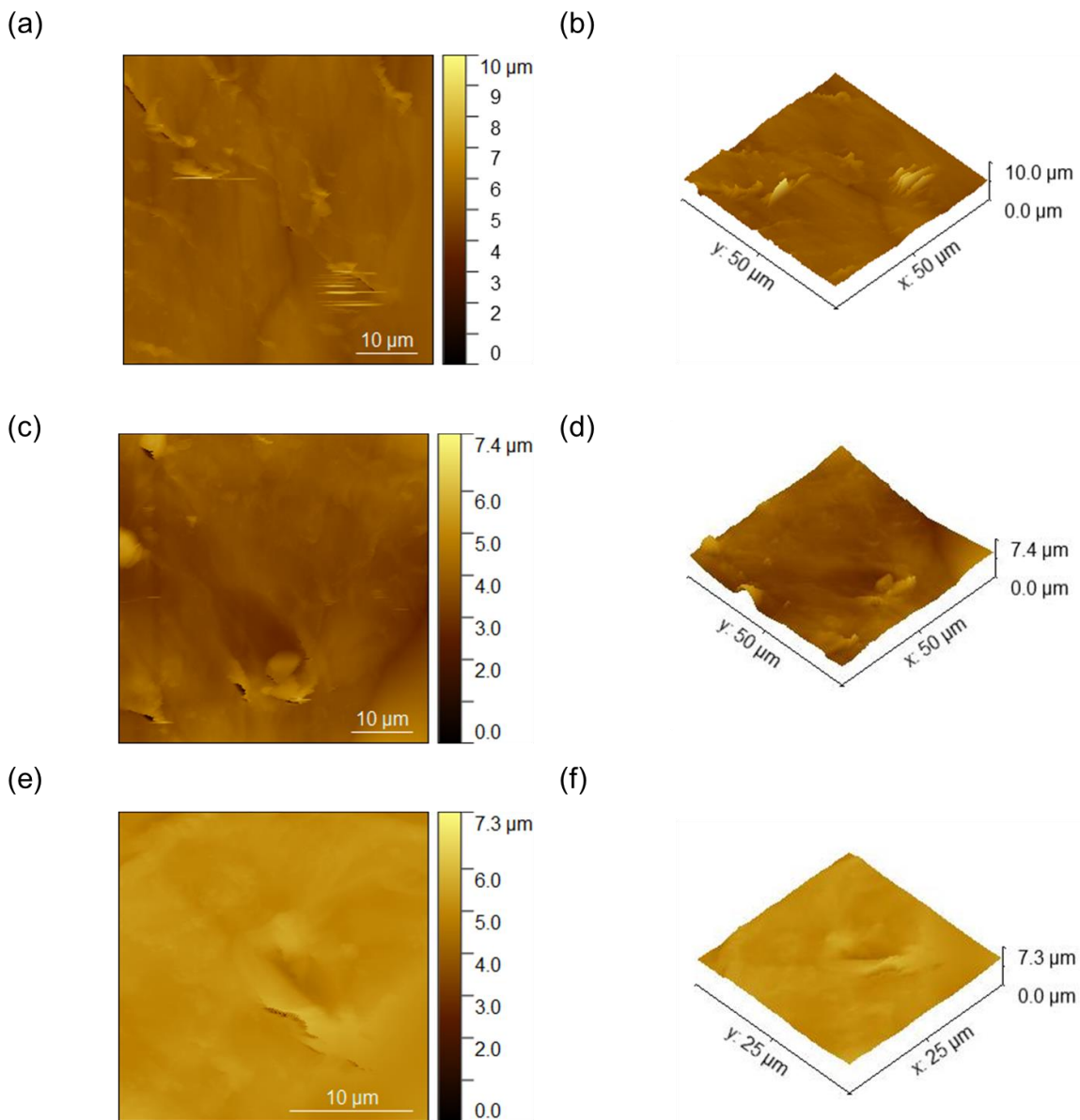


Figure C1. AFM analysis showing surface roughness of MPs in (a) 2D (b) 3D for pristine MPs (c) 2D and (d) 3D for Na<sub>2</sub>S treated MPs (e) 2D and (f) 3D for NOM-loaded MPs



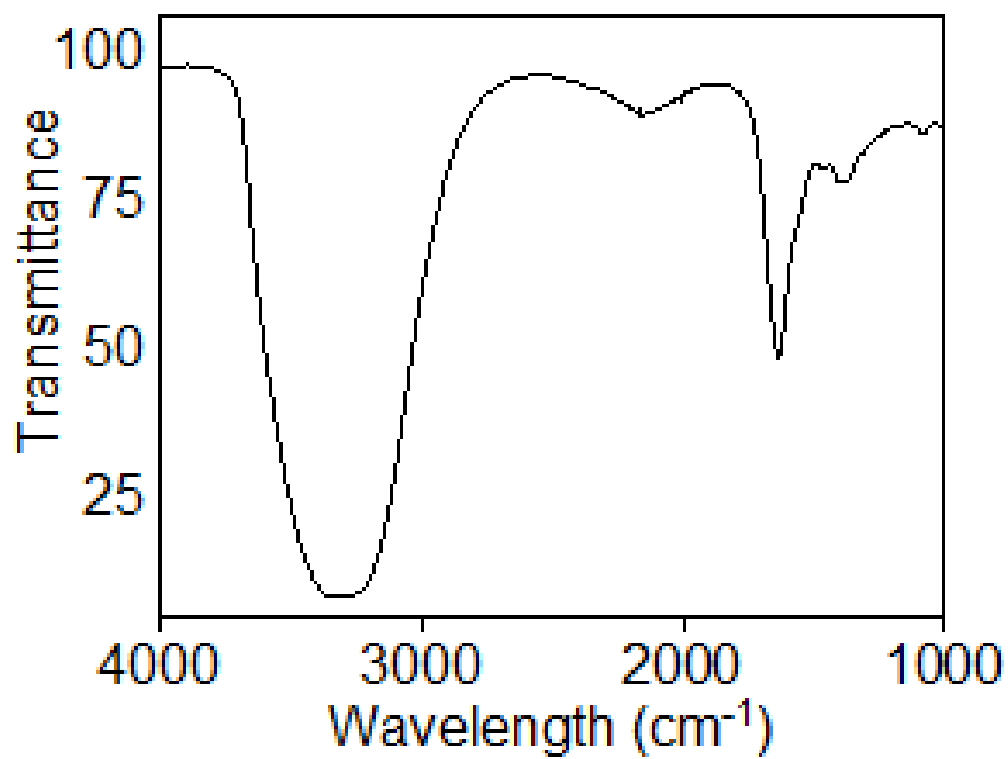
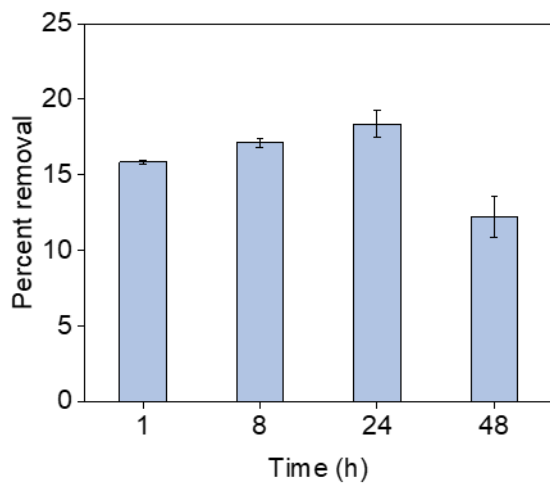


Figure C2. FTIR spectrum of NOM solution.

(a)



(b)

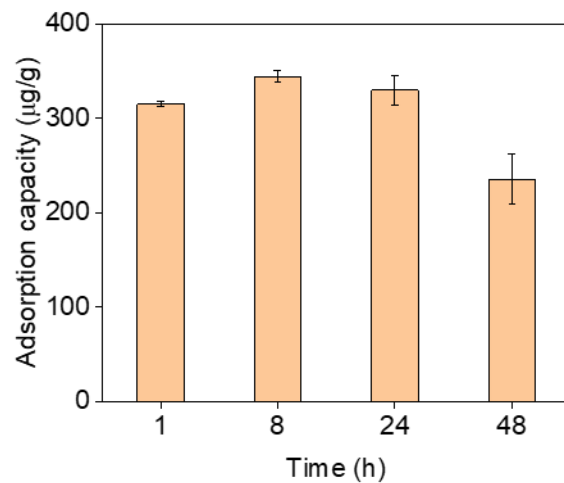


Figure C3. (a) Percent removal and (b) adsorption capacity of peptone adsorbed onto secondary PET MPs

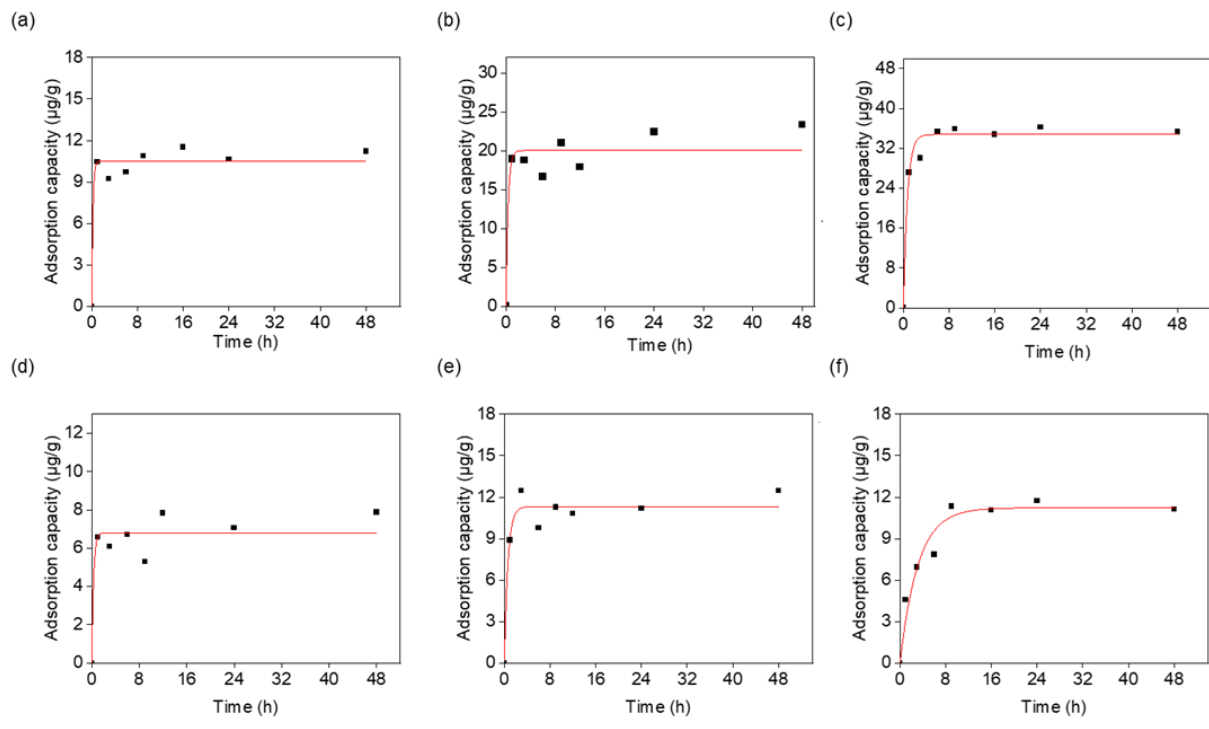


Figure C4. Adsorption capacity at different times of the pristine MPs for (a) PFOA (b) PFOS (c) FOSA (d) PFBA (e) PFBS (f) GenX in deionized water

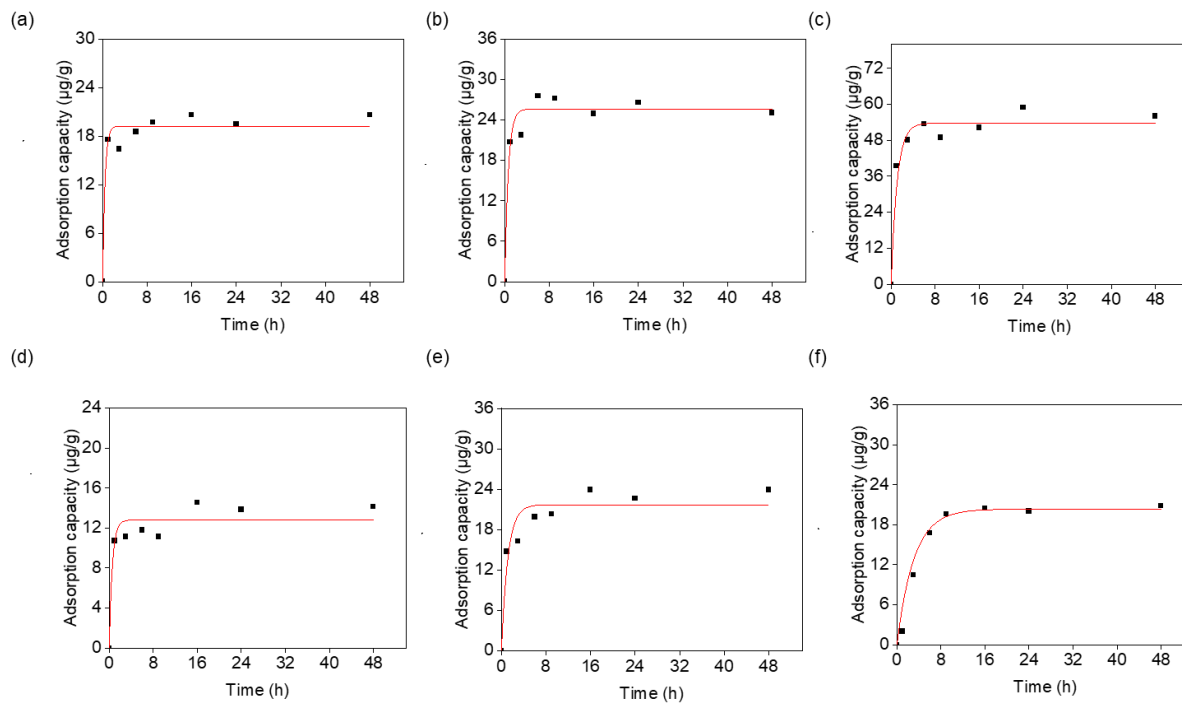


Figure C5. Adsorption capacity at different times of the  $\text{Na}_2\text{S}$  treated MPs for (a) PFOA (b) PFOS (c) FOSA (d) PFBA (e) PFBS (f) GenX in deionized water.

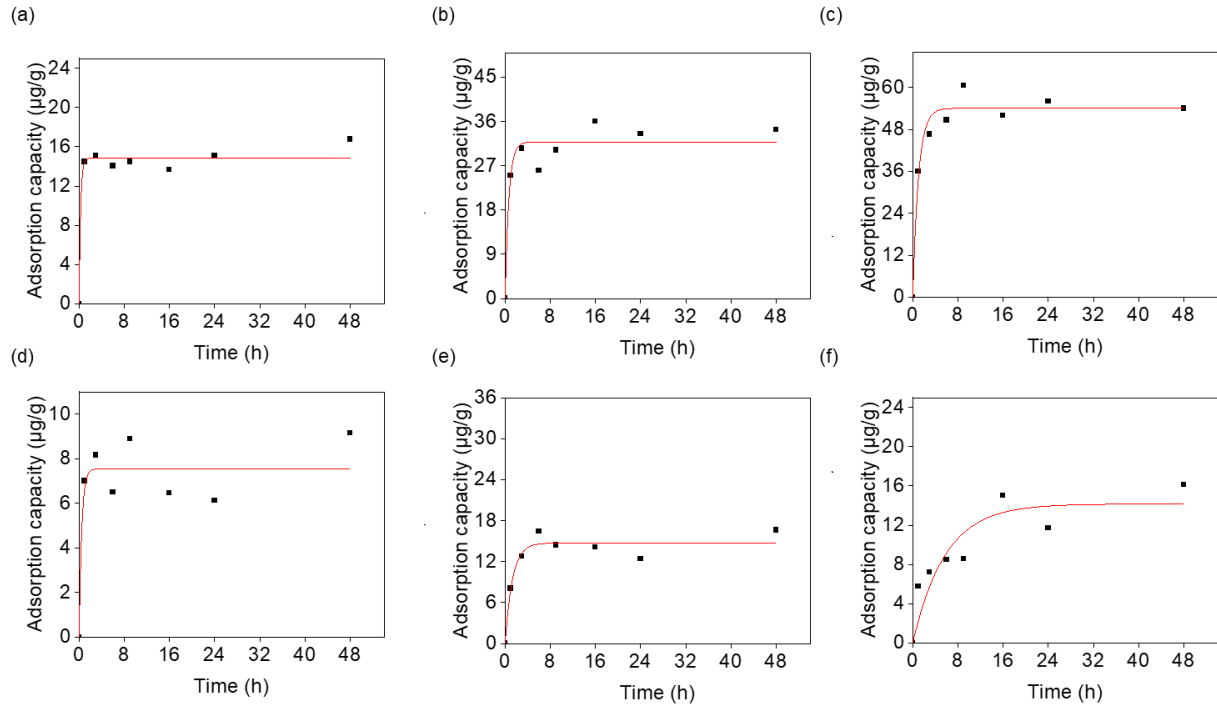


Figure C6. Adsorption capacity at different times of the NOM-loaded MPs for (a) PFOA (b) PFOS (c) FOSA (d) PFBA (e) PFBS (f) GenX in deionized water

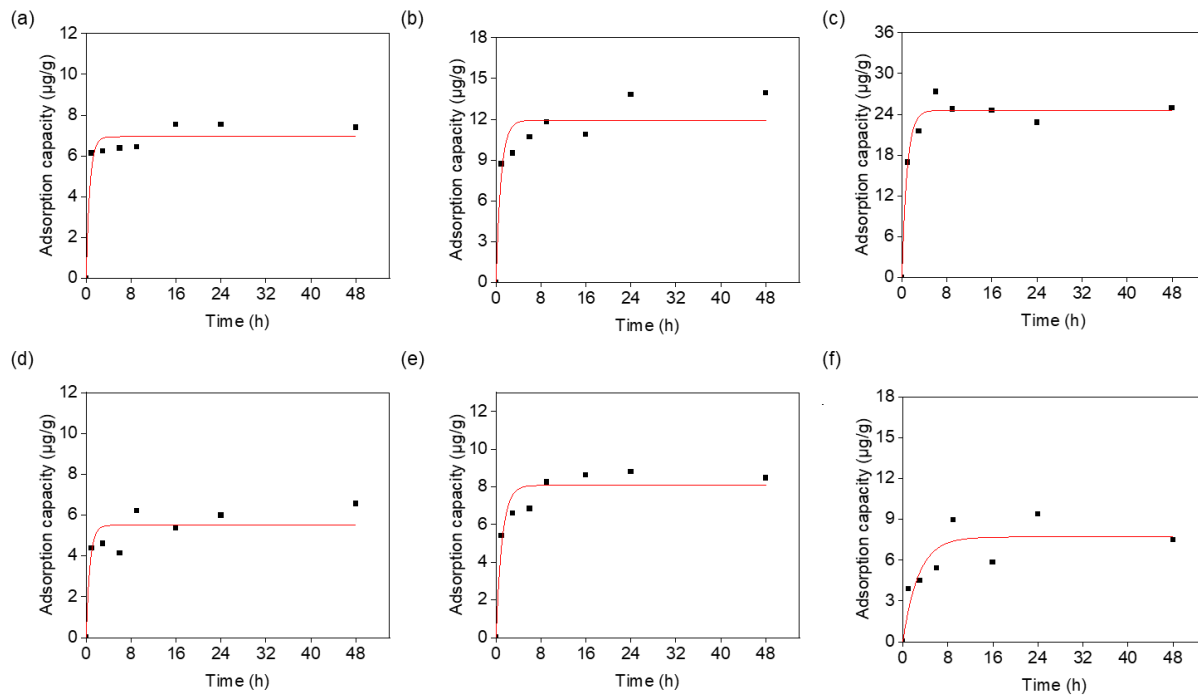


Figure C7. Adsorption capacity at different times of the pristine MPs for (a) PFOA (b) PFOS (c) FOSA (d) PFBA (e) PFBS (f) GenX in synthetic water

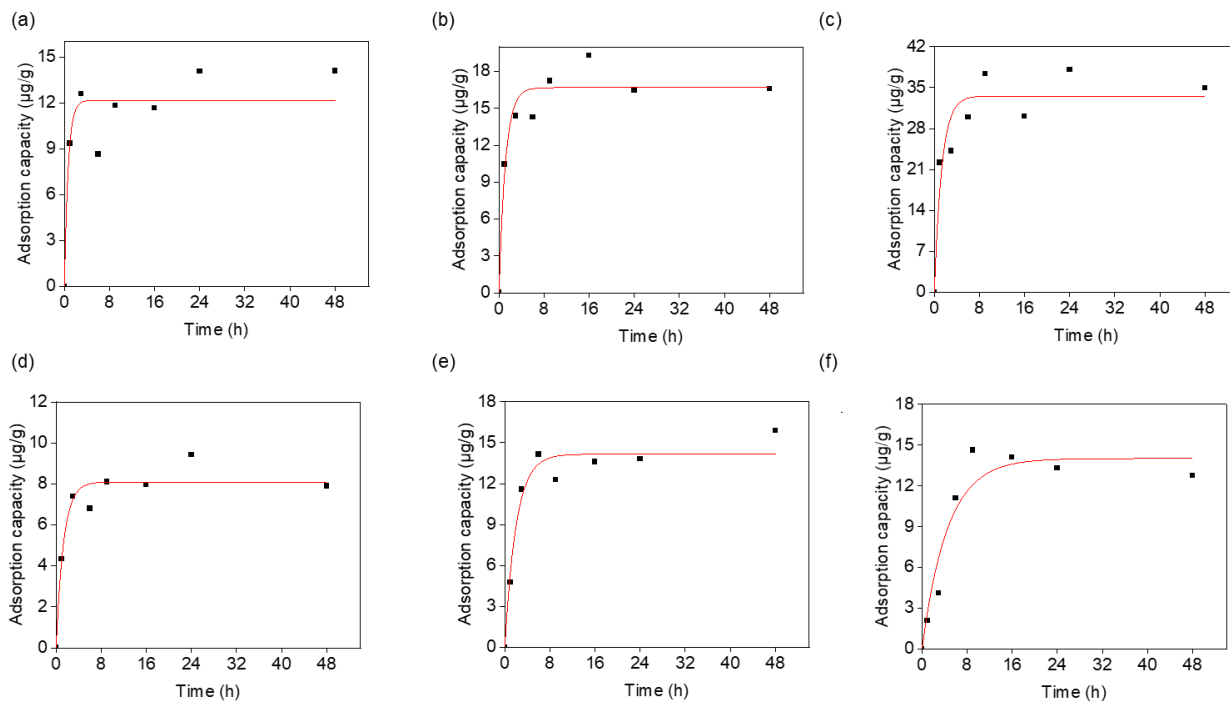


Figure C8. Adsorption capacity at different times of the Na<sub>2</sub>S treated MPs for (a) PFOA (b) PFOS (c) FOSA (d) PFBA (e) PFBS (f) GenX in synthetic water

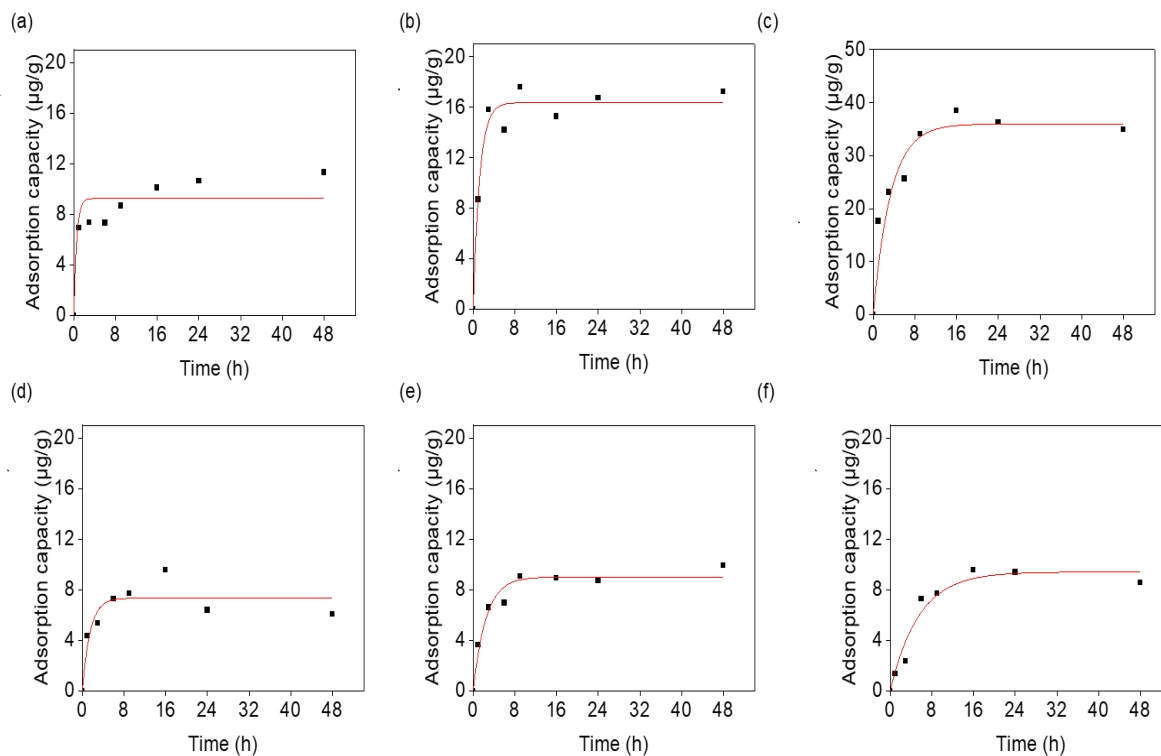


Figure C9. Adsorption capacity at different times of the NOM-loaded MPs for (a) PFOA (b) PFOS (c) FOSA (d) PFBA (e) PFBS (f) GenX in synthetic water



Table C1. Constituents of the synthetic wastewater (Limbach et al., 2008; OECD, 2001)

Constituents	Concentration (mg/L)
Peptone	4000
Meat extract	2750
Urea	750
Sodium chloride	175
CaCl <sub>2</sub> ·2H <sub>2</sub> O	100
MgSO <sub>4</sub> ·7H <sub>2</sub> O	50
K <sub>2</sub> HPO <sub>4</sub>	700
NaHCO <sub>3</sub>	4900

Table C2. Elemental composition of aged MPs based on XPS analyses

Microplastics	O-C=O	O-C	C-C	C-O	C=O	Total C	Total O	Total N	O/C ratio
Pristine	23.2	27.6	49.2	14.9	85.1	64	14	22	0.22
Na <sub>2</sub> S treated	25.3	30.2	44.5	8.2	91.8	61	17	22	0.28
NOM-loaded	16.2	26.4	57.4	34	66	74	23	3	0.31

Table C3. Kinetics parameters derived from non-linear pseudo first order (PFO) fitting for PFAS adsorption onto microplastics in different aqueous systems.

Parameter		PFBS	PFOS	PFBA	PFOA	GenX	FOSA
<i>Deionized water</i>							
		Average $\pm$ SD	Average $\pm$ SD	Average $\pm$ SD	Average $\pm$ SD	Average $\pm$ SD	Average $\pm$ SD
Pristine	$q_e$ ( $\mu\text{g/g}$ )	11.31 $\pm$ 0.39	20.04 $\pm$ 0.99	6.81 $\pm$ 0.37	10.53 $\pm$ 0.33	11.22 $\pm$ 0.56	34.79 $\pm$ 0.81
	$k_1$ (1/min)	1.59 $\pm$ 0.44	2.89 $\pm$ 2.34	3.32 $\pm$ 1.06	4.82 $\pm$ 1.25	0.32 $\pm$ 0.06	1.42 $\pm$ 0.24
	R <sup>2</sup>	0.95	0.91	0.89	0.96	0.95	0.98
Sulfided	$q_e$ ( $\mu\text{g/g}$ )	21.68 $\pm$ 1.66	25.60 $\pm$ 0.78	12.81 $\pm$ 0.59	19.23 $\pm$ 0.59	21.39 $\pm$ 1.19	53.7 $\pm$ 1.44
	$k_1$ (1/min)	0.87 $\pm$ 0.22	1.56 $\pm$ 0.37	1.74 $\pm$ 0.68	2.39 $\pm$ 0.88	0.28 $\pm$ 0.09	0.92 $\pm$ 0.15
	R <sup>2</sup>	0.92	0.96	0.91	0.96	0.92	0.97
NOM-loaded	$q_e$ ( $\mu\text{g/g}$ )	14.59 $\pm$ 2.18	32.55 $\pm$ 6.78	7.35 $\pm$ 1.87	14.89 $\pm$ 1.53	14.36 $\pm$ 3.52	56.01 $\pm$ 4.66
	$k_1$ (1/min)	0.78 $\pm$ 0.57	1.52 $\pm$ 0.76	2.49 $\pm$ 0.27	4.46 $\pm$ 0.78	0.20 $\pm$ 0.07	0.92 $\pm$ 0.3
	R <sup>2</sup>	0.84	0.93	0.85	0.97	0.82	0.97
<i>Synthetic wastewater</i>							
Pristine	$q_e$ ( $\mu\text{g/g}$ )	8.08 $\pm$ 0.34	11.92 $\pm$ 0.67	5.50 $\pm$ 0.36	6.92 $\pm$ 0.22	7.86 $\pm$ 0.39	25.05 $\pm$ 0.58
	$k_1$ (1/min)	0.93 $\pm$ 0.25	1.12 $\pm$ 0.41	1.47 $\pm$ 0.72	2.14 $\pm$ 0.83	0.25 $\pm$ 0.04	1.02 $\pm$ 0.17
	R <sup>2</sup>	0.94	0.89	0.85	0.95	0.79	0.97
Sulfided	$q_e$ ( $\mu\text{g/g}$ )	14.09 $\pm$ 1.08	16.64 $\pm$ 0.51	8.32 $\pm$ 0.38	12.500 $\pm$ 0.38	13.9 $\pm$ 0.77	34.91 $\pm$ 0.94
	$k_1$ (1/min)	0.48 $\pm$ 0.01	0.86 $\pm$ 0.20	1.31 $\pm$ 0.48	1.31 $\pm$ 0.48	0.15 $\pm$ 0.05	0.70 $\pm$ 0.08
	R <sup>2</sup>	0.96	0.94	0.95	0.95	0.93	0.89
NOM-loaded	$q_e$ ( $\mu\text{g/g}$ )	9.37 $\pm$ 1.54	16.98 $\pm$ 1.90	7.04 $\pm$ 2.53	9.08 $\pm$ 1.08	9.09 $\pm$ 0.89	35.32 $\pm$ 2.34
	$k_1$ (1/min)	0.45 $\pm$ 0.32	0.81 $\pm$ 0.26	0.71 $\pm$ 0.52	1.35 $\pm$ 0.19	0.08 $\pm$ 0.06	0.46 $\pm$ 0.18
	R <sup>2</sup>	0.96	0.96	0.84	0.96	0.95	0.92